Exploring ^{1}H NMR Relaxometry for Wine Traceability and Authenticity Assessment

Andrea Zava

Dissertation to obtain a Master's Degree in

Viticulture and Oenology Engineering

Supervisor: PhD Sofia Catarino, Assistant Professor, Instituto Superior de Agronomia, Universidade de Lisboa

Supervisor: PhD Pedro Josè Oliveira Sebastião, Associated Professor, Instituto Superior Técnico, Universidade de Lisboa

Jury:

PRESIDENT
PhD Jorge Manuel Rodrigues Ricardo da Silva, Full Professor at Instituto Superior de Agronomia, Universidade de Lisboa.

MEMBERS
PhD António Mário Pereira Ferraz, Assistant Professor at Instituto Superior Técnico, Universidade de Lisboa;
PhD Sofia Cristina Gomes Catarino, Assistant Professor at Instituto Superior de Agronomia, Universidade de Lisboa.

2019/2020

Abstract

Keywords: Authenticity, Isotopes, NMR, Relaxometry, Wine.

The development of analytical methodologies for wine authenticity assessment is one of the most challenging issues for the scientific community. In this study, the potential analytical applications of ^{1}H NMR relaxometry, in view to wine authenticity investigation, were explored. For that, proton longitudinal relaxation rate dispersions in the range 0.04-300 MHz were investigated in three white and three red varietal wines from Tapada da Ajuda (Lisbon), obtained from *Vitis vinifera* L. grape varieties, namely Alvarinho, Arinto, Cabernet Sauvignon, Moscatel Graúdo, Touriga Nacional and Trincadeira, from vintages 2008 and 2017 for a total of twelve bottles. To evaluate rain as an environmental source of variability pluviometric data were considered. Dispersions associable to the presence of paramagnetic ions were observed at low frequencies but the results for wine iron content cannot explain the effect. Correlations between the wine characters and the areas drawn by the most representative relaxometry models show an effect of alcoholic strength by volume, glycerol and total dry matter suggesting wine viscosity to modulate relaxivity. To the best of our knowledge, for the first time wine physical-chemical characteristics and glycerol content have been compared to NMR relaxation rate profiles. To investigate the paramagnetic relaxation and evaluate the relaxation associated to wine hydro-alcoholic matrix, water-ethanol mixtures were tested, and linear regressions were obtained. Comparing the results with bibliographic sources, the paramagnetic enhancement on relaxation profiles was associated to the presence of manganese(II), but no parameters have been fitted from the models. The dispersions highlighted possible cross relaxations in the 1.5-6 MHz frequency range. The presence of nitrogen diluted into the wine could explain this behaviour. To inspect how each physical-chemical parameter impacts on wine relaxation profiles the knowledge of manganese content is crucial.

Resumo

Palavras-chave: Autenticidade, Isótopos, NMR, Relaxometria, Vinho.

O desenvolvimento de metodologias analíticas para avaliação da autenticidade do vinho representa um enorme desafio para a comunidade científica. Neste estudo, pretendeu-se explorar as potencialidades da técnica de relaxometria ^{1}H NMR, com vista à sua aplicação para avaliação da autenticidade do vinho. Para tal, foram avaliadas as dispersões da taxa de relaxamento do protão na faixa de 0,04-300 MHz, em doze vinhos monovarietais, brancos e tintos, originários da Tapada da Ajuda (Lisboa), produzidos a partir de variedades *Vitis vinifera* L., nomeadamente Alvarinho, Arinto, Cabernet Sauvignon, Moscatel Graúdo, Touriga Nacional e Trincadeira das vindimas de 2008 e 2017. O potencial efeito da precipitação foi avaliado através da análise de dados pluviométricos. Foram observadas, no espectro de baixas frequências, dispersões associadas à presença de íões, não explicadas pelo teor de ferro nos vinhos. A avaliação da correlação entre as características físico-químicas dos vinhos e as áreas desenhadas pelos modelos de relaxometria mais representativos, mostram a influência do teor alcoólico, glicerol e extracto seco total, sugerindo um efeito de modulação da viscosidade na relaxividade. Para investigar o relaxamento paramagnético e avaliar o relaxamento associado à matriz hidroalcoólica do vinho, foram realizados ensaios com soluções água-etanol, tendo sido obtidas regressões lineares entre o teor alcoólico e a taxa de relaxamento. Comparando os resultados com fontes bibliográficas, o incremento nas taxas de relaxamento foi associado à presença de manganês. As dispersões evidenciam possíveis relaxamentos cruzados na faixa de frequência de 1,5-6 MHz. A presença de azoto no vinho poderá explicar este comportamento. Para avaliar o efeito de cada parâmetro físico-químico nos perfis de relaxamento do vinho, o conhecimento do teor de manganês parece ser crucial. Pela primeira vez, as características físico-químicas do vinho, incluindo o teor em glicerol, foram relacionadas com os perfis de taxa de relaxamento.

Resumo Alargado

A avaliação da autenticidade do vinho é um tema importante, uma vez que o aumento do valor acrescentado dos vinhos produzidos com menções específicas tem como consequência tornar a rotulagem errada do vinho economicamente interessante. Na primeira secção deste documento, os principais desenvolvimentos sobre autenticidade e rastreabilidade do vinho são revistos juntamente com a variabilidade da composição orgânica, mineral e isotópica. O presente trabalho apresenta uma introdução teórica de relaxometria por ressonância magnética nuclear, sendo explicadas as grandezas físicas, os modelos matemáticos e alguns exemplos aplicativos. A componente experimental apresentada sob a forma de artigo científico, descrevendo a primeira abordagem para a aplicação desta técnica analítica ao vinho. Deve salientar-se que é a primeira vez que os parâmetros físico-químicos do vinho são relacionados aos perfis de relaxamento.de protões.

Devido à complexidade da composição do vinho, não é possível detectar uma adulteração através da inspecção da concentração absoluta e/ou relativa de algumas famílias de compostos. Somente a aplicação de ferramentas estatísticas multivariadas permite inspeccionar a variabilidade composicional e rastrear as discrepâncias. De acordo com a bibliografia, tem sido obtidos bons resultados com a aplicação de espectroscopias de infravermelho médio, infravermelho próximo, visível, ultravioleta e ressonância magnética nuclear de protões, já que estas técnicas permitem inspeccionar mais de um grupo químico ao mesmo tempo. Até agora, apenas a técnica de fraccionamento de isótopos naturais NMR foi aceite como uma ferramenta para detecção de chaptalização (adição de açúcar). Nos últimos anos têm sido feitos desenvolvimentos interessantes que permitem discriminar os vinhos de acordo com as condições pedo-geológicas dos solos de origem. Os perfis dos elementos de terras raras obtidos é uma das ferramentas mais promissoras na discriminação da origem geográfica dos vinhos. Uma abordagem semelhante demonstrou que a relação isotópica de estrôncio permanece estável durante toda a produção de vinho, tornando possível discriminar a origem dos vinhos de acordo com a composição da rocha mãe do solo e a idade. Algumas práticas enológicas, tais como o loteamento, uso de bentonite, filtração, adição de dióxido de enxofre, e contaminações diminuem a fiabilidade desta abordagem analítica, uma vez que contribuem para a variabilidade composicional de uma forma imprevisível.

Neste estudo, pretendeu-se explorar as potencialidades da técnica de relaxometria ^{1}H NMR, com vista à sua aplicação para avaliação da autenticidade do vinho. Mais exactamente, foram obtidos perfis da taxa de relaxamento para doze vinhos monovarietais, brancos e tintos, originários de vinhas próximas (Tapada da Ajuda, Lisboa), e de duas vindimas (2008 e 2017),

a partir das castas Alvarinho, Arinto, Moscatel Graúdo, Arinto, Touriga Nacional, Trincadeira, e Cabernet Sauvignon. Os perfis foram obtidos na faixa de frequência 0,04-300 MHz. Para avaliação do impacto da precipitação, foram consultados e analisados dados pluviométricos. Foram observadas dispersões associáveis à presença de iões paramagnéticos não explicadas pelo teor de ferro dos vinhos. De facto, um estudo recente provou que o manganês(II) é o principal ião no vinho que contribui para a taxa de relaxamento paramagnético. As correlações entre as características físico-químicas do vinho e as áreas desenhadas pelos modelos de relaxometria mais representativos destacaram um efeito do teor alcoólico, glicerol e extracto seco total, sugerindo que a viscosidade do vinho poderá modular a relaxividade. Os modelos foram desenhados considerando as contribuições diamagnéticas cumulativas e paramagnética. Sem conhecer o conteúdo exacto de manganês(II), não foi possível extrair parâmetros fisicamente confiáveis dos modelos. Para investigar singularmente os perfis de relaxamento paramagnético e avaliar o relaxamento associado apenas ao solvente do vinho (matriz hidroalcoólica) foram realizados ensaios com soluções água-etanol, tendo sido observadas, regressões lineares entre o teor de etanol e a taxa de relaxamento. Após transformação dos dados relativos à taxa de relaxamento paramagnético, as novas dispersões evidenciaram possíveis relaxamentos cruzados na faixa de frequência de 1,5-6 MHz. A presença de nitrogénio no vinho sob a forma de nitróxidos, aminoácidos e/ou proteínas poderá explicar este comportamento. Em conclusão, não foi possível discriminar entre castas e/ou vindimas, sendo necessária informação sobre o teor de manganês para comparação dos tempos de correlação correspondentes a cada vinho. O instrumento analítico FFC-NMR utilizado revelou limitações na discriminação de vinhos de acordo com a variedade, vindimas, no entanto poderá ter interesse para inspecção das interacções entre grupos de moléculas na determinação da viscosidade e do corpo do vinho.

Table of Contents

List of Figures

List of Tables

List of Abbreviations and Symbols

Abbreviations

AAS	Atomic Absorption Spectroscopy
Al	Alvarinho
ANOVA	Analysis of Variance
AOC	Appellation d'Origine Controllée
Ar	Arinto
BPP	Bloembergen-Purcell-Pound Model
CPMG	Carr-Purcell-Meiboom-Gill (Sequence)
CS	Cabernet Sauvignon
DD	Dipole-Dipole
DO	Denominación de Origen
DOF	Degrees of Freedom
DOC	Denominação de Origem Controlada, Denominazione di Origine Controllata
DOCG	Denominazione di Origine Controllata e Garantita
DNA	Deoxyribonucleic acid
EC	European Commission
EMA	Economically Motivated Adulterations
EU	European Union
FDA	U.S. Food and Drug Administration
FFC-NMR	Fast-Field-Cycling - Nuclear Magnetic Resonance
FID	Free Induction Decay
FT	Fourier Transform
FTIR	Fourier Transform Infrared Spectroscopy
GI	Geographical Indication
GIS	Geographic Information System
GABA	γ-Aminobutyric Acid
HCA	Hierarchical Cluster Analysis
HCTA	Hydroxycinnamoyl Tartaric Acids
HPICE	High-Performance Ion Chromatography Exclusion
ICP-OES	Inductively Coupled Plasma Optical Emission Spectroscopy
ICP-MS	Inductively Coupled Plasma Mass Spectroscopy
ICSI	National R&D Institute for Cryogenics and Isotopic Technologies (Romania)
IR	Inversion Recovery (Sequence)
IS	Inner-Sphere
k-NN	k-Nearest Neigh
LC	Liquid Chromatography
LDA	Linear Discriminant Analysis
LSR	Least Square Regression
LUA	Landesuntersuchungsamt
LOOCV	Leave-one-out cross validation
mDP	mean degree of polymerization (wine flavanols)
MG	Moscatel Graúdo
MIR	Medium Infrared (Frequency Spectrum)

MRI	Magnetic Resonance Imaging
NA (%)	Natural Abundance (%)
NCEI	U.S. National Centers for Environmental Information
NIR	Near Infrared
NMR	Nuclear Magnetic Resonance
NOAA	U.S. National Oceanic and Atmospheric Administration
OS	Outer-Sphere
OIV	Organisation Internationale de la Vigne et du Vin - International Organization of Vine and Wine
PAC	Proanthocyanins
PCA	Principal Component Analysis
PC	Principal Component
PCR	Principal Component Regression
PI	Paramagnetic Integral
PLS-DA	Partial Least Square Discriminant Analysis
PDO	Protected Denomination of Origin
PLS-R	Partial Least Square Regression
PR proteins	Pathogenesis Related proteins
REE	Rare Earth Elements
RF	Radio Frequency
SC	Scalar
SIMCA	Soft Independent Modelling by Class Analogy
SIRA	Stable Isotope Ratio Analysis
SNIF-NMR	Site-Specific Natural Isotopic Fractionation-Nuclear Magnetic Resonance
TMS	Tetramethylsilane
TN	Touriga Nacional
Tr	Trincadeira
U.S.	United States
Uv	Ultraviolet (Frequency Spectrum)
Vis	Visible (Frequency Spectrum)

Symbols

a	Distance of Minimum Approach
A	Mass Number
B_0	Static Magnetic Field
B_1	Pulsed Radiofrequency Field
B_d	Detection Field (FFC-NMR)
B_p	Polarization Field (FFC-NMR)
B_r	Relaxation Field (FFC-NMR)
D, D_I, D_S	Diffusion, Proton Diffusion and Electron Diffusion Coefficients
I	Current Intensity
$j_k(\omega)$	Spectral Density
L	Angular Moment
n	Average Spin Density
n_m	Number of Paramagnetic Particles

n_s	Number of Solvent Molecules
N_A	Avogadro's Number
h	Planck Constant
$\vec{\mathrm{M}}$	Macroscopic Magnetization Vector
M_0	Magnitude of $\vec{\mathrm{M}}$ at Thermal Equilibrium
M_x, M_y, M_z	Axial Components of $\vec{\mathrm{M}}$
q	Number of Coordinate Water Molecules per Ion
p	p-value (Probability Value)
PT	Portugal
r	Molecular Radius
r	Length of the *I-S* Bound, also Pearson's Correlation Coefficient
r_v^{Mg}	Manganese Paramagnetic Relaxivity (at frequency v)
R	Resistance
R_1^{IS}	Longitudinal Inner-Sphere Relaxation Rate
R_1^{OS}	Longitudinal Outer-Sphere Relaxation Rate
R_{diam}	Diamagnetic Contribution to the Relaxation Rate
R_{obs}	Observed Relaxation Rate
R_{Sample}	Sample Isotopic Ratio
$R_{Standard}$	Standard Isotopic Ratio
$\langle r \rangle$	Average Spin Distance
Re	Reynolds Number
R^2	Coefficient of Determination
t	Time
T	Temperature
T_1	Longitudinal Relaxation Time
T_2	Transversal Relaxation Time
TI	Total Integral
S	Electronic Spin
Z	Atomic Number
$1/T_1$	Longitudinal Relaxation Rate
$1/T_{1m}$	Proton Mean Relaxation Time
$1/T_1^{DD}$	Dipole-Dipole Relaxation Rate Contribution
$1/T_1^{SC}$	Scalar Relaxation Rate Contribution
$1/T_1^{SD}$	Self-Diffusion Longitudinal Relaxation Rate
$1/T_{i,diam}$	Diamagnetic Relaxation Rate (i = 1,2)
$1/T_{i,para}$	Paramagnetic Relaxation Rate (i = 1,2)
$\left(1/T_{i,p}\right)^{IS}$	Inner-Sphere Contribution to Longitudinal (i = 1) and Transversal (i = 2) Paramagnetic Relaxation Rate
$\left(1/T_{i,p}\right)^{OS}$	Outer-Sphere Contribution to Longitudinal (i = 1) and Transversal (i = 2) Paramagnetic Relaxation Rate
$(1/T_{ie})^{ZFS}$	Zero Field Splitting Contribution to Longitudinal (i = 1) and Transversal (i = 2) Paramagnetic Relaxation Rate
$(\mathrm{D/H})_{\mathrm{S}}^{\mathrm{Q}}$	Hydrogen (Water) Isotopic Ratio After the Fermentation
$(\mathrm{D/H})_{\mathrm{W}}^{\mathrm{S}}$	Hydrogen (Water) Isotopic Ratio Before the Fermentation
$\Delta(\mathrm{D/H})_{\mathrm{W}}^{\mathrm{QS}}$	Hydrogen (Water) Isotopic Ratio Variation

γ	Gyromagnetic Ratio
γ_I	Nuclear Gyromagnetic Ratio
γ_p	Proton Gyromagnetic Ratio
γ_S	Electron Gyromagnetic Ratio
δ_{ppm}	Chemical Shift
$\delta‰$	Isotopic Deviation from International Standard Value
ε	Electromotive Force
η	Viscosity
θ	Angle
Δ^2	Mean Square Fluctuation of the Zero Field Splitting
μ	Magnetic Moment
μ_z	*Magnetic Moment z Axis Component*
μ_0	Vacuum Permeability
ν_L	Larmor Frequency (Hz)
ν_{Sample}	Precession Frequency (Hz) of a Specific Chemical Group
ν_{TMS}	Tetramethylsilane Precession Frequency (^{1}H NMR Internal Standard)
ρ	Density
τ	Torque Moment
τ_{ci}	Correlation Time Modulating the Dipole-Dipole Paramagnetic Longitudinal (i = 1) or Transversal (i = 2) Relaxation Contribution
τ_{ei}	Electron Longitudinal (i = 1) or Transversal (i = 2) Relaxation Time
τ_i	The Time Between Pulses During an NMR Pulse Sequence
τ_{ie}	Zero Field Splitting (ZFS) Longitudinal (i = 1) or Transversal (i = 2) Relaxation Time
τ_m	Half-Life of the Ions-Water Bounds
τ_o	Rotation-Diffusion Correlation Time (BPP)
τ_r	Rotational Corrlation Rime modulating the Dipole-Dipole Contribution to the Inner-Sphere Relaxation Rate
τ_v	Correlation Time for the Modulation of the Zero Field Splitting (ZFS)
Φ_{B}	Magnetic Flux Density Associated to Magnetic Field B
χ^2	Chi-Squared
ω_I	Proton Spin Larmor Frequency (rad s^{-1})
ω_L	Larmor Frequency (rad s^{-1})
ω_p	Precession Frequency (rad s^{-1})
ω_S	Electron Spin Larmor Frequency (rad s^{-1})
$(1/\tau_{1e})^{ZFS}$	Zero Field Splitting (ZFS) Contribution to Relaxation Rate
%vol	Alcoholic Strength by Volume

Literary Review

1. General Introduction

During the last decades, it has been observed an increasing attention in the regard of foodstuff quality and composition this includes the assessment of alimentary characteristics, such as nutritional parameters, shelf life and healthiness. Together with the public interest, the producers themselves start to understand the economic benefits linked the authenticity of some specific products and the increasing in number of economically motivated adulterations (EMA), also known as food frauds, can have strong impacts on human health and/or on the specific markets (Everstine et al. 2013). According to the U.S. Food and Drug Administration (FDA) an aliment can be defined as adulterated when *"any valuable constituent has been in whole or in part omitted (…) or if any substance has been substituted wholly or in part (…) or if any substance has been added thereto (…) so as to increase its bulk or weight, or reduce its quality or strength, or make it appear better or greater value than it is"* (U.S. Food and Drugs Administration 2010). To increase the traceability and to grant the particular food and beverage characteristics, the European Union Countries developed restrictions and regulations per each specific sector through creation of certification bodies or, Protected Designation of Origin (PDO). Denominação de Origem Controlada (DOC) in Portugal, denominazione di origine controllata and denominazione di origine controllata e garantita (DOC and DOCG) in Italy, appellation d'origine controllée (AOC) in France and Switzerland and denominación de origen (DO) in Spain (Meloni and Swinnen 2013) are just examples.

The interest on "authenticity assessment" as a research field has increased over the last twenty-five years, and wine takes second place in terms of number of publications beaten only by grouped cereals, fruit and vegetables (Danezis et al. 2016). The high added value of some wine Designations of Origin induces the undesirable effect to make economically interesting the use of not certified grapes and wines, to mislead consumers, producing products under fake mentions. It is not rare to read about this type of fraudulent actions: for instance, during 2009 about two millions of litres of high quality level wine (Brunello di Montalcino DOCG) have been downgraded in Tuscany (IT) due to blending with non-authorized grapes (Asimov 2009). A similar case was found in France, where a producer was discovered to relabel imported wines under the Bordeaux Appellation (Paris 2002). Even if these types of frauds do not affect directly on human health, the negative impact of single cases on consumers perception could cause huge economic repercussions on the producing territories (Holmberg 2010). Together with mislabelling, the main fraud case involves chaptalisation or, the adding in exogenous

sugar with the intent of increasing the alcoholic potential of wines, and the dilution with water to both decrease the alcoholic potential increasing production. The last two fraud examples are better legally defined as adulterations. To give an idea about the number of fraudulent wines on market, in 2002 the Landesuntersuchungsamt (LUA) started an investigation on more than 6000 Germans and non-German wine labels. The investigation continued until 2008 and around 4% of wines were found to contain illegally added water or other substances, or to be produced starting from not-authorized grapes (Holmberg 2010). The need for well-developed and discussed analytical procedures to detect such adulterations and consumer frauds is obvious and essential to maintain or even increase the purchaser confidence on PDO. In the following section, an introduction on fraud detection through the isotopic ratio analysis is given both to follow chronologically the research and because of the current interest on this topic. After that, the main wine variability in terms of chemical composition will be briefly treated in order to find possible information linkable to wine variety, geographical origin and/or vintage. These are in some extent coded into analytical patterns which can be extracted throw the application of spectral analysis: the most recent developments in ^{1}H NMR spectroscopy (Godelmann et al. 2013; Godelmann et al. 2016) are example on how to increase the investigation on this analytical tool is of extreme interest.

1.1. Objectives

The aim of this work is to assess the possible application of proton relaxometry on wine, namely, to find common grouping characteristics to provide in some extent a link to their vintage and/or variety. Before achieving reliable results, the physical-chemical wine properties must be tested against the relaxometry profiles. Bibliographic datasets were attempted to provide the main information for topic comprehension, identifying the sources of wine compositional variability and how these can be expressed in terms of the belonging categories. Since all the environmental and technological conditions which vineyard and wine are subjected are rarely known, different compositional variability sources were inspected. Great importance was given to wine isotopic composition because of the importance it has had in food frauds detection history. Also, the environmental conditions during each vintage and their interaction with plants genotype were set as responsible for compositional differences and are proposed as a modern technique for the wine “a priori” characterization. The document is organized in two sections: the first starts introducing the main developments on wine authenticity and then a description of relaxometry models and NMR theory provides instrument for a better comprehension of the experimental part; the second is organized as a paper draft version.

2. Evaluating Wine Authenticity: How to Study Isotopic Profiling Helps Fraud and Mislabelling Detection

In the 1982 the physical organic chemistry laboratory of the Nantes Science Faculty started developing an analytical protocol to determine the origin of natural alcohols by the relative deuterium content (Martin et al. 1982); eight years later, it became the first official method to be adopted by the European Commission (EC) (Christoph et al. 2015). Hydrogen, together with oxygen and carbon isotope fractionation process, has been under studies for years: the goal was to find a reasonable pattern to recognize wine provenance in terms of geographical origin, vintage, variety and adopted technologies. The technique to experimentally determine the deuterium relative intermolecular isotope concentration is called site-specific natural isotopic fractionation-nuclear magnetic resonance (SNIF-NMR) and it represents only one example of stable isotope ratio analysis (SIRA). More recently, the strontium (Sr) isotopic ratio has been considered as a suitable marker in wine geographic origin characterization (Martins et al. 2014; Kaya et al. 2017). Nowadays, thanks also to instrumental and analytical strategy innovations, new approaches are under study as the rare-earth elements (REE) profile (Catarino et al. 2011; Catarino et al. 2018) and/or the ^{1}H NMR spectroscopy (Godelmann et al. 2013; Godelmann et al. 2016).

2.1. The Isotopes

The Rutherford-Bohr model describes the atoms structure: these are composed in a central nucleus formed by nucleons, or protons and neutrons, around which electrons orbit. Both electrons and protons possess an electric charge almost equal in intensity but opposite in sign while neutrons, as the name suggests, do not possess any electric property (Halliday et al. 2013a). Following the Dmitrij Ivanovic Mendeleev elements classification, these can be grouped and sorted according to the atomic number (Z), or the quantity of protons which are present inside the nucleus. When an element's Z term corresponds to the number of electrons in orbit around the nucleus, the atom does not have a net electric charge; contrary, when one of these two values exceeds the other, the atom is referred to as ion (Shriver et al. 2014). The second index which is used as a discriminator is the mass number (A): this value corresponds to the summation between protons and neutrons quantities. Generally, elements exist in nature in different isotopic form each of which possesses the same number of protons but different of neutrons. Consequently, any isotope can be identified thanks to both the A and Z value (Shriver et al. 2014). Let us take as example the simplest atom: hydrogen is tenth for abundance on Earth but in biological sciences it assumes great importance as it is a crucial component in

most of the organic molecules. In nature, it is possible to find H atoms under two different isotopic forms: ^{1}H simply called hydrogen, or protium, and ^{2}H (or D) which takes the name deuterium.

2.2. The Isotopic Ratio

The ones shown in Table 1 are standard IUPAC reference values (Meija et al. 2016); the indicated ranges have been obtained during several investigation on different types of samples (food, inorganic matter, …). Therefore, we define a standard value called Natural Abundance (Eq. 1) (NA), which represents the ratio (in percentage) between the environmental concentration of a given isotope and its total abundance in nature (Schmidt 2003):

$$\mathrm{NA}\ (\%) = \frac{{}^{A}X_j}{\sum_{j=1}^{n}\left[{}^{A}X_j\right]} \cdot 100 \qquad (1)$$

When classifying specific samples' isotopic content, it is mandatory to observe the "deviation (δ) relative to international standard" (Eq. 2, Christoph et al. 2015, Schmidt 2003):

$$R = \frac{{}^{m}\mathrm{X}}{{}^{n}\mathrm{X}} \qquad \delta\ (‰) = \frac{R_{Sample} - R_{Standard}}{R_{Standard}} \cdot 1000 = \left(\frac{R_{Sample}}{R_{Standard}} - 1\right) \cdot 1000 \qquad (2)$$

where n is the mass number of the heavier isotope and m is the mass of another isotope of the X element, respectively considered in nature or into the sample.

To give an idea about the magnitude of the standard values, the $R_{Standard}$ for hydrogen is equal to $1.5576 \cdot 10^{-4}$. The two mainly studied deviations are the deuterium (δD) and ^{18}oxygen ($\delta^{18}O$) ones: these are evaluated in terms of deviation from the VSMOW (Vienna Standard Mean Ocean Water) standard values (Christoph et al. 2015; Craig 1961).

Table 1. Isotopes of interest for wine traceability and authenticity assessment: atomic and mass number and their abundance in nature (Haynes et al. 2016; Meija et al. 2016).

Symbol	Atomic Number (Z)	Mass Number (A)	Range of Natural Variation (at.%)	**Representative Isotope Composition** (at.%)
^{1}H	1	1	[99.972, 99.999]	99.9885
^{2}H	1	2	[0.001, 0.028]	0.0115
^{10}B	5	10	[18.9, 20.4]	19.82
^{11}B	5	11	[79.6, 81.1]	80.18
^{12}C	6	12	[98.84, 99.04]	98.93
^{13}C	6	13	[0.96, 1.16]	1.07
^{16}O	8	16	[99.738, 99.776]	99.757
^{18}O	8	18	[0.187, 0.222]	0.205
^{86}Sr	38	86	[9.75, 9.99]	9.86
^{87}Sr	38	87	[6.94, 7.14]	7
^{204}Pb	82	204	[1.04, 1.65]	1.04
^{206}Pb	82	206	[20.84, 27.48]	24.1
^{207}Pb	82	207	[17.62, 23.65]	22.1
^{208}Pb	82	208	[51.28, 56.21]	52.4

2.3. Stable Isotope Fractionation Process

The main isotopic abundance ratios considered, still in course of study in the anti-fraud field, are $^{2}H/^{1}H$ (also referred to as D/H), $^{13}C/^{12}C$, $^{18}O/^{16}O$ and $^{87}Sr/^{86}Sr$. If these values were constant over the entire Earth's surface, and/or within each type of analysed matrix, it would not be possible to use them as discriminating factors attempting to distinguish between samples. Luckily, in nature exists a process called "stable isotope fractionation" which causes alteration in the distribution of isotopes both within biomolecules and vegetable water (Christoph et al. 2015). It is possible to distinguish between two main sources of isotopic fractionation: biotic and abiotic. Analysing these phenomena in detail, it is possible to understand the sources of variability which affecting samples according to specific categorical variables (e.g. geographic origin).

2.3.1. Abiotic Fractionation

The evapotranspiration activity is capable itself to alter the isotopic distribution (D/H and $^{18}O/^{16}O$) in vegetal water samples with respect to the values found in the soil (Dunbar 1982); this directly affects the relative and absolute concentration of isotopes within juices deriving

from different fruits and therefore, in products obtained after their fermentation (e.g. wine). The accumulation of the ^{18}O isotope inside of the leaves has been positively correlated to the combined effect of the increase of both relative humidity and air temperature (Dongmann et al. 1974). In this case, the greater volatility of lighter and smaller atoms composing water molecules explains the phenomenon (Christoph et al. 2015). Consequently, to disadvantage the conditions for stomatal transpiration and water evaporation causes an increase in the concentration of the heavier isotopes: the higher volatility of lighter oxygen isotopes leads the heavier isotopes to concentrate in all water sources (Gill et al. 2007); a vintage and/or geographical origin effect follows, and it could be studied through the samples differences in the δ (Eq. 2) values (Breas et al. 1994). The D/H and $^{18}O/^{16}O$ ratios in the rainfall water are not constant: in fact, these vary according to (Craig 1961; Christoph et al. 2015):

- **Latitude and altitude -** Lower presence in heavier isotopes are shown at higher latitude due to greater precipitation rate;
- **Continental effect -** A decrease in the presence of heavy isotopes is shown to the extent that it moves away from coastal areas;
- **Temperature -** Concentration effect due to greater volatility of lighter isotopes.

Therefore, both the D/H and $^{18}O/^{16}O$ ratios partially code for samples' geographical origin (Craig 1961). In any case, it is important to pay attention to meteorological data in order to justify anomalies in the isotopic ratios during musts and wines analysis: in fact, in case of rainfall during the last grape maturation phase, an important dilution effect on deuterium concentration have been reported by Dunbar (1982).

2.3.2 Biotic Fractionation

The isotopic concentration within plant products (e.g. wine) is not predetermined solely by their natural distribution, and therefore by abiotic fractionation, but also depends on plant-environment interactions. Biotic fractionation refers to the physiological processes, including biosynthetic pathways, that cause an alteration of isotopic abundance within plant tissues and/or between plant and environment. According to Schmidt (2003) the redistribution processes are regulated by thermodynamic or enzymatic kinetic laws which in turn represents the genotypic and phenotypic expression of plants (interaction between plant and environment). Therefore, pH, temperature and metal ions concentration affect the fractionation intensity (O'Leary 1978). In general, during the photosynthetic pathway, the plants discriminate in favour of lighter isotopes (Bender 1971) even if C3 and C4 plants show different behaviour

in this sense (Martin et al. 1991). The main difference in these two vegetal classes lies in the photosynthetic pathway, or in the CO_2 fixation, and leads to different biotic fractionation intensity. The greater efficiency of the C4 pathway causes a reduction of the $^{13}C/^{12}C$ ratio in favour of higher ^{13}C concentration and, therefore, by comparing this parameter to the one of other plant type, it is possible to distinguish the origin of sugar molecules (Martin et al. 1991). In addition, it has been observed a discrimination factor in the CO_2 diffusion into liquid phase (Farquhar et al. 1982) which varies in turn by the different plant reactions (stomatal conductance) under water stress condition (Tramontini et al. 2013). Other biological fractionation effects on carbon isotopic ratio are discussed by Tcherkez et al. (2011). Regarding the D/H and $^{18}O/^{16}O$ values, no interesting biological fractionation have been reported at vegetal tissues level; the heavy isotope concentration is therefore related, as previously discussed, mainly to the evapotranspiration requirement and to the distribution within the environmental water.

Finally, the fractionation phenomena can be studied as a global phenomenon (infra-molecular natural fractionation) or more localized (site specific natural isotopic fractionation) (Christoph et al. 2015). The possibility to localize within the biosynthetic and/or catalytic pathway the elements origin, more precisely hydrogen isotopes which constitute specific ethanol chemical groups, led to the development of the first analytical method recognized by the European Union (EU) for must chaptalization identification (Martin et al. 1983).

2.4. Isotopes as Chemical Markers for Wine Fraud Assessment

The fermentation process does not seem to significantly affect the D/H and $^{18}O/^{16}O$ ratios in pre- and post-fermentation samples. Equation 3 quantifies the changes in water hydrogen isotopic ratio:

$$\Delta(D/H)_W^{QS}=(D/H)_W^{Q} - (D/H)_W^{S} \quad (3)$$

where, $(D/H)_W^{S}$ and $(D/H)_W^{Q}$ are respectively the water deuterium isotopic ration before and after the fermentation; $\Delta(D/H)_W^{QS}$ value was find to be directly correlated, through a first degree relation, with the must starting fermentable sugar content (Martin et al. 1991). Contrary, the yeast fermentation does not seem to directly affect the oxygen isotope concentrations.

As previously mentioned, it was developed an analytical procedure for specific chemical groups isotopic inspection which allows to discriminate solutions depending on the glucides plant origin (C3 vs. C4 plants).

Table 2. Variations in the deuterium abundance ratio sample of ethanol obtained from the fermentation of different substrates (Martin et al. 1982). $(D/H)_I$ and $(D/H)_{II}$ respectively identify the hydrogen isotopic ratios on the methyl and methylene groups. Values for grapes have been extrapolated "Compendium of international methods of wine and must analysis" (OIV 2019b). In some cases, standard deviation values were not available.

	Grape[a]	Corn	Sugar Cane	Wheat[a]	Potato	Sugar Beet	Apple[a]
$(D/H)_I$	**102.2**	111.6 ± 2	111.2 ± 2.5	103.5	97.3 ± 4	94.1 ± 2	100.9
$(D/H)_{II}$	**129.7**	123.9 ± 2	127.8 ± 2.5	128.3	131.8 ± 4	128.0 ± 2	129.7

[a] Standard deviation values not available.

The technology is called site specific natural isotope fractionation – NMR (SNIF-NMR) and, in some cases, its application made it possible to detect fraudulent wine chaptalisation. The discrimination is made according to the $(D/H)_I$ value (Tab. 2), inspecting the hydrogen isotopic ration on the ethanol's methyl and methylene chemical groups. Since the concentration of deuterium in wine samples is strongly influenced both by the area of production origin and by local rainfalls (Craig 1961; Dunbar 1982), not all the results were clearly justifiable; in case of controversies, it is possible to implement the method investigating also the $\delta^{13}C$ value. The $^{18}O/^{16}O$ ratio analysis in wine water (Dunbar 1982) showed to be directly correlated to the ^{18}O natural abundance. Since almost of vine and wine oxygen derives by the water absorbed through vine roots during productive cycle (Schmidt 2003), the information carried by this atom could code in some extent for geographical origin and vintage during samples discrimination (Breas et al. 1994). There would seem to be no "coded" information by the carbon isotopic ratio (Breas et al. 1994) since, even if used during archaeological studies for dating the organic remains, the readings range of error is between 50 and 100 years (Diamond 2005; Gill et al. 2007).

More recent studies have demonstrated the possibility to geolocate wine samples depending on their strontium isotopic abundance and strontium isotopic ratio ($^{87}Sr/^{86}Sr$). This element possesses four natural isotopes (Tab. 1). In this case, the discrimination between wine samples is possible due to fractionation phenomena absence during radical absorption, xylem translocation, and plant metabolism (Petrini et al. 2015). This, together with the fact that fractionation does not occur during strontium dissolution from soil's mother rock (English et al. 2001), means that isotopic distribution within plant tissues it is not only representative of that the circulating solution one (Petrini et al. 2015) but, it can be associated to the soil of origin composition (English et al. 2001). According to the same authors, the soil strontium

composition does not solely depend on the mother rock but also on the rubidium (Rb) concentration at its formation. In addition, in some areas, the atmospheric sand is able to give a four-time greater contribution in comparison to the last two mentioned;Therefore, the $R_{Standard}$ (Eq. 2) must be continuously maintained up to date depending on local weather patterns.

What the relationship depends on $^{87}Sr/^{86}Sr$ and why is it a good indicator of geographical origin? The formation of strontium 87 isotope is a radioactive decay consequence of another element: rubidium (Rb). The speed at which occurs depends solely on the ^{87}Rb half-life and consequently, both $^{87}Rb/^{87}Sr$ and $^{87}Sr/^{86}Sr$ values are proportional to the age of rocks (Faure and Powell 1972).

Some noteworthy developments showed how the strontium isotopic ratio to be a reliable tool for the traceability of Portuguese DO wines, where soils were developed on different geological formations (Martins et al. 2014). Since Strontium can to replace Calcium (Ca) during igneous rocks formation while, Rb replaces Potassium (K) in the silicate rocks (such as mica rock and potassium feldspar) formation (Faure and Powell 1972), to observe the distribution of such elements, together with the $^{87}Rb/^{87}Sr$ and $^{87}Sr/^{86}Sr$ ratios, increases the chances to predict the wines' geographical origin. The National R&D Institute for Cryogenics and Isotopic Technologies (ICSI) in Vilcea (RO) (Geană et al. 2017) has managed to classify, with 100% of success, the geographical origin of 21 red wines with denomination of origin (PDO) or geographical indication (GI). The developed method combines the Sr isotopic ratio quantification and Ca/Rb ratio determination to other elements quantitation (e.g. Gallium, Sr, Aluminium). More recently, the $^{204}Pb/^{206}Pb$, $^{208}Pb/^{206}Pb$, $^{207}Pb/^{206}Pb$ ratios demonstrated their utility in wine sample discrimination according to geographical origin in Romania (Bora et al. 2018). It must be stated that the Pb isotopic composition in wine can be modified in some extent by the presence of atmospheric lead which depending on the local leaded-gasoline use (Medina et al. 2010): the heavy metal contamination problem is decresed after the removal of this type of fuel from market. Anyway, further investigation regarding the technological treatment effect on metals isotopic ratio have been carried out (Kaya et al. 2017; Moreira et al. 2017) confirming what was discovered before from Martins et al. (2014): depending on the vines growing country, the strontium isotopic ration can be used to geographically discriminate the wine producing area.

In conclusion, the research has demonstrated how to inspect the information coding for wines geographical origin in the boron isotopic ratio ($^{11}B/^{10}B$) permits a discrimination whether they are produced in different countries (Coetzee & Vanhaecke 2005) or within the same borders (Vorster et al. 2010).

2.5. Uncertainty Sources

As highlighted in the previous paragraphs, each isotopic ratio encodes one or more categorical variables; therefore, their magnitude variation is to some extent a function of:

- Genotype or, varietal phenotypic expression;
- Vintage;
- Geographical origin.

However, it is not possible to limit the observations to these parameters as they can be altered by unpredictable external factors: still to be evaluated their variation during bottle aging or as a consequence of direct contact with polluting material. What would happen during a dry vintage to the $^{18}O/^{16}O$ values in case of irrigation? As for the $^{87}Sr/^{86}Sr$ ratio, there may exist producing areas with common geological origin. One of the solutions lies from the possibility to inspect multiple markers (Vorster et al. 2010). The Increasing in the number of identified markers leads to higher robustness during statistical analysis. If only a few markers are chosen to characterize a specific mention/area, some of the analysed wines could result associable to several geographic groups making the analytical technique inadequate for mislabelling detection. The increasing in the number of markers will reduce the groups dimensionalities since increases the number discriminant factors. The capability of isotopic ratio to discriminate variety and vintage has been proven by Dinca et al. (2015) but, to discuss relations between sample discrimination and the date of rainfall event more hydrogeological and environmental data are needed.

If the goal is to combat mislabelling, it is necessary to increase the amount of information linkable to the listed above categories (Ogrinc et al. 2001); there are many official analytical techniques which allow to investigate the wine chemical composition (OIV 2019a,b) but, since it is unthinkable to develop a model that includes them all, it is necessary to inspect the application of advanced spectroscopic analytical techniques, such as the ones associated to: proton nuclear magnetic resonance (^{1}H NMR), ultraviolet (Uv), visible (Vis), near infrared (NIR), medium infrared (MIR) and/or Raman. Through the information amount increasing, it would be possible to create chemical fingerprint which, as for human DNA, will univocally code per each categorical variable. As shown by (Geană et al. 2017), it is essential to determine where these information are coded to create models and, because of that, the combination of chemometrics, bioinformatic and Geographic Information System (GIS) data, is essential to integrate and translate analytical data (Danezis et al. 2016).

In 1993 the European Commission created a wine databank with the purpose to collect isotopic ($^{13}C/^{12}C$, $^{18}O/^{16}O$, $^{2}H/^{1}H$) values to be used in alcohol, sugar and water addition detection. Contemporary, the association of each determination to the specific geographical origin will make it possible to observe the average differences between specific mentions and assess the labels' correctness.

3. Wine Chemical Composition as an Information Source for Its Traceability

This paragraph is intended to give a general overview about wine chemical species of interest to underline possible sources of varietal, geographical origin, and vintage information. The main division lies between inorganic and organic chemical species.

3.1. Mineral Elements

The main inorganic compound in terms of concentration in wine is the water which, as widely discussed in Paragraph 2, can convey interesting information regarding geographical origin and vintage during its isotopic ratio investigations. Wine geographical origin assessment through the mineral element analysis is one of the main topics regarding foodstuff mislabelling detection: Geană et al. (2017) provided interesting observations about wine samples discrimination according to their elemental composition. In these terms, significant differences were found in the concentration of Ca, Ga, Sr, Al and in the Ca/Sr ratio according to different specific production areas; it means that these elements are to some extent predictive of wine geographical origin or, their variation could partially code for that. However, the possibility to observe changes in Ca, Al and Ga profile during must to wine transformation should be considered. In fact, during the vinification process, these elements are subject to fluctuations whose intensity is often unpredictable: Ca concentration varies as a consequence of calcium tartrate insolubility and consequently, precipitation can occur during both vinification and wine storage. The other two are part of a larger group of contaminant element which concentration is strongly affected by sulphur dioxide addition and/or by oenological practices such as bentonite fining and filtration (Catarino et al. 2008a,b; Redan et al. 2019). Still the different rootstocks absorption rate with respect to the individual elements, also according on the pluviometric trend and their assimilability, need to be registered. In addition, some technological treatment, as destemming (Cheng and Liang 2012), can affect the must/wine mineral composition: this has been demonstrated after a 90 days of aging with staves addition (Kaya et al. 2017) for Sr, manganese (Mg), nickel (Ni), cobalt (Co) and vanadium (V). To study how technological treatment could influence the multi-elemental composition during the wine vinification process is a key-point in the identification of possible elemental fingerprinting to assess wine geographical origin: in fact, it is not possible in all the cases to assume the direct correlation between soil mineral composition and wine elemental profile (Catarino et al. 2008b). In addition, different behaviour in rootstocks capability to absorb water and mineral has been explained (Marguerit et al. 2012) to be in some extent, genetically controlled; this

creates another variability source during wine sample classification and a varietal per vintage per rootstock interaction effect.

Despite these concerns, studies developed by Catarino et al. (2011; 2018) demonstrate that rare-earth elements (REE) should be considered: in fact, their chemical similarity and the absence in biotic and abiotic fractionation processes both during rootstock absorption and vinification make these elements interesting targets in wine geographic characterization. The soil/must/wine system change affects mainly the REE total content as is it clear in Figure 1 where their concentration pattern seems in most cases to follow the soil one. It is interesting to stress the similarity between both the B and C patterns, whether we consider soil or wine samples, because these two productions arise from the same region (Óbidos).

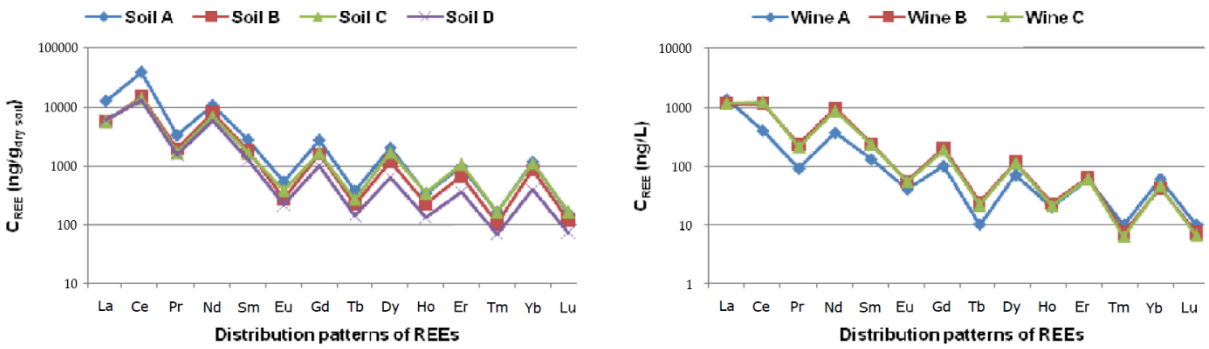

Figure 1. Chondrite normalised REE concentration (CREE) in soil (ng $g^{-1}_{dry\ soil}$) and corresponding wines (ng L^{-1}) (Catarino et al. 2011). Wine and related soils of origin are indicated using the same colours: wine A and wine B share the same pattern and "Denominação de Origem" (Óbidos D.O.P.). Soils A (Dão region) and B (Palmela region) show different composition patterns; wine A differs from wines B and C in the lighter REE concentrations.

Though in this case the correlation soil-wine composition in terms of rare-earth elements is around 0.9, it must be stressed the must and wine fining agents, as bentonite and other silica derivates, large influence on REE profiles (Rossano et al. 2007). These adjuvants are largely used to prevent protein casse in white wines and therefore, for now the applicability of this elemental fingerprinting should be limited on red wines.

3.2. Organic Compounds

The main classes of wine organic molecules are: Organic acids, Nitrogen compounds (amino acids, peptides and proteins), Polyphenols, Lipids, Carbohydrates and Aromas (terpenes, norisoprenoids, thiols and esters) (Ribéreau-Gayon et al. 2006). Many are the external and genetical influences on their concentration, absolute and/or relative. Therefore, knowing the sources of this variability is essential to use them as chemical fingerprints (Danezis et al. 2016).

3.2.1. Phenols

This category includes two subgroups that respectively take the name of "Flavonoids" and "non-Flavonoids" (Ribéreau-Gayon et al. 2006c). This paragraph purpose is not to treat all the facets and possible evolutions during wine aging but to underline internal and external elements that contribute to their variability.

3.2.1.1. Flavonoids

The term "flavonoid" groups different phenolic categories, including flavan-3-ols, flavonols and anthocyanidin-3-o-glucosides: these can be found into the berry, mainly concentrated in the skin layers, and their variation is mainly result of the genome-environment interaction. Expression changes of the biosynthetic pathway have been reported by Castellarin et al. (2007): following water stress situations, an increase in expression of genes which encode for enzymes asserting to the anthocyanin pathway is shown; according to the same author, as a result of a greater exposure of the berries to sunlight, an increase in the synthesis rate of flavonols, as biomolecules produced to protect from excessive Uv irradiation, has been proven. The same direct radiation alters the anthocyanin profile (relative concentrations) which, although strongly dependent on variety (Jin et al. 2009), seems to be subject to changes during limiting environmental conditions. Flavonoids content in wine is also function of technological treatment during grape processing, just think to the *"blanc de noir"* vinification, or the different maceration technologies (Sacchi et al. 2005) for white and red wines.

The term anthocyanins refers to a class of pigments found in many plant species within flowers, leaves and fruits. Their colours vary, depending on oxidation level and the pH of the medium within which they are dissolved, from red to blue (Ribéreau-Gayon et al. 2006c). The anthocyanins absolute and relative contents in grapes depends mainly on cultivar (Bautista-Ortín et al. 2016), training system, maturity, and vintage (Canals et al. 2005).

Flavan-3-ols are another class of compounds present in grapes and wine; these are organized into polymeric structures of concatenated sub-units, called proanthocyanins (PAC), whose mean degree of polymerization (mDP) into berries skin cells varies as a result of environmental trends and vineyard management (Ribéreau-Gayon et al. 2006c). Flavanol polymerization with other molecules, including anthocyanins, causes many compounds to originate and, the so occurring reaction products are mainly studied according to their size and colouring characteristics (Ribéreau-Gayon et al. 2006c). In addition, from the polymerization between anthocyanins and carbonyl (ethanal, pyruvic acid, …) molecules, which originates mainly

during fermentation, vitisins arise (Romano et al. 1994). This latter, together with pinotins, flavanyl-pyranoanthocyanins, portisins and pyranoanthocyanins' dimers, belong to the pyranoanthocyanins chemical group or a class of coloured compounds which are interesting because of their chemical stability. Since pyranoanthocyanins arise from chemical reactions occurring the whole wine vinification and aging process, their concentration is lower than the anthocyanins one. Quaglieri et al. (2017) observed lower pH and higher oxygenation to be responsible for higher chemical synthesis rate. In fact, oxygen is a key constituent since it causes the ethanol chemical oxidation to ethanal.

The possibility to technologically manage the flavonoid composition, in terms of concentration and mDP, has been largely discussed and represents one of the main wine research topics (Canals et al. 2005; Bosso et al. 2009; Lerno et al. 2015; Smith et al. 2015). From the previous statements it is possible to gather useful information for sample characterization according to variety, geographical origin and vintage: all these compounds are subject to variations strictly connected to vine genotype, and genes regulation depends on environmental conditions. This, together with vinification vineyard management and wine aging practices, explains itself the complexity in connecting categorical information to few chemical absolute and relative concentrations (Pereira et al. 2006). However, it is still noticeable how these data convey information that encode the environmental characteristics linked to vintage and wine production area. In conclusion, since the varietal compositional variability of flavonoids still remain to be completely discovered, the role of pyranoanthocyanins in colour stabilization (Berrueta et al. 2020) and, in some cases, enhancement (He et al. 2012) needs in more detailed explanations. pyranoanthocyanin dimers have been proven to cooperate to wine colour causing a bathochromic shift to blue tonalities (680-730 nm), this molecular class assumes major role during specific fortified wines aging (Oliveira et al. 2010) and could be cautiously used to detect mislabelling in really hold vintage Port wines.

3.2.1.2. Non-Flavonoids

Non-flavonoids are divided into three main groups: gallotannins and ellagitannins, phenolic acids and stilbenes. The formers are polymers of different shapes and sizes which are extracted by the contact between wine and wood; they consist in gallic and ellagic acid subunits which concentration in wine mainly depends on the type of wood and contact time (Ribéreau-Gayon et a. 2006c). They can therefore be considered as possible indicators of the process/refinement/aging that characterize certain denominations more than others. Phenolic acids, on the other hand, are highly concentrated within the berry; these are mainly present in the form of hydroxycinnamoyl tartaric acids (HCTA) even if during vinification are also released

through tartaric acid hydrolysis. Coumaric, caffeic, ferulic and gallic acid are the ones known until now; their concentration seems to be affected by varietal components but not by weather changes (Ferrandino et al.2012; Šuklje et al. 2012).

Finally, stilbenes are a very important class for the food industry as they are designed and used as food additives for their high antioxidant activity. Their concentration may vary depending on the weather (vintage), altitude, but is also strongly influenced by the genetic component (variety) (Bavaresco et al. 2007).

3.2.2. Organic Acids

The main organic acids in wine generally come from four sources: grapes, yeasts, lactic and/or acetic bacteria physiological activity and intentionally added (Ribéreau-Gayon et al. 2006a). As for the addition of exogenous acids, little has to do with this discussion purpose; however, it is important to be aware about all treatments at which wine has been subjected since, the use of additives can reduce the quantity of categorical coded information because of compositional changes. The most important are tartaric, malic, lactic and acetic acids, to which others are added whose concentration mainly depends on the fermentative course (Ribéreau-Gayon et al. 2006a). Tartaric and malic acids are synthesized during the vegetative phase of berry development; these accumulate until veraison. During berry maturation, malic acid is used as a carbon source instead of glucose: depending on temperature, its concentration decreases due to cellular respiration (Pereira et al. 2006); during some vinifications, mainly the red wine ones, its transformation into lactic acid by lactic bacteria is required (Ribéreau-Gayon et al. 2006a); in addition, it is possible to achieve similar results thank to the use of particular yeast strains such as Schizosaccharomyces pombe (Sousa et al. 1991; Loira et al. 2018). In order to increase the malic to lactic acid conversion manageability, these two techniques can be substituted directly adding the malolactic enzyme to the wines or by the use of specific membranes as sustain (Formisyn et al. 1997; Maicas 2001).

3.2.3. Nitrogenous Substances

Protein and peptide concentrations in the wine greatly differs comparing white to red wines but, also varietal differences are shown (Pocock et al. 2000): in fact, tanning compounds present in the latter precipitate the majority of proteins before bottling (Ribéreau-Gayon et al. 2006b). Concentration also varies as a consequence of bentonite treatments (Waters et al. 2005). Pereira et al. (2006) has demonstrated the effect of different bunches exposures

(microclimates) on histidine, γ-aminobutyric acid (GABA), alanine, and arginine concentration; this proof how the environmental conditions affects amino acid wine profile. Pathogenesis related proteins (PR proteins) is an important protein class because of their technological role in white wines instability (Ferreira et al. 2001). As regards their relative concentration, wines obtained from different geographical areas, varieties and years showed non-dissimilar compositions (Ferreira et al. 2000). In conclusion, unlike the polypeptide composition, both the profile and the amino acid concentration can be important targets for wine fingerprinting. The tannins capability to interact with nitrogenous substances is responsible for the differences in white and red wine protein/amino acids content. Some of the latter compounds could remain in solution trapped into polyphenolic polymers making the nitrogenous chemical fraction dependent on flavonoid/non-flavonoid concentration and type.

4. New Approaches to Recognise Compositional Patterns: Metabolomics and Chemometrics

Metabolomics regroups both quantitative or qualitative analysis, depending on whether you work in targeted or non-targeted analysis, of the entire metabolome or a selected subset. Through spectroscopic analysis associated with specific chemometrics tools it is possible to identify patterns statistically correlated to specific sample. Comparing several wines compositions and spectra, it is possible to find the mains variability sources as the same as it had been shown for isotopic ratio (Danezis et al. 2016). According to Godelmann et al. (2013): *"The information on latent parameters such as grape variety, origin, and vintage is coded in multivariate patterns of multiple parameters in the NMR spectra rather coded in single spectrum markers"*. It means that three categorical variables of interest (variety, geographical origin and vintage) cannot be summarized by the variation of one or a few analytical parameters or, only the combination of a large number of information (multivariate patterns) is able to describe them. This phenomenon is called "synergistic effect" and can include isotopic data fusion (Monakhova et al. 2014).

Chemometrics is a particular branch of chemistry that studies how the application of mathematical and statistical models on analytical data can help in their interpretation; this proves very useful especially when the quantity of information exceeds by far the number of categorical variables under investigation. For this purpose, statistical tools, as principal component analysis (PCA), have been developed to allow the elimination of that part of the information that is not relevant (spurious information); it is possible to regroup such tools into three categories: exploratory analysis, classification analysis and regression analysis (Medina et al. 2019). During sample characterization in terms of geographical origin, vintage and/or variety, chemometrics tools are used to screen into analytical spectra in search of variability sources linked to these categorical variables. It is important to distinguish between two approaches that characterize one or the other statistical tool. A supervised approach is a process of organizing or describing data according to a predefined criterion; an example comes from the linear and multiple regression model: the least square criterion tries to minimize the difference between groups of variables from a regression function. Contrary, the opposite approach follows an unsupervised criterion: this requires data to be viewed in their entirety in search of an a priori (latent) criterion capable to regroup them into clusters. This type of approach must be associated to model validation procedures (Marini 2013).

4.1. Target vs. non-Target Analysis

Compositional analysis on wines and other food matrices can be carried in two different ways; note that one does not exclude the other and intermediate ways are possible. Profiling and fingerprinting are the two main strategies (Fan et al. 2018): the first refers to the application of targeted analysis or the determination of the absolute and/or relative concentration of specific chemical species; the second approach involves the application of spectroscopic strategies combined with multivariate statistical methods (chemometrics) without the needing in the sample composition identification. The second one allows to investigate information that would not be taken into account through targeted analysis making the latter a useful approach for investigations in food sector, especially if used in association with NMR spectroscopy (Christoph et al. 2015; Danezis et al. 2016; Fan et al. 2018; Godelmann et al. 2013). In support of this statement, it has been shown in detail by Godelmann et al. (2013) how to increase the information during exploratory analysis makes it possible to discriminate more effectively wine samples, according to variety and/or geographical origin.

4.2. Exploratory Analysis

The first step in chemometrics methods is the application of an unsupervised criterion in the clustering of datasets in analysis. As anticipated, the aim is to reduce the size, and therefore the complexity, of the set of numerical data. The main statistical tools used in this phase of the experimental model are hierarchical cluster analysis (HCA) and PCA (Medina et al. 2019). Agglomerative HCA works through a reiterated procedure:

- Identification of the two most similar objects which are the ones with the highest similarity degree;
- Creation of a cluster containing the two mentioned objects;
- Similarity comparison between the created cluster and all the other objects.

The PCA instead is one of the most used statistical tools in the mining of analytical data; this tool allows to reduce the number of information explaining most of the variability through the bilinear projection in two components (PCs), or latent variable, which result from the composition of the starting ones (Marini 2013). The two new components explain the highest variance levels and at the same time identify the variable responsible of sample clustering (Medina et al. 2019). The PCA has shown itself to be a useful tool facing data collinearity problem management during regression and discriminant analysis models realization (Næs et al. 2001). In model realization, collinearity means a direct correlation between the explaining

variables or, the variation one parameter is coded in some extent in another portion of the dataset itself: including two correlated variable in the same model means consider more than once a latent variable (Dowdy et al. 2004).

4.3. Classification or Discriminant Analysis

Classification procedures involve the use of statistical tools to associate samples to one or more classes defined *"a priori"* (supervised method) (Medina et al. 2019). Once the clusters have been identified, through exploratory chemometrics procedures, it is important to generate a method able to associate each sample to an exclusive class: this means identifying within the geometric space, generated starting from the analytical dataset, the areas asserting to the various clusters (Marini 2013). Partial least square discriminant analysis (PLS-DA) and linear discriminant analysis (LDA) are the two mainly used tools in foodstuff authentication and adulteration identification (Medina et al. 2019).

The first classification tool (LDA) works by comparing, within the space defined above, the distance of all values, one at a time, from the centroids of the *"a priori"* clusters through a linear combination of the starting variables. This method has two problems: first, the association to a cluster is forced even if there is no real connection; second, the statistical tool does not give good results if working with a few categorical variables against many continuous variables (Medina et al. 2019). One solution to the latter problem is to replace the initial variables with those selected through PCA (Melucci 2015). By the other hand, the use of PLS-DA is recommended because of the possibility to keep track on the variables forcing the classes differentiation (Granato et al. 2018).

In conclusion, some observation are needed: Rodionova et al. (2016) discussed about the discrimination method non eligibility in term of authenticity assessment: in fact PLS-DA and soft independent modelling by class analogy (SIMCA) are not able to correctly classify samples, or group of them, if the models are not implemented by default with their classes. It means that if the class is not defined *"a priori"* the sample will be wrongly associated to the less dissimilar class.

4.4. Regression Analysis

Partial least square regression (PLS-R) is the most used prediction model during foodstuff authentication (Medina et al. 2019): starting from a complete dataset, it generates a matrix of

predicted values to describe through an equation the separation between classes. The model goodness is expressed through the coefficient of determination (R^2) which varies between zero (no variability explanation) and one (total variability explanation, Dowdy et al. 2004). Model validation is required to prove the model data-generating process correspond to the natural real-data generating one or, in wine sample classification case, the statistical clustering corresponds to the real sample grouping; Leave-one-out cross validation (LOOCV) and k-fold cross-validation are just two possibilities (Medina et al. 2019). Another less common but equally interesting tool is the k-nearest neighbour (k-NN); in fact, it permits both classification of categorical variables and/or regression of continuous variables without relying on any reference distribution (Granato et al. 2018).

However, during the creation of models, one or more regressors (variables) can result each other's correlated: in this case data mining procedures (e.g. backward elimination, forward selection, stepwise regression) must be applied to overcome this problem (Dowdy et al. 2004). Collinearity is an issue that also affects classification analysis. In both cases the solution may lie in the manual decreasing in variable number by the selection of the largest ones (Næs et al. 2001). According to the same author, the use of principal component regression (PCR) makes it possible to overcome collinearity problems between variables and therefore, if the number of dependent variables far exceeds that of independent ones the least square regression (LSR) is preferable.

5. Nuclear Magnetic Resonance: A Tool to Deeply Inspect Molecular Dynamics

The growing interest in nuclear magnetic resonance (NMR) spectroscopic technology finds its reason in sample preparation simplicity, which reduces possibilities to incur in error, and in the high analytical methods reproducibility (Godelmann et al. 2016), which both are essential for analytical procedures to be implemented at legislative level (Tyagi et al. 2010). Generally, the NMR takes place in research field in obtaining high-resolution structural information on a wide range of chemical species (Danezis et al. 2016) but, through the application of specific mathematical algorithms (Fourier transform) it is also possible to extract compositional (spectral) information (Farrar et al. 1971a). Furthermore, it is possible to use NMR in association with separation techniques, as liquid chromatography (LC) or capillary electrophoresis (Košir et al. 2002), for the identification of new chemical species present within the wine or other complex alimentary matrix (Medina et al. 2019).

Magnetic resonance is a physical phenomenon that implies the capacity of atomic nuclei inserted within a static magnetic field ($\vec{B}_0$), in the case of ^{1}H NMR we refer to hydrogen, to acquire energy when subjected to an oscillating electromagnetic pulse. This phenomenon has important applications in the medical field through an imaging technique called magnetic resonance imaging (MRI). As far as the food sector is concerned, a distinction should be made between relaxometry and spectroscopy analytical techniques. To understand the nuclear magnetic resonance applicability, an introduction to mathematical handling of the resonance physical phenomenon is needed.

5.1. Angular Moment and Precession Motion

It is not possible to introduce the NMR analytical technique without giving some clear information about precession motion the main physical parameter which are involved in a rotating system. Referring to the Figure 2a, the angular moment (L) in a rotating body can be defined as the physical motion quantity which remains constant if the considered systems remains closed (Halliday et al. 2013b). In alternative can be seen as the rotational dynamics equivalent of linear momentum.

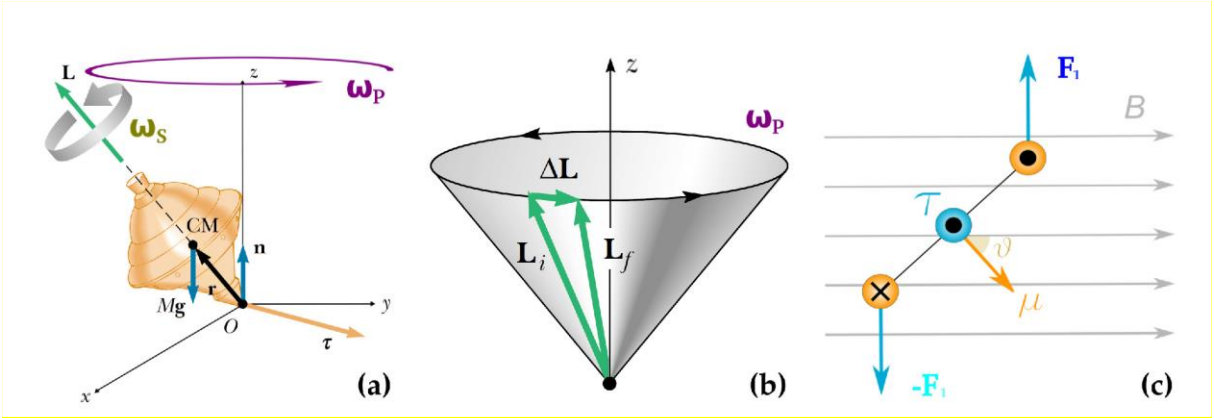

Figure 2. Figures a (Halliday et al. 2013b) and b summarise the spinning top motion while c (retrieved from https://upload.wikimedia.org/wikipedia/commons/7/7a/Momento_torcente_magnetico.svg) shows the couple of forces ($F_1, -F_1$) exerting a torsion (τ) on a particle possessing an intrinsic magnetic moment (μ) as a consequence of the external magnetic field (B).

Let us now consider the motion of a spinning top (2a): the term indicated as ω_p in Figure 2a,b represents the precession frequency (pulsation). It is defined as the time (t) necessary to the rotation axis to draw a perfect circumference or, the time needed to describe an angle equal to 2π. The torque moment τ arises from composition of vectors *Mg* and *r*. In the proposed spinning top model, the resulting ω_p is proportional to the applied *Mg* force and to the torque moment (τ) depending on the following expression:

$$\omega_p = \frac{\partial \varphi}{\partial t} = \frac{Mgr}{L} \qquad \tau = \frac{\partial \vec{L}}{\partial t} \qquad (4)$$

where $\partial\varphi$ refers to the angular variation of $\vec{L}$ on the xy plane while r is the vertical distance between Mg and n origins. At the same time, it is shown the relation between τ and the spinning top angular moment (L) (Halliday et al. 2013f).

5.2. Magnetic Moment

To introduce the NMR technology, it is good to clarify what magnetic moment represents: this physical quantity serves to quantify the force that a magnet exerts on an electrical current or, the torque (τ) that an external magnetic field ($\vec{B}_0$) exerts on a magnetic dipole (μ) (Halliday et al. 2013g). It is recognised for electrically charged particles as electrons and protons to possess an intrinsic magnetic moment other than zero. Even if neutrons are not recognised to be positively or negatively charged, the possibility to develop an intrinsic magnetic moment is explained by the quark model or, it arise from the magnetic moment vectorial composition of his elementary particles (quarks, Bertini et al. 2017).

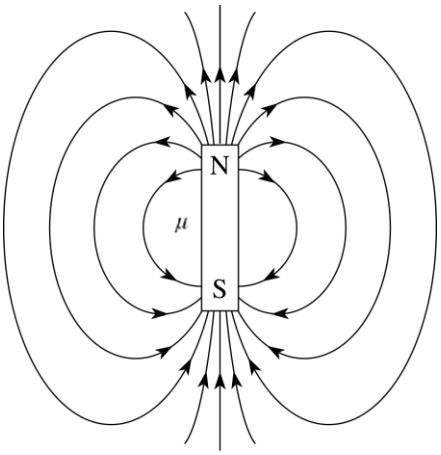

Figure 3. Vectorial representation of a magnetic dipole/moment μ characterized by north (N) and south (S) polarities. The graphic shows the force lines arising which density is proportional to the magnetic centre distance (image retrived from https://www.cleanpng.com/png-magnetic-field-magnetism-craft-magnets-field-line-650603/preview.html).

Another way to discuss a magnetic moment is to figure it as a magnetic dipole characterized by north (N) and south (S) polarities. In Equation 3 such magnetic field is represented through force lines whose direction is determined by the poles' orientation. By positioning inside a static magnetic field an object characterized by a not-null moment of magnetic dipole (Fig. 2c), it will be submitted to a pair of forces (F_1, $-\mathrm{F}_1$), parallels and equal in magnitude, which force the alignment of moment toward the static magnetic field. Since both forces exert at a distance ($\vec{r}$) from the centre pivot, as it happens for the spinning top model (Fig. 2a), they arise a couple of torque moment ($\vec{\tau}$) which direction, perpendicular to the external magnetic field ($\vec{\mathrm{B}}_0$), can be established by the right-hand rule.

$$\vec{\tau} = \vec{\tau}_1 + \vec{\tau}_2 \qquad \vec{\tau}_{1,2} = \pm \vec{\mathrm{F}}_1 \times \vec{r}_{1,2} \qquad (5)$$

Summing up, the application of a force at a certain distance from the point where it exerts generates a torsional moment perpendicular thereto; it results in a precession motion whose frequency ω_p is directly proportional to the applied forces themselves. Applying the same reasoning to a magnetizable particle (e.g. proton), the pair of forces that are generated induce a single twist which carries the magnetic moment associated with the dipole in a precession around the magnetic field ($\vec{\mathrm{B}}_0$) direction. Unlike the spinning top model, the graphical representation of all the force contribution to the torque is more complicated since it depends on the force lines number and density. Nevertheless, it is possible to express the resulting motion as a function of the external magnetic field and magnetic dipole intensities (Eq. 6).

$$\frac{\partial \vec{\mu}}{\partial t} = \gamma \vec{\mu} \times \vec{\mathrm{B}}_0 \quad (6)$$

In a purely conservative system, where all these vectors maintain their magnitude (thermodynamic stability), the first term of Equation 6 does not change during time or, the precession frequency can be assumed to be conserved. Only atoms possessing a nuclear quantum state (I) different from zero (non-null) are sensible to an external magnetic field presence since this quantity arises by the nucleons' (protons and neutrons) spin vectorial composition. According to rational mechanics the nuclear magnetic moment

$$\mu = I\gamma\frac{h}{2\pi} \quad (7)$$

is proportional to the nuclear quantum state, the gyromagnetic ratio (γ), i.e. the ratio between the magnetic moment and the angular moment of the considered particle, and the Planck constant (h).

We define Zeeman effect as the separation of the spectral lines in the presence of a magnetic field; this effect, related to nuclear orbitals, consists in the energy levels' separation of the orbitals: since the hydrogen (^{1}H) nuclei are composed of a single unpaired proton ($I = \pm 1/2$), it results in the formation of two energetic levels equal in magnitude but with opposite direction.

If one describes a sample containing only water molecules, considering the Zeeman effect exerted on hydrogen ions, it will be possible to divide their motion into two classes according to their direction (Fig. 4). We use angular velocity ω_p, or pulsation

$$\omega_p = \gamma \mathrm{B}_0 \quad (8)$$

to characterize their motion. Since each particle possesses a fixed gyromagnetic ratio (γ_p = 2.675221900(18)10^8 rad s^{-1} T^{-1}, Haynes et al. 2014), the precession frequency of the latter can be directly modified by exerting changes on the external magnetic field $\vec{\mathrm{B}}_0$. At the same time, any departure of an experimental system from the one just described could mean the presence of local magnetic fields. When we consider protons inside molecules (-CH_4, -OH) we can easily imagine how the functional groups conformation alone modifies the interaction between nuclear and/or electric magnetic moments: this translates into the arising of more than two "motion classes".

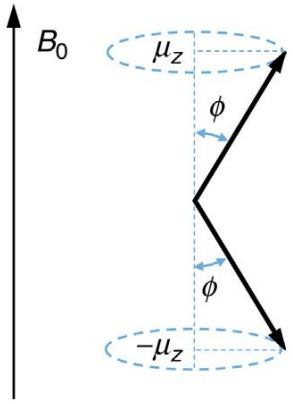

Figure 4. Graphical representation of the two possible hydrogen nuclear magnetic moment when subjected to a static magnetic field ($\vec{\mathrm{B}}_0$); the term μ_z refers to the projection of μ on the z axis (Bertini et al. 2017).

5.3. Resonance

After reaching an equilibrium condition (ω_p conserved) you want now to consider the case when more than one magnetic field contributes to the overall magnetic moment motion. Altering the energy state of a proton in a magnetic field is possible only if it exists an instrument to transmit energy; this will result in its nuclear magnetic moment reorientation. It is possible to observe the resonance effect if an oscillating magnetic field is applied to a precessing magnetizable system when the frequency of the first one is equal or nearly equal to the second one (Halliday et al. 2013f): during the ^{1}H NMR analysis, it translates into altering the proton orbital energy through the application of an electromagnetic radiation conveyed by a radiofrequency (RF) pulse (Farrar et al. 1971e).

Starting from Equation 6, we want to describe the torque ($\partial\vec{\mu}/\partial t$) exerted on a single proton with spin $1/2$ in the case of a second magnetic field B_1 oscillating at ω_p frequency is applied orthogonally to the first $\vec{\mathrm{B}}_0$:

$$\frac{\partial\vec{\mu}}{\partial t} = \gamma\vec{\mu} \times \left[\vec{\mathrm{B}}_0 + \vec{\mathrm{B}}_1(t)\right] \tag{9}$$

Since to describe this system through the application of fixed Cartesian coordinates (laboratory frame of reference) is quite difficult, it is useful to introduce a new reference system (x', y', z') assuming a rotation of the xy plane around the z axis at an angular speed equal to ω_p in the same precession direction of the nuclear magnetic moment. This new reference system is called rotating frame of reference. In the particular case in which the B_1 field is applied parallel

to the x' axis to the exact precession speed of the nuclear magnetic moment, the new system corresponds to the nuclear magnetic moment precession around x' itself; in other words, the magnetization component along the z axis will be cancelled out by the presence of a fictitious magnetic field (ω_p/γ) (Farrar et al. 1971a). The torque acting on m can be described as

$$\frac{\partial \vec{\mu}}{\partial t} = \gamma \vec{\mu} \times \vec{\mathrm{B}}_1 \qquad (10)$$

or, in the laboratory frame, the magnetic field associated with the nuclear magnetic moment precesses only on the $x'z$ plane (Farrar et al. 1971a). Since the application time of the second magnetic field is extremely short, this analytical technique is also called pulsed nuclear magnetic resonance. The resonance frequency, namely the frequency (RF) at which the B_1 magnetic field is generated

$$\nu_L = -\frac{\gamma \mathrm{B}_0}{2\pi} \quad \text{or} \quad \omega_L = -\gamma \mathrm{B}_0 \qquad (11)$$

is called Larmor frequency: it is defined as the frequency of the applied oscillating magnetic field to which a magnetic moment (μ) must be subjected, regardless of its angle, in order for it to undergo such a torsion as to induce a motion of precession in the direction of the field itself (Farrar et al. 1971a).

5.4. The ^{1}H NMR Signal

Up to this point, the behaviour of a single hydrogen atom immerged into a static magnetic field (B_0) and subjected to a second pulsed magnetic field at resonant frequency (ω_p) has been described. The phenomenon has also been observed within two different reference systems in order to simplify its mathematical handling. Trying to summarize the laboratory conditions, in which the nature of the sample is much more complex than the one considered so far, it is good to sum up the magnetization component considering it as the composition of all the vector ($\sum \vec{\mu}_k = \vec{\mathrm{M}}$) associated with each of the nuclei present in the sample. Since the torque (Eq. 6) generated by (B_0) imposes phase coherence only in the precession around the direction of the field itself or, the sum of the nuclear magnetic moments results not null only in the directions $-z$ and $+z$, the projection of $\vec{\mathrm{M}}$ into the x, y and z components can be summarized as follows:

$$\sum M_z \cong M_z \cos\theta - M_{-z} \cos\theta$$

$$\sum M_x \cong 0 \qquad (12)$$

$$\sum M_y \cong 0$$

where θ represents the $\vec{\mathrm{M}}$ tilt in respect to the z axis.

As observed in Equation 12, starting from the assumption that within the static magnetic field the single nuclear magnetic moments are oriented with the same probability toward the two directions $\vec{\mathrm{B}}_0$ and $-\vec{\mathrm{B}}_0$ the resultant along the three (x, y, z) spatial directions will be null. According to the Boltzmann equation applied to the energy level distribution, all the systems which not at thermodynamic equilibrium will assume the lower possible one (Doan et al. 2013). regarding the considered system (Fig. 4), the number of spins precessing in the same direction of $\vec{\mathrm{B}}_0$ will be greater than the ones precessing in the opposite ($-\vec{\mathrm{B}}_0$) direction resulting into a non-null $\sum M_z$ net magnetization (Eq. 12). As discussed above, the application of a second pulsed magnetic field (B_1) along the x axis allows to alter the energy level of the analysed nuclei. When the chosen frequency is exactly equivalent to the pulsation of M (Eq. 11), we will observe a variation of the incidence angle (θ) proportional to the intensity of the B_1 field itself. Therefore, by exploiting the resonance phenomenon, it is possible to control the nuclear magnetic moments orientation.

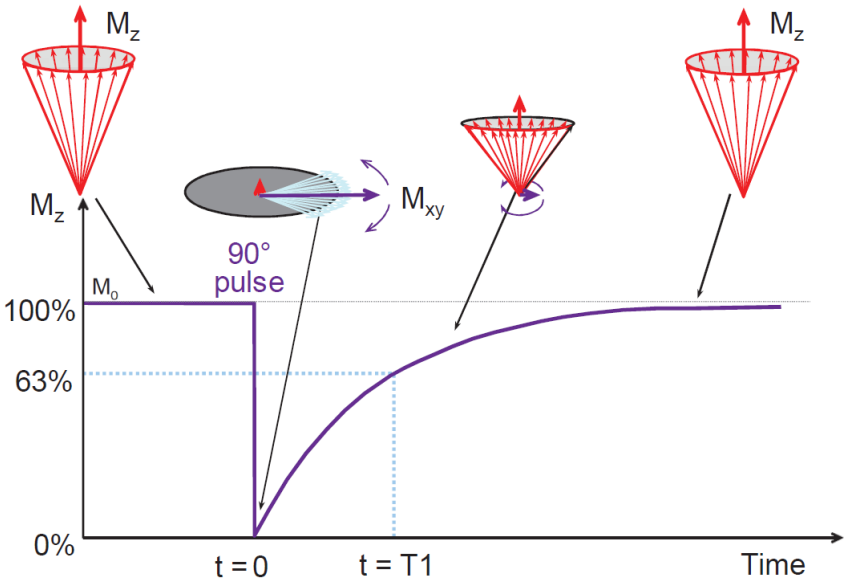

Figure 5. Representation of the initial magnetization (M_0) variation after a 90 degree pulse (B_1). The vector intensity at time 0 s^{-1} (after the pulse) is essentially null (Bushberg et al. 2011).

We define the 90 degree pulse (Fig. 5) as the radiofrequency pulse whose power is able to perfectly project the magnetization vector (M_z) on the xy plane perpendicularly to the static magnetic field (Farrar et al. 1971a). As we will discuss in the next paragraph, this sequence allows to draw the overall magnetization variation in time with the purpose to extrapolate its initial magnitude.

5.4.1. From Magnetization to Signal: The Faraday-Lenz-Neumann Law

In order to strengthen the understanding on how the results obtained during ^{1}H NMR analysis are interpreted, a brief explanation on the interconnection between magnetic fields and electricity follows. As you can see from Figure 3, the distribution of magnetic fields in space is represented by a series of lines called field lines which originate from the ends of the magnetic dipoles and whose density decreases as they come out of the source. Equation 13 quantifies the magnetic flux (Φ_{B}) as the field lines density crossing a surface of known area (A) (Halliday et al. 2013h).

$$\Phi_{\mathrm{B}} = \int \mathrm{B} \cdot d\mathrm{A} \tag{13}$$

Assuming the magnetic field constant, if all the field lines fall perpendicularly on the surface, Φ_{B} will be null since the incoming and outgoing field lines are equal in number and intensity. When perturbations in the magnetic field occurs, for example when the magnetic field associated with hydrogen nuclei approaches the direction perpendicular to A, the last statement is no longer valid and it is possible to define the entity of its variation as $\partial\Phi_{\mathrm{B}}/\partial t$. The importance of this variation during NMR analysis is linked to Faraday's law which states: *"the temporal variation of the magnetic flux across a surface of known area, which is embraced by an electric circuit in tension, generates in the circuit itself an electromotive force (ε) that opposes this variation"* (Halliday et al. 2013c).

$$\varepsilon = -\frac{\partial\Phi_{\mathrm{B}}}{\partial t} \qquad with \qquad \mathrm{I} = \frac{\varepsilon}{\mathrm{R}} \tag{14}$$

where the R and I terms respectively correspond to the resistance, that is the tendency of a circuit to oppose the passage of an electric current, and the intensity of the current itself. Considering both Equations 14 and 13, one can see the proportionality between the intensity of the magnetic field B applied through a solenoid and variation of the current flowing through

it. Therefore, it has been shown how it is possible to translate the alterations of a magnetic field along a given direction into an electrical signal.

5.4.2. Phenomenological Handling: The Block Proposal

The mathematical characterization of all the alterations to which spinning particles are subjected if drown into external magnetic fields was proposed by the Swiss physicist Fenix Bloch in 1946 (Bloch 1946). After we apply the 90 degree pulse, assuming the static magnetic field constant, it is possible to quantify the time needed by the system to return to the starting equilibrium (Fig. 5). The time dependence is strictly correlated to the interactions occurring between the spin and the surrounding laex. This last term refers to the degrees of freedom of the bulk-solvent system in which the atoms are dispersed. In fact, the particles freedom to rotate and/or diffuse will translates into faster or slower magnetization variations. We will consider the longitudinal magnetization M_z reorientation after a 90 degree pulse as:

$$\frac{dM_z}{dt} = \frac{(M_0 - M_1)}{T_1} \tag{15}$$

where $(M_0 - M_1)$ is the magnetization variation on the z axis and T_1 is the time needed by the spin system to recover 63% of the starting M_0. The T_1 parameter is called longitudinal relaxation time and it is consequence of spin-lattice relaxation phenomena (Farrar et al. 1971a). Since the static magnetic field B_0 remains active even during and after the imposition of the second magnetic field B_1, Equation 16 must consider also the torsion it exerts on the nuclear magnetic moments along the z axis.

$$\frac{d\vec{M}_z}{dt} = \gamma\left(\vec{\mathrm{M}} \times \vec{\mathrm{B}}_0\right)_z + \frac{(M_0 - M_1)}{T_1} \tag{16}$$

In turn, to explain the overall $\vec{\mathrm{M}}$ variation as a function of time, the x and y components and their relaxation time must be considered as follow:

$$\frac{d\vec{\mathrm{M}}}{dt} = \gamma\vec{M} \times \vec{B} - \frac{\left(\vec{M}_x - \vec{M}_y\right)}{T_2} - \frac{(M_z + M_0)}{T_1}\hat{k} \tag{17}$$

where T_2 represents the transversal relaxation time or the time needed to completely relax the magnetization on the xy plane after the B_1 pulse. Contrary to the longitudinal

relaxation, this last one is mainly affected by spin-spin interactions. According to Block et al. (1946), the magnetization variations time dependence can be extracted from Equation 17 by independently integrating the second and third terms. The transverse and longitudinal magnetizations variation laws

$$M_z(t) = M_0\left(1 - e^{-\frac{t}{T_1}}\right) \qquad \text{and} \qquad M_{xy}(t) = M_0 e^{-\frac{t}{T_2}} \qquad (18)$$

both showing to follow an exponential decay. This last sentence can be generically accepted exclusively for systems which are characterizable by only one precession frequency. In fact, more than one exponential decay could be expected in multi-solvent samples.

5.4.3. Free Induction Decay (FID)

As explained at the end of paragraph 5.4, depending on the pulsed signal B_1 power, it is possible to adjust the magnetization vector's angle of incidence until it lies on the xy plane. The possibility to detect the magnetic flux variation ($\partial\Phi_{\mathrm{B}}/\partial t$) along a specific direction translating it into an electric signal has already been discussed in Paragraph 5.4.1; after we apply a 90 degree pulse, the graphic representation of such electric current variation through a coil is called free induction decay (FID) (Farrar et al. 1971a). As it is shown in Figure 6, the magnetization vector precession causes the current to fluctuate between maxima and minima values. The peaks intensity decreases as a function of time elapsed after the pulsed field (B_1) is applied. If you consider the system into the rotating frame of reference, where the xy plane rotates at an angular speed equal to the magnetic moments precession, the result is the magnetization exponential decay representation along the y' axis.

Depending on the instrumentation, the NMR can mount one or two different coils: in the first case the task of transmitting the radio-frequency impulse and that of receiving the signal is carried out by the same equipment. To do not incur in spurious readings, it is important to put attention on the timing between the RF pulse and the switch to antenna. In the second case the NMR presents two different instrumental parts (coils): *"receiver"* and *"transmitter"* (Farrar et al. 1971c). What has been described so far, that can be summarized with a signal similar to the one shown in Figure 6d, is an ideal case in which no turbulences in the B_0 and B_1 magnetic fields are presents and the nuclear magnetic moments associated to the hydrogen atoms spins all possess the same angular speed.

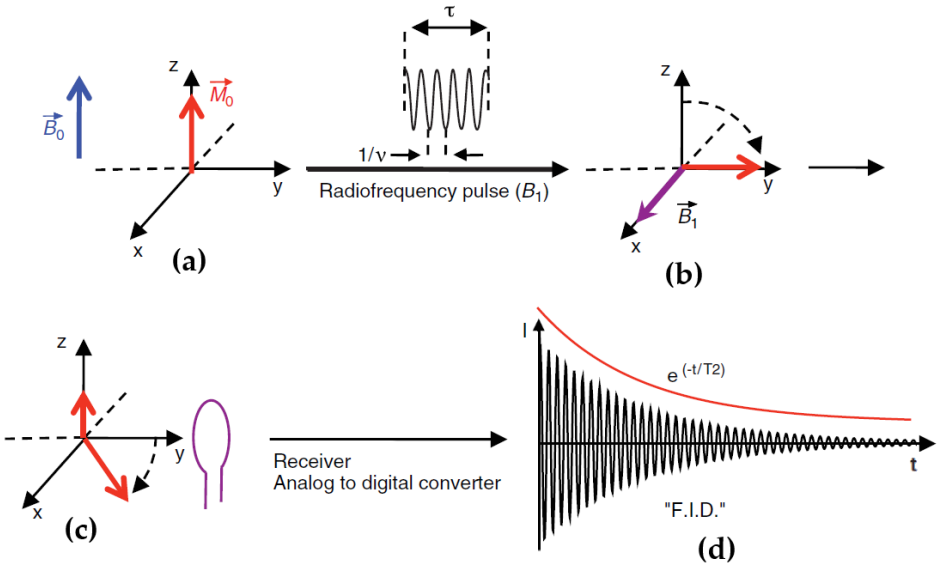

Figure 6. Graphical representation the magnetization vector ($\vec{M}_0$): (a) termodynamic equilibrium; (b) magnetization lying to the xy plane immediately after a 90 degree pulse (B_1); (c) relaxation phenomena in the only static magnetic field (B_0) bring the system back to the condition (a); (d) free induction decay (FID) of the transverse signal as a function of time graphical representation (Doan et al. 2013).

Since the experiment designs always involve the presence of field B_0 inhomogeneities, such problem is solved by the analysis of the complex part of the FID which arises by the signal representation on the (M_y, t) plane. The aim of this treatment was to make the reader aware of dimensionalities and phenomena involved during the nuclear magnetic resonance analysis. The same observations can be applied to experiments on isotopes other than ^{1}H (e.g. ^{2}H, ^{13}C, ^{14}N, ...). In addition, it is important to take into account the intensity of the signal to be directly proportional to the concentration of the analysed atoms and to the external field intensity (Farrar et al. 1971a); this is extremely important during ^{1}H NMR spectroscopy techniques application to metabolomic studies: in samples where water is the main component, the applicaztion of specific suppression sequences is required in order to reveal the signal arising from others than water hydrogen nuclei (Godelmann et al. 2016).

5.5. Acquisition Sequences

Due to the problems related to fields inhomogeneity during signal acquisition, to get a nonspurious set of data, it is necessary to use specific reading sequences. The application of a single 90 degree pulse allows to obtain only the transverse relaxation time (T_2) arising from spin-spin relaxation mechanism: it means no information about the longitudinal magnetization decay would be detectable. Two examples on how experimentally handle these issues are given namely, the use of Inversion Recovery (IR) and Carr-Purcell-Meiboom-Gill (CPMG)

sequences. In addition, the use of fast field-cycling relaxometers will be presented as technological solution to obtain relaxation times also in in the low frequency spectrum.

5.5.1. Inversion Recovery (IR) Sequence

What follows is the most used sequence to determine the longitudinal relaxation time T_1. Let us consider a pure water sample where the only signal generated is the one characteristic of the M magnetization arising from of the water hydrogen spins. The procedure to determine the 90 degree pulse power consist in: identify the pulse power which makes the longitudinal magnetization completely null (180 degree pulse), make that power half expecting to obtain the maximum signal intensity (90 degree pulse). To achieve this, it is both possible to set the pulse duration or the signal amplitude. The inversion recovery (IR) sequence exploits a series of alternating 180-τ_i-90 degree pulses during which, at each iteration, the τ_i value, which represents the waiting time between the first and second pulse, increases (Farrar et al. 1971b). The first pulse (180 degree) will force the magnetization from the starting M_0 magnitude to a $-M_0$ value; the following relaxation phenomenon is summarized by Equation 18 and, it would allow to obtain the longitudinal relaxation time if it was not that the antenna is only sensitive to the magnetic flux variations on the xy plane. The second pulse (90 degree) aims is to overcome this problem by projecting the magnetizing vector on the $-y$ direction allowing a "longitudinal magnetization photography" at a certain time (τ_i) to be taken. Since during the latency between the first and second pulse the longitudinal magnetization tends to return to equilibrium through the spin-lattice relaxation mechanisms, the FID intensity representation as a function of τ_i (Fig. 7) allows to extrapolate the longitudinal relaxation time T_1.

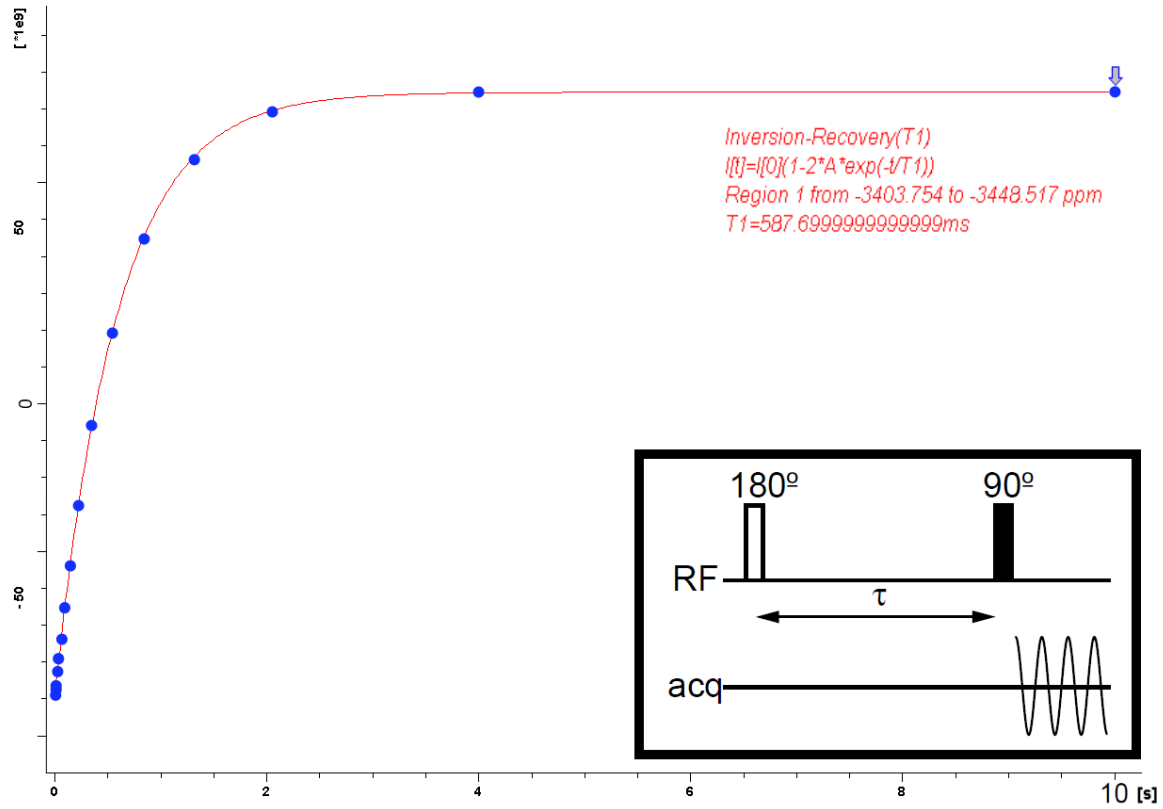

Figure 7. Graphical representation of an inversion recovery acquisition sequence: each point corresponds to the initial FID intensity after the 90 degree pulse. During the experiment sixteen τ_i (i=16) where used to estimate T_1. Depending on the type of experiment the list of τ can be modified in order to better fit the model; in this case the last (τ_{16}) was equal to 10 seconds. A graphic representation of the sequence is shown in the black box (bottom right).

After the 90 degree pulse the spin-spin mechanisms takes place; therefore, in order to avoid transversal relaxation to occur, it is important to set the signal acquisition as close as possible to the B_1 pulse ending. The term inversion recovery means that the magnetization will be initially forced to a minimum ($-M_0$) and then gradually let it rise to the maximum one (M_{inf})

$$M_z(\tau_i) = M_{inf} + \left(M_0 + M_{inf}\right)e^{-\frac{\tau_i}{T_1}} \qquad (19)$$

to extrapolate the T_1 value. The M_z (Eq. 19) decay is obtained by the general Bloch equations (not included) considering M_x and M_y equal to zero (Farrar et al. 1971b). In order to separate each (180°-τ_i-90°) cycle it is a good rule to let time pass at least five times the expected T_1 value; the choice is made in order to guarantee an almost complete reacquisition of the initial M_0magnitude. If complete relaxation between each sequence is not allowed, it will cause a systematic error or, the recording of a T_1 value lower than the real one (Farrar et al. 1971b).

5.5.2. Carr-Purcell-Meiboom-Gill (CPMG) Sequence

As anticipated, inhomogeneity in the magnetic field B_0 is one of the main problems. When measuring T_2 on solid samples you can apply a simple sequence called spin-echo or Hahn sequence: this consists of a 90°-τ_i-180° serie with acquisition after $2\tau_i$ following the last pulse. This sequence thus makes it possible to neutralize the systematic error on the T_2 readings which are related to the different precession frequency of the individual magnetic moment μ_k subjected to different static magnetic fields (Farrar et al. 1971b). In case the sample is in liquid state, to the inhomogeneity of the B_0 field also problems related to molecular self-diffusion can spoil the readings: hydrogen nuclei are never motionless but, they tend to diffuse (D) within the sample according to Einstein-Stokes law:

$$D = \frac{k\mathrm{T}}{6\pi\mathrm{r}\eta} \tag{20}$$

where k refers to specific substances' kinetic proportionality to temperature (T), r is the particle radius and η the viscosity. In addition, a problem of inhomogeneity in the B_1 field is added: during simple acquisition sequences (e.g. inversion recovery), inhomogeneity in the order of 5% is accepted. However, because of the reiteration of pulses the associated error adds up by significantly altering the recorded T_1. The experimental solution derives from the Carr-Purcell-Meiboom-Gill (CPMG) sequence: it consists in a 90°-τ-180°- 2τ -180°- 2τ -180°- ... sequence in which the 180 degree pulses are applied along the y_0 axis so that the magnetization is rotated around the y_0 axis itself. The signal acquisition starts 4τ after the application of the 90 degree pulse and each following 2τ until the signal completely disappears. Therefore, through the acquisition of the echoes' intensity, it is possible to extrapolate a T_2 value purged by errors (Farrar et al. 1971b). Choosing the shortest τ values further reduces the possibility for proton spins to diffuse through the sample allowing more reliable results.

5.5.3. Fast Field-Cycling (FFC-NMR)

As has been shown (Eq. 8), the magnetic moments precession frequency is directly proportional to the applied magnetic field (B_0). In turn, the magnetization vector intensity M_z, and therefore the NMR signal, depends on the $\vec{M}_0$ incidence angle which varies according to the induced torsion (Eq. 4). During the NMR readings, noise is an experimental parameter always considered: its quantitation is possible through the signal-to-noise ratio (S/N) value. When the experimental conditions allow to operate at high Larmor frequencies, the signal

intensity is not a limiting factor; therefore, in this case it is possible to use one of the discussed sequences. However, it is of major interest to inspect the T_1 and T_2 dependency to the acquisition frequency; the reasons will be discussed above. Investigating the noise sources is beyond the scope of this document. Anyway, it must be stressed the S/N proportionality to the Larmor frequency and therefore to the static magnetic field intensity (Kimmich et al. 2004). In order to allow relaxation times detection even at low frequencies, the field-cycling technology and related sequences were introduced: unlike the inversion-recovery sequence, the static magnetic field is never totally turned off, but it is controlled by switches turning it in between of two or more known magnitudes (Fig. 8). It follows the signal intensity to remain acceptable even at frequencies even below 0.1 MHz making it possible the relaxation time evaluation into lower frequencies ranges.

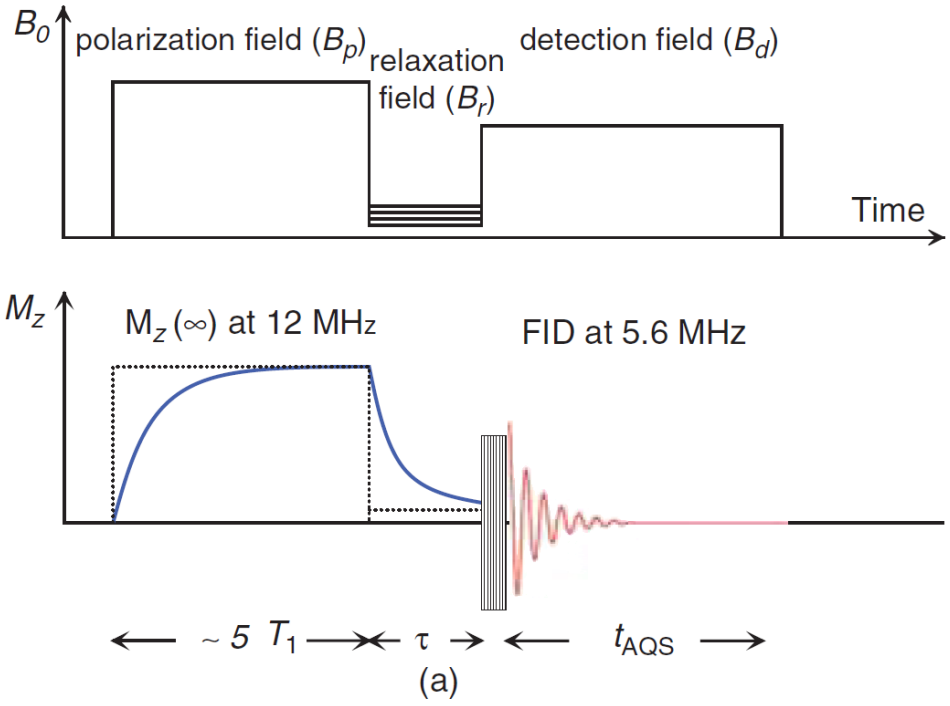

Figure 8. Working scheme of an FFC-NMR relaxometer: variation of both the magnetic field B and longitudinal magnetization M_z one field-cycle. The two B_p and B_d fields can have the same magnitude (Tóth et al. 2013).

The possibility to inspect low-frequency molecular motions is limited by samples (e.g. the "local fields" effect could exceed the external applied field) and/or technical (e.g. molecular motions could occur faster than the field switching needed time) characteristics. To collect data on extremely fast molecular motions, the fast field-cycling switches should be electronically controlled (Kimmich et al. 2004). Depending on the instrumentation type and used frequency more than one sequence can be applied. The one depicted in working scheme (Fig. 8) is just one of the recurrent repetitions needed for relaxation time extrapolation. In contrast to the previous cases, a 90 degree pulse is used to project the magnetization along the antenna

acquisition axis: the RF pulse is exerted during detection phase followed by signal acquisition. It is essential the magnetization M_z to reach its maximum value before the polarization phase starts otherwise the reading will suffer of systematic errors. The field switch at a lower (B_r) intensity is followed by relaxation phenomena. After a certain τ_i time the static field intensity is increased to a $\mathrm{B}_d > \mathrm{B}_r$ value and a 90 degree pulse allows the corresponding M_z value sampling. Through the Bloch equations (Bloch 1946) by sampling at incremental τ_i values, it is possible to trace the relaxation times associated to the B_p field. Those treated are just some of the parameters involved during the fast field-cycling experimental design. The timing required for the magnetic field and antenna switches and the choice of the last τ_i sampling value should also be considered since they directly affect the experiment duration. Regardless of that, the correct setting should always made in order to reduce the occurrence of systematic errors.

5.5.4. Fourier Transform Method

Until now, a sample composed by a single molecular species, namely water, has been examined: what if more than one precession frequency arises during a complex mixture analysis? As has been observed nuclear magnetic moments can be summarized as magnetic dipoles (Fig. 3) which associated magnetic field spreads in the surrounding acting on other magnetic nuclei as the external magnets does. Therefore, these influence each other depending on their orientation and proximity. In fact, when a homogeneous sample is considered, the spatial organisation and chemical composition of the aforementioned translates into a well-defined precession. Contrary, if the same sample is added with a certain amount of ethanol (CH_3CH_2OH), the new solvent will be characterised by different types of hydrogen each of which will locally experience different magnetic field interferences. By setting a static magnetic field B_0 again you can rewrite the torque Equation 6 as:

$$\frac{\partial \vec{\mu}}{\partial t} = \gamma \vec{\mu} \times \left(\vec{\mathrm{B}}_0 + \vec{\mathrm{B}}_i\right) \tag{21}$$

where $\vec{\mathrm{B}}_i$ summarizes the local magnetic field exerting on a specific hydrogen. From an experimental point of view, how does the signal (FID) look when nuclear magnetic moments precess at different frequencies? The undulatory nature of an electromagnetic wave can be explained by a pair of sines, one (magnetic field) orthogonal to the other (electric field) (Halliday et al. 2013d). Trying to express the magnetic moment $\vec{\mathrm{M}}$ displacement as a function of time you will also discover it can be represented through a sine function (the ability of the first to

resonate with the second is closely related to their oscillatory nature). Back to the water-ethanol mixture, the FID obtained after a 90° pulse will result from the different spin precessions signal composition. The Fourier transform (FT) is a particular integral transform that finds its application in the harmonic analysis or, the branch of mathematics which studies signals as a composition of fundamentals waves: its application allows to divide a complex signal or, a signal arising from the interaction of more than one waves, into an infinite series of sine and/or cosine functions; the results it is called Fourier series (Doan et al. 2013; Farrar et al. 1971a; Farrar et al. 1971b):

$$f(t) = \sum_{n=0}^{\infty} \left[A_n \cos\left(\frac{n\pi}{T}\right) t\right] + \sum_{n=0}^{\infty} \left[B_n \sin\left(\frac{n\pi}{T}\right) t\right] \quad (22)$$

At the same time, when the Fourier transform is applied to the magnetization exponential decay it results in the representation of the same phenomenon in the form of intensity as a function of frequency; it means the exponential function in time domain is the Fourier transform of a Lorentzian function in frequency domain (Farrar et al. 1971a).

$$\frac{T_2}{[1 + T_2^2(\omega - \omega_0)^2]} = \int_0^{\infty} e^{-\frac{t}{T_2}} \cos(\omega - \omega_0)\, dt \quad (23)$$

The expression $(\omega - \omega_0)$ indicates the off-resonance phenomenon or, the angular velocities which the different hydrogen classes of hydrogen experience, that results in a chemical shift between the spectral lines (Fig. 9) (Farrar et al. 1971b). Let us consider a water-ethanol solution spectrum obtained through an inversion recovery sequence (Fig. 9): thanks to the application of a Fourier transform each precession frequency is extracted and singularly analysed. This procedure results into three spectral "lines" each of which coding per one or more functional groups. Therefore, from each spectrum it is possible to extract both an averaged relaxation time or inspect each one of the different lines to characterize more than one T_1 and T_2 per sample. In conclusion, the analytical procedure involving the application of Fourier transform acquires particular importance in complex matrices' metabolomics characterization: if it is possible to identify the compound whose concentration can be summarized through a specific spectral line density (area), this analytical technique may also have quantitative value (Godelmann et al. 2016).

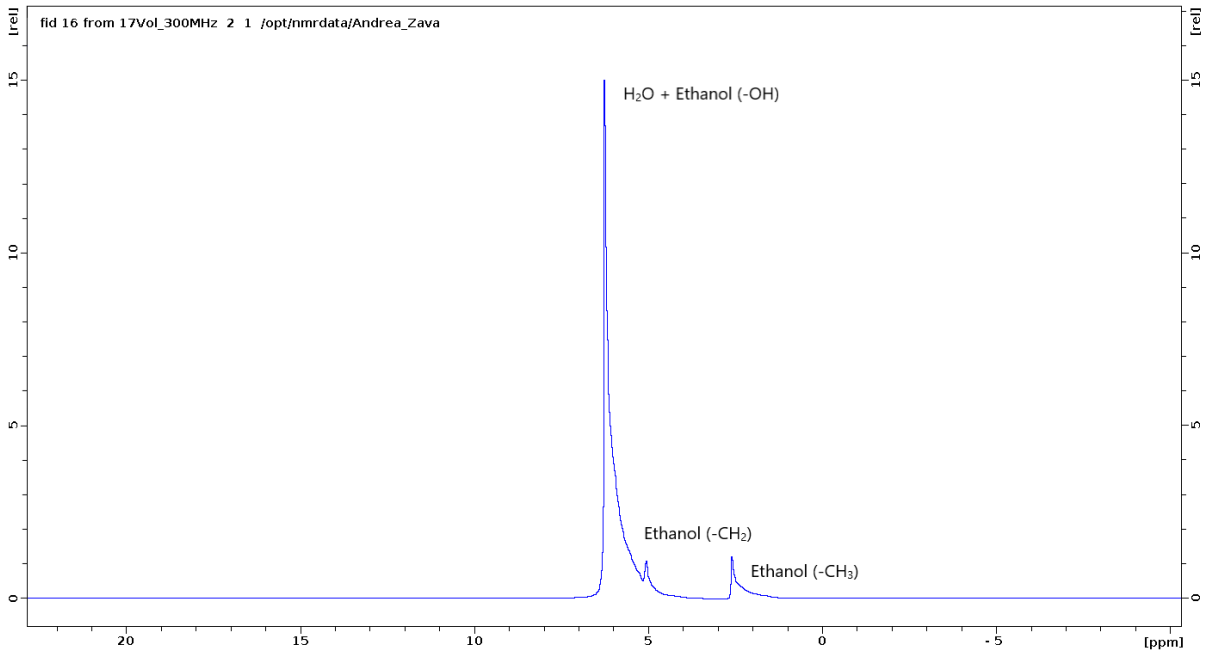

Figure 9. Water-ethanol mixture at 17 % vol; spectrum obtained through TopSpin software. The three spectral lines show, starting from left, the intensity of water hydrogens, together with the signal coming from the ethanol hydroxyl group (-OH), the ethanol methylene group (-CH_2) and the ethanol methyl group (-CH_3).

5.6. Molecular Motions and Their Effect on Relaxometry Models

The term relaxometry refers to one of the analytical techniques which are currently used to characterize samples molecular dynamics (e.g. rotation, diffusion). The dipole-dipole interaction between magnetic moments causes local field fluctuations which are the responsible for spin energy level degeneration (Farrar et al. 1971a). Therefore, the samples physical-chemical characteristics will affect the whole magnetic moment possibility to interact in a time dependent scale or, different water relaxation rate are expected depending on the lattice capability to affect the proton dynamics. These information arise from a range of analytical techniques designed to characterize the evolution of relaxation times, namely T_1 and T_2, as a function of experimental parameters including resonance frequency (ν_L), temperature (T), pH and chemical composition. The answers are studied in the form of dispersion of the measured values through the application of models; the choice of the latter is a consequence of the question to which an attempt is made to give an answer. These models were developed on samples of known composition as water, aqueous solutions, or crystals so that it was possible to observe how relaxation times were affected by the variation of one of the experimental conditions mentioned. The next step involves investigating which physical properties explain the sample molecular dynamics to quantify variables and constants to be used for the characterization of more sophisticated samples. An interesting application in the

medical field is the study of paramagnetic elements and/or compounds, as gadolinium(III) complexes, for the development of the contrast agents to be used during magnetic resonance imaging (MRI) analysis: when these solutions are injected into tissues, their main feature is to induce a drastic reduction in relaxation times creating or increasing the required contrast to obtain sharp imaging (Doan et al. 2013). This behaviour is summarized by the Solomon-Bloembergen-Morgan, the Fries-Belorizky, and Albrand models (Tóth et al. 2013).

Consider a water solution containing a paramagnetic particle (Mg^{2+}): the relaxation rate can be described by the cumulative model

$$\frac{1}{T_{i,obs}} = \frac{1}{T_{i,diam}} + \frac{1}{T_{i,para}} \tag{24}$$

containing the diamagnetic contribution ($1/T_{i,diam}$), or the water solution relaxation rate in absence of paramagnetic species, and the paramagnetic contribution ($1/T_{i,para}$) which is linearly dependent to the paramagnetic particle concentration (Tóth et al. 2013). It must be stressed the diamagnetic contribution to be generally obtained by the additive self-diffusion and solvent rotational relaxation rates. Bodart et al. (2020) proposed to extract this information through a sample characterization after the complete paramagnetic particle removal by acidic cation exchange resins pre-treatment.

5.6.1. The Diamagnetic Relaxation Rate: Rotation-Diffusion Contributions

It is easy to imagine a molecule to be free to translate in space (diffuse) and to rotate, both in time scale, as consequence of the interaction with surroundings. Level and type of structural organization of a sample affect molecular movement freedom. The term "liquid" is often associated with isotropy, which refers to the total randomness in the distribution of molecules. When the organization increases, we talk instead of "nematic" or "smectic" liquid; depending on physical, conditions such as temperature, some liquids change the level and type of organization: these differences are identified as "phases". The time dependence molecular motions are responsible for different dipole-dipole interaction intensity between magnetic centres and therefore, the relaxation rate will change depending on the sample molecular organization. In fact, more than one relaxation models exist depending on the analysed liquid phase:

- Torrey model for self-diffusion relaxation rate ($1/T_1^{SD}$) in isotropic phases (Torrey 1953);

- Žumer and Vilfan (Vilfan et al. 1980; Žumer et al. 1978) model numerically adapted to characterize nematic and smectic A phases;
- The Bloembergen-Purcell-Pound (BPP) model (Bloembergen et al. 1948) explains the rotation-diffusion relaxation rate contribution.

The subtraction of diffusion relaxation rate from the BPP model allows to extract the individual rotation contribution. Considering each sample molecule as spherical, we can assume the Stokes law valid in a low turbulence state ($\mathrm{Re} < 10^4$) or, each particle will be subjected to a viscous friction force which opposes to its motion direction proportionally to the solvent viscosity (η) and molecular radius (r) (Halliday et al. 2013e). This limits the molecular diffusion causing, according to the Torrey model, the longitudinal relaxation rate ($1/T_1$) to be enhanced as follows:

$$\frac{1}{T_1} = \frac{9}{8}\left(\frac{\mu_0}{4\pi}\right)^2 \gamma \left(\frac{h}{2\pi}\right)^2 [j_1(\omega) + j_2(2\omega)] \tag{25}$$

where μ_0 is the vacuum (magnetic) permeability (Halliday et al. 2013h), $h/2\pi$ the reduced Planck constant (Halliday et al. 2013b) and $j_k(\omega)$:

$$j_k(\omega)^{SD} = \frac{n\tau_D}{d^3} j_k^{SD}\left(\omega\tau_D, \frac{\langle r\rangle^2}{12d^2}\right) \tag{26}$$

Despite in multiple molecular systems more than one self-diffusion value can be observed, it is always possible to obtain an estimation on the overall contribution to sample relaxation rate. In this case average spin-density (n), molecular width (d) and average spin distance $\langle r\rangle$ values are considered. The easiest BPP model expression for ^{1}H protons is given by:

$$\left(\frac{1}{T_1}\right)^{BPP} = A^{BPP}\left[\frac{\tau}{1+\omega^2\tau^2} + \frac{4\tau}{1+4\omega^2\tau^2}\right] \tag{27}$$

with

$$A^{BPP} = 1.70888 \times 10^{-49}\left\langle\frac{1}{r^6}\right\rangle \tag{28}$$

The r term (Eq. 28) can be calculated through software for molecular simulations (e.g. Avogadro) while the τ values are the corresponding correlation time which explain the time dependence of the phenomenon.

5.6.2. Paramagnetic Relaxation Rate

The term paramagnetic refers to chemical species characterized by possessing an intrinsic weak magnetic moment; the latter, in the absence of an external magnetic field, randomly orients itself in space. If a static magnetic field is externally applied, their magnetic moment will try to align with it as described in Paragraph 5.2. This phenomenon is opposed to that of diamagnetism which sees the alignment of the magnetic moments of the diamagnetic chemical species in the opposite direction to that of the applied magnetic field (Halliday et al. 2013h). Among the paramagnetic chemical species are: molecular oxygen (O_2), gadolinium(III) (Gd^{3+}) manganese(II) (Mn^{2+}) and iron(III) (Fe^{3+}). The paramagnetic relaxation rate results by the summation of two mechanisms related to the presence of paramagnetic chemical species: inner-sphere (IS) and outer-sphere (OS) relaxation (Tóth et al. 2013). The two contributions separately considered in Figure 10 for a 2 mmol L^{-1} manganese(II) chloride ($MnCl_2$) pure water solution. In this case, only the red (IS) and the blue (OS) relaxation rate values have been used to characterize the dispersion curve (black line) ($R_{1,p} = R_1^{IS} + R_1^{OS}$).

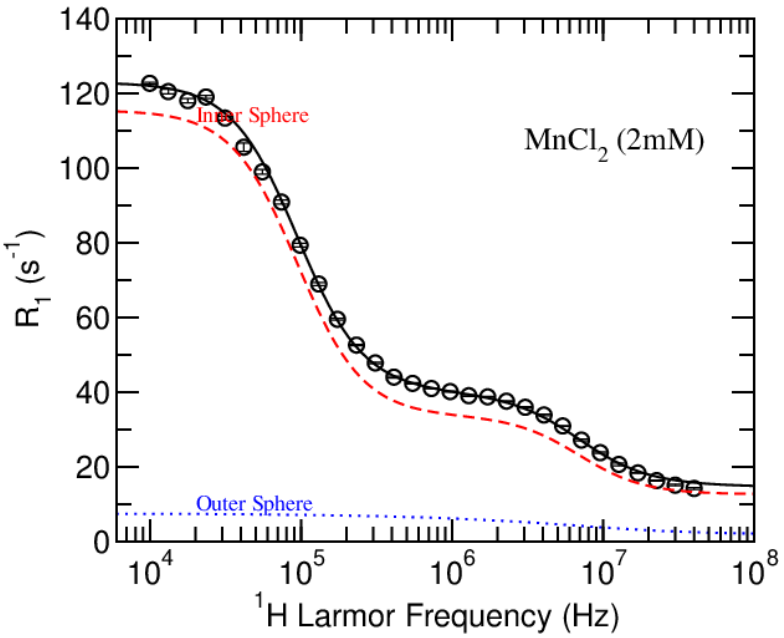

Figure 10. The graph represents the hydrogen relaxation rate R_1 (s^{-1}) values dispersion between 10 kHz and 50 MHz for a 2 millimolar manganese chlorine $MgCl_2$ solution: the red and blue lines respectively represent the inner-sphere and the outer-sphere contributions to the total relaxation rate. The data are obtained during experiments in the Instituto Superior Técnico (IST) of Lisbon. Available on: http://www.fitiwiki.net/.

Instead of expressing the total relaxation rate as in Equation 24, under certain circumstances it is considered useful to quantify the paramagnetic particle molar contribution

$$R = R_0 + r_v^{\mathrm{Mn}}[\mathrm{Mn}] \tag{29}$$

through the relaxivity (r_v); the R_0 term in Equation 29 refers to the solvent observed relaxation rate in the absence of paramagnetic species. The linear relation, fixed at each specific frequency, can be obtained considering the relaxation rate enhancement at increasing paramagnetic species concentration. It must be stressed the relaxivity values to be affected, as it will be explained in the next paragraphs, by solvent chemical composition and physical state.

5.6.3. Inner-Sphere Proton Relaxivity

One of the two models explaining the presence of paramagnetic chemical species contribution to relaxation time is called Solomon-Bloembergen-Morgan model (Bloembergen and Morgan 1961). Only the longitudinal relaxation time is considered since the transverse relaxation mechanism is beyond the scope of this manuscript:

$$\left(\frac{1}{T_1}\right)^{IS} = P_m \frac{1}{T_{1m} + \tau_m} \qquad P_m = q\frac{n_m}{n_s} \tag{30}$$

where T_{1m} is the proton mean relaxation time, τ_m is average half-life of the particle solvent bounds, q is number of coordinated solvent molecules per paramagnetic particle, n_m the number of paramagnetic particles and n_s the number of solvent molecules. It is possible to estimate the $n_{m,s}$ value starting by the solvent viscosity determination by having information about his composition and the components' molecular molar mass. This model shows how the interactions between paramagnetic species and solvent hydrogen atoms induces an increase longitudinal relaxation rate depending on nature and concentration of the particle. Since the paramagnetic particles themselves exercise the external magnetic field presence, the relaxation of water proton is governed two mechanisms namely the dipole-dipole (DD) and scalar (SC) (Tóth et al. 2013):

$$\frac{1}{T_{1m}} = \frac{1}{T_1^{DD}} + \frac{1}{T_1^{SC}}$$

$$\frac{1}{T_1^{DD}} = \frac{2}{5}\frac{\gamma_I^2\gamma_S^2}{r^6}\left(\frac{h}{2\pi}\right)^2 S(S+1)\left(\frac{\mu_0}{4\pi}\right)^2\left(\frac{3\tau_{c1}}{1+\omega_I^2\tau_{c1}^2} + \frac{7\tau_{c2}}{1+\omega_S^2\tau_{c2}^2}\right) \tag{31}$$

$$\frac{1}{T_1^{SD}} = \frac{2}{3}S(S+1)\left(\frac{A2\pi}{h}\right)^2\left(\frac{\tau_{e2}}{1+\omega_S^2\tau_{e2}^2}\right)$$

While T_{1m}^{DD} is depends on the water-electron spin vector re-orientation and the water-particle bond duration, the T_{1m}^{DD} remains unaffected by the first depending only on the electron spin relaxation and proton exchange (Tóth et al. 2013). The scalar (or contact) effect refers to the contribution coming from the electronic wave function delocalization to the I physical centre (Bodart et al. 2020). The $\gamma_{I,S}$ and $\gamma_{I,S}$ terms refer to gyromagnetic ratios and Larmor frequencies of protons and electrons respectively. S represents the electronic spin; only species with electron spin greater than or equal to $1/2$ are paramagnetic centres and able to affect hydrogen relaxivity (Farrar et al. 1971d). The enhancement is proportional to the number of unpaired electron but also to the distance spearing the S and I centres (r) and the water molecule coordination number (q). Therefore, the overall inner-sphere paramagnetic contribution to the relaxation rate is not only affected by the concentration of the specific particle but also the number of unpaired electrons.

Regarding the solvent effect, the characteristics correlation time τ_{ci} is itself affected by the solvent composition: depending on the type molecules coordinated to the paramagnetic centre specific proton-metal rotation correlation time (τ_R) are expected.

$$\frac{1}{\tau_{ci}} = \frac{1}{\tau_R} + \frac{1}{\tau_{ie}} + \frac{1}{\tau_m}$$

$$\frac{1}{\tau_{ei}} = \frac{1}{T_{ie}} + \frac{1}{\tau_m} \qquad (32)$$

$$i = 1{,}2$$

According to the Debye-Stokes-Newton law for molecular diffusion into non-viscous liquids (Lauffer 1987), the τ_R value is directly proportional the solvent viscosity itself or, the higher the

solvent viscosity the lower the inner-sphere relaxation rate will be. The $1/T_{ie}$ value refers to the zero field spitting (ZFS) contribution to the relaxation rate (Eq. 33). The Zeeman effect on ions which presents more than one unpaired electron gives rise to degenerated energy. The electronic shell fluctuation is another source of paramagnetic relaxation contribution which is summarized by the Bloembergen-Morgan theory of paramagnetic electron spin

$$\left(\frac{1}{T_{1e}}\right)^{ZFS} = \frac{2}{50}\Delta^2\tau_v[4S(S+1)-3]\left(\frac{\tau}{1+\omega_S^2\tau_v^2}+\frac{4\tau}{1+\omega_S^2\tau_v^2}\right) \quad (33)$$

where Δ^2 is mean square fluctuation of the zero field-splitting in s^{-1} and τ_v the correlation time for the field fluctuation (Tóth et al. 2013).

By inspecting the relaxation enhancement at specific frequency it is possible to understand which of the correlation constant dominates the relaxation phenomena: for instance, in aqueous solution the increasing in relaxation rate at frequency lower than 0.1 MHz ($\omega_S\tau_e = 1$) is well known to be related to the dominant scalar coupling contribution (Bertini et al. 1993). Equations 30-33 together resume the Solomon-Bloembergen-Morgan solution for inner-sphere theory which quantifies the relaxation rate enhancement due to direct bounding of proton and paramagnetic particles. As we will see, the hydrogen magnetic moment will be experiencing the presence of fluctuations in the local magnetic fields even at distances higher than r.

5.6.4. Outer-Sphere Proton Relaxivity

The use of this model often serves to justify a decrease in relaxation time which could not be explained only by inner-sphere model: the presence of paramagnetic centres does not affect only the adjacent magnetic moments. In fact, both a second-sphere and an outer-sphere (OS) relaxation rate can be identified: since it is not always possible to distinguish between them, the OS model generally ends up summarizing them both (Tóth et al. 2013). Let us consider the differences between a free metal ion and a hardly chelated paramagnetic particle in solution: the bond between solvent molecules and paramagnetic particles will make the inner-sphere relaxation rate enhancement predominant on the total paramagnetic relaxation rate. Contrary, an increasing the steric hindrance radius will make the outer-sphere relaxation rate more evident.

To consider the relaxation rate related to the solvent molecule translation/diffusion in the paramagnetic centre proximity we refer to Fries and Belorizky (1978) and Albrand et al. (1983) models

$$\left(\frac{1}{T_{i,p}}\right)^{OS} = G[j_2(\omega_I-\omega_S)+3j_1(\omega_I)+6j_2(\omega_I+\omega_S)] \quad (34)$$

with

$$G = \frac{32\pi}{405}\left(\frac{\mu_0}{4\pi}\right)^2 \gamma_I \gamma_S \left(\frac{h}{2\pi}\right)^2 \frac{n_m N_A}{aD} S(S+1) \quad (35)$$

where N_a is the Avogadro's number, D the summation between the two I and S magnetic centres diffusion coefficient ($D = D_I + D_S$). The electronic and proton spin distance of minimum approach (a), or the minimum distance between proton and paramagnetic particle centres, should not be lower than r (Eq. 31). Depending on the ion steric hindrance, we can imagine the a value to increase in highly chelated particles because of the geometric disturbance of other nuclei. The $j_k(\omega)$ term represents the spectral density or, the Fourier transform of the correlation function (Ayant et al. 1975).

$$j_i(\omega) = Re\left(\frac{1+\frac{z}{4}}{1+z+\frac{4z^2}{9}+\frac{z^3}{9}}\right) \quad (36)$$

with

$$z = \sqrt{i\omega\tau + \frac{\tau}{T_{1e}}} \qquad \tau = \frac{a^2}{D} \quad (37)$$

Someone can easily claim the S and paramagnetic particle concentration importance on the final R^{OS} relaxation rate; in addition, also the inverse proportional effect of diffusion or, the probable proportionality between viscosity and outer-sphere effect, should be stressed.

6. ^{1}H NMR Applicability on Wines

The next paragraphs will be dedicated to possible ^{1}H NMR applications on wine: by associating sample chemical composition information to specific wine categories is essential in order to implement anti-fraud analytical procedures.

6.1. ^{1}H NMR Spectroscopy in Wine Characterization: Two Strategies

The possibility to obtain compositional information from ^{1}H NMR spectra has been explained in paragraph 5.5.4. Wine is a complex alimentary matrix: the large amount of involved chemical species during metabolomics studies makes the use of this analytical technique extremely interesting, as make it possible to inspect the overall chemical composition of samples (Godelmann et al. 2016). Before introducing the ^{1}H NMR spectroscopy applicability some observations are needed. Since the signal intensity is proportional to the originating protons concentration, by inspecting aqueous solutions (e.g. hydro-alcoholic mixture), most of the compositional information will be hidden by the solvent corresponding spectra. An invasive solution is to entirely substitute the sample water with its deuterated version (H_2O): since deuterium ions differ from simple protons in the number of spinning nucleons, their Larmor frequency at specific field intensities results completely different. The water hydration shell is responsible for the stability of several chemical species (e.g. proteins) and affects the formation of insoluble salts. Together with this, during water removal processes, temperature increasing, oxidation and light exposure could origin chemical alteration on the analysed wines. Therefore, this procedure should be avoided in metabolomics and chemical sample classification studies. As an effecting alternative, the pre-saturation sequences together with specific R_1-filters can be used in order to null part of the frequency signals making the other spectral lines to arise (López-Rituerto et al. 2012; Mazzei, Spaccini, et al. 2013). Thanks to this approach it was made possible to extract many compositional information of wines increasing the statistical robustness during sample cross comparison (Godelmann et al. 2013). Even if the technology needs to be deeply inspected, its applicability still remain evident even outside research laboratories.

Thanks to the Fourier transform method, it is possible to trace the harmonic frequencies (continuous sinusoidal signals) composing the FID (Eq. 22, 23) or, hydrogen nuclei that differ in the precession frequency, regardless of the reason, are represented with independent ^{1}H NMR spectral lines. Starting from this assumption, how is it possible to extract compositional information from a spectrum and again, how can we use this information to assess wine variety,

vintage, and/or geographical origin? In Germany, both the already discussed targeted and non-targeted approaches were applied comparing more than 600 wine samples to judge the amount of information coded by their spectra (Godelmann, Fang, et al. 2013). These two strategies are respectively called profiling and fingerprinting.

6.1.1. ^{1}H NMR Profiling

The targeted approach works after associating spectroscopic peaks with certain previously identified molecules (Fig. 11): this qualitative approach is made possible through the addition of an internal standard (tetramethylsilane, TMS) and expressing the distance, also referred as chemical shift (δ_{ppm}), of all other peaks from this last one (Keeler 2002):

$$\delta_{ppm} = \frac{\left(\nu_{Sample} - \nu_{TMS}\right)}{\nu_{TMS}} \cdot 10^{6} \tag{38}$$

Furthermore, the compounds can be quantified by comparing the specific spectral line (peak) area to that of the reference compound (Keeler 2002). This analytical strategy in conjunction with the application of chemometrics tools allowed to track variability sources of samples with different geographical origins (Son et al. 2008), variety (Aru et al. 2018) and, in some cases, vintage (Anastasiadi et al. 2009). It is interesting to stress the possibility to work directly on wine without a pre-analytical sample preparation procedure (e.g. separation, drying, ...) which could otherwise decrease its accuracy (Aru et al. 2018).

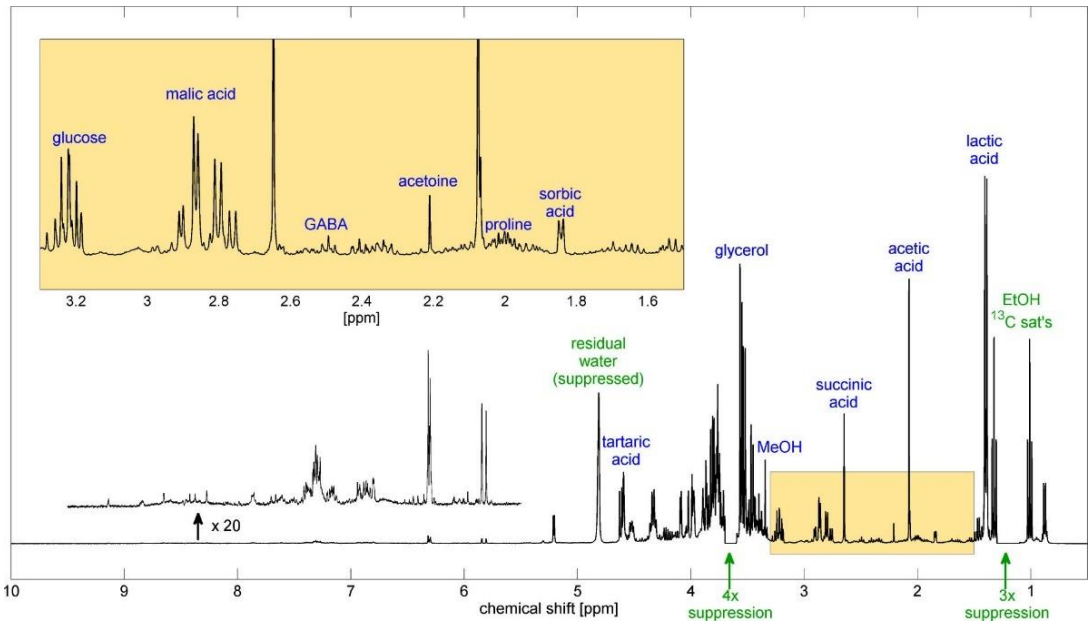

Figure 11. Wine ^{1}H NMR spectra with eight suppressed frequency ranges. Some peak-molecules associations are given (Godelmann et al. 2013).

Even if there are cheaper and faster analytical methods giving comparable results, (Danezis et al. 2016), the minimum sample preparation, the automation possibility, and the high throughput information amount (Godelmann et al. 2016) make this technique extremely interesting. Still many peaks need to be correctly associated to the corresponding chemical species: the difficulty lies in wine compositional complexity. One solution comes by the application of hyphenated techniques, namely pre-analytical chromatographic separation, followed by individual chemical species association to each chemical shift value. During both exploratory and discriminant analysis, followed by model validation with Montecarlo resampling tests, the association of wine samples to their variety were performed with an 80% of success on average (Godelmann, et al. 2013).

According to the same author, the possibility to use information coming from not classified peaks makes it possible to increase the model predictability up to 95% or, the application of chemometrics tools together with non-targeted approaches allows an higher amount of information extraction from the NMR spectra. Nevertheless, the targeted approach still remains an effective analytical tool for wine provenience classification: the possibility to discriminate wine according their nationality (Brescia et al. 2003) or even between closer production areas (Brescia et al. 2002) should not be neglected. In fact, the aforementioned authors proved the data extracted from NMR spectra to be more informing if compared to the one obtained through classical analysis, namely high-performance ion chromatography exclusion (HPICE) in hyphenation with inductively coupled plasma optical emission spectroscopy (ICP-OES).

6.1.2. ^{1}H NMR Fingerprinting

As it can be seen in Figure 11, minor peaks, to which no compositional information is associated, are present. Thanks to the binning procedure, the spectrum is divided into smaller intervals, to proceed calculating the area below the NMR line (Fan et al. 2018). Binning operation is a pre-analytical data treatment used to both reduce the amount of data and explore unknown variability sources. These areas are used as variables during multivariate statistical analysis (Godelmann et al. 2013), making each spectrum as a unique wine fingerprint. The information amount extracted from each sample is much larger than the ones obtained applying a targeted approach. As highlighted in Paragraphs 4.2.1. and 4.2.3., the increase in number of variables used during wine samples classification could lead to collinearity problems (Næs et al. 2001); in addition, since the real parameters explaining the wine chemical variability sources are not known, it is possible to incur in overfitting issue (Melucci 2015). The increasing in amount of information could clarify the model behaviour. Both these problems can find solution by the application of data mining or other statistical tools. The PCA is the most applied

exploratory analysis during NMR spectra interpretation since, beside solving the abovementioned issues, it permits to regroup sample through non-guided clustering. Contemporary, the possibility to inspect the variable affecting each principal component (PC) informs on the source of variability of the dataset: inspecting several chemical species could allow to decrypt conditions (environmental, technological,...) which are affecting their concentration. Recently, thanks to fingerprinting approach, many wine classification advances in terms of vintage, geographical origin, variety, and applied technology have been done. The possibility to relate wine terroir, intended as microclimate, soil composition and applied technologies, has been demonstrated (Mazzei et al. 2010). Differences between wines fermented by commercial yeasts strains or autochthonous ones was also shown (Mazzei et al. 2013) indicating another source of data variability. In both projects sample differentiation was obtained, and the greatest data explanation came by the lactic acid, glycerol, fructose, succinic acid, and glucose spectral areas. Both these examples showed wine characterization fermentation (alcoholic and malolactic) related compounds is possible. During varietal wine characterization both targeted and non-targeted approaches was compared (Godelmann et al. 2013) showing an increasing in correct sample prediction (from 80% to 95%) in case of whole ^{1}H NMR spectra use. According to the same author, the procedure made it possible to correctly associate the samples to their geographical origin (> 90%) and vintage (97.5% on average). These are just examples about ^{1}H NMR spectroscopy application on wine since similar approaches were effectively used to inspect different food matrices characteristics (Esteki et al. 2018) proving the technology plasticity.

Both the fingerprinting and profiling procedures require the possibility to compare spectral data with pre-existing databases. In order to contribute to the wine and honey authenticity assessment, Bruker company started collecting wine samples from different varietal, vintage and geographical origin to create a specific database containing all this information. By continuously updating the stored data it will be possible in the future to reduce the error associated to the compositional variability of wines during multivariate statistical analysis thus reducing producers' tools for wine mislabelling.

6.2. Wine ^{1}H NMR Relaxometry Modelling as a Tool for Mislabelling Detection

We have seen how the use of harmonic analysis (Fourier transform) in relaxation models allows to extract wines compositional information. These procedures involve obtaining spectra at a specific wavelength, so as to make the spectral line densities comparable through a "concentration as a function of peak area" proportionality. As discussed, the application of

relaxation models (BPP, IS, OS) allows to obtain molecular motion information by extracting the correlation time (τ_i) starting from relaxation variation as a function of the applied field intensity. In fact, the ability to relax the magnetization induced by the applied magnetic field is a consequence of samples composition and physical state. The inspection of paramagnetic ions behaviours, namely gadolinium(III) and manganese(II), in aqueous solution has the main goal to optimise their use as contrast agents during magnetic resonance imaging. However, the possibility to use such particle as chemical probes for wine classification remains to be discussed. According to the inner- and outer-sphere models, the linear proportionality between paramagnetic species concentration and sample relaxation enhancement always depends on the relaxivity value (Eq. 28). In principle, this term is specific per each type of ion and varies as a function of the corresponding acquisition frequency but, since they also result by all the correlation times coordination, we should not run to conclude the sample classification to be possible only according to the relaxation rate magnitude. In addition, the wine compositional complexity does not allow to exclude *"a priori"* the presence two or more paramagnetic contributions. By changing prospective to look at this as a positive situation, the amount of information conveyed by the differences in relaxivity values is much higher. If we assume the r_v value to be always the same, even changing the wine type and/or its composition, the use of IS and OS models will be interesting only for quantitation purpose.

Through mathematical modelling software, some generic (e.g. MATLAB, Origin, R) while others more specific (https://sites.google.com/tecnico.ulisboa.pt/fitteia), together with error minimization techniques (e.g. least square minimization), it is possible to draw non-linear models to explain the relaxation dispersion as a function of frequency: this procedure is called chi square-fitting (William et al. 2002). To do that, it is essential the number of free parameters, namely the unknown variable characterizing the function envelope, to be smaller than the dataset degrees of freedom (DOF). The number of variable and parameter which are involved in this type of modelling is extremely high; in order to optimize the fitting procedure, some of them can be obtained thanks to the application of other analytical technique (X-ray, densimeter, ...) or rather extracted by bibliographic databases. After the best fitting parameters have been obtained, to compare the latter with other know systems (hydroalcoholic, water-ions solutions) make it possible to draw conclusion regarding sample molecular dynamics and the differences' sources in the relaxation rate dispersions. These final assumptions should be strengthened by other sample analytical characterizations: for this purpose, wine viscosity, pH, glycerol content, alcoholic volume and other physical-chemical information will be extremely important.

There are several bibliographic cases trying to explain the relaxation rate in samples differing in the type of solvent: Ludwig (1995) found a reduction in relaxation time as the concentration of alcohols such as methanol (CH_4O), ethanol (C_2H_6O) and 1-propanol (C_3H_8O) increases. This behaviour is explained by a simultaneous increase in the dielectric (τ_d) and rotational (τ_c) correlation constants of water molecules. The two phenomena considered individually are respectively explained by the reduction of spin density and "hydrophobic hydration" phenomena. What about to use a paramagnetic particle as a probe in different solvent systems? During the characterization of water/glycerol mixtures in the presence of manganese particles (Mn^{2+}) (Bertini 1993), at increasing concentrations of the second solvent, two independent effects were highlighted (Fig. 12): as far as low frequency dispersion (< 0.1 MHz) is concerned, after the addition of glycerol, it was possible to report an increase in the relaxation rate; this phenomenon is caused by a substantial τ_e reduction (Eq. 30). Similarly, the increase in glycerol concentration show itself even at in the high frequencies range (> 10 MHz) because of the reduction of the rotational correlation constant τ_R (dipolar coupling, Eq. 31).

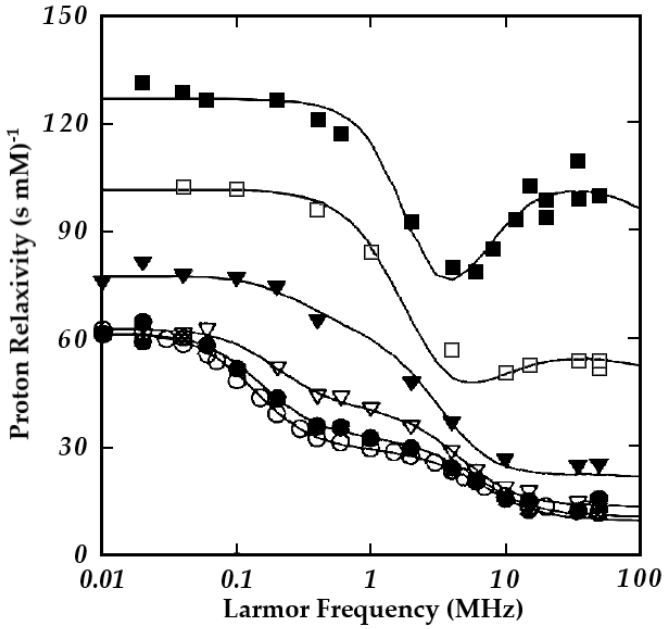

Figure 12. Water ^{1}H NMRD profiles of $Mn(OH)_6^{2+}$ (hexaaqua) solutions at 288 K in pure water (○) and with increasing amounts of d8-glycerol: 10% (●), 20% (▽), 35% (▼), 55% (□), 65% (■) (Bertini et al. 1993).

More recently, Bodart et al. (2020) tried to create an analytical protocol to quantify wine manganese content from relaxation rate profile/reading in the low-frequency region (< 10 MHz); still an evaluation on how other paramagnetic elements (e.g. Fe^{3+}) and/or changes in their oxidation state could affect each wine type relaxivity. Such information can be obtained by changing wine composition or analytical conditions: one possibility is to obtain the same

relaxation rate dispersion at different temperatures to eliminate some competing sources of variability.

6.2.1. Modelling on Wine Samples

Thanks to the joint use of fast field-cycling and super magnet relaxometer, together with specific sequences application, the relaxation dependence on frequency for a wine sample is shown in Figure 13. Since wine is known to contain different paramagnetic elements, namely Fe, Mn, Cu, Ni (Nickel) and Cd (Cadmium) (Bodart et al. 2020), the possibility to inspect low frequency ($<$ 10 MHz) relaxation rate dispersions is crucial for sample characterization purpose. During wine production the use bentonite is well known responsible for elemental profile changes in all of these mineral elements (Catarino et al. 2008a,b) so, the possibility to assess sample characterization according to geographical origin, vintage and variety should by discussed. Focussing on wine iron and manganese contents, important changes during the alcoholic fermentation can occur; in particular, red wines show an increasing in mineral loss probably as a consequence of the higher pH values. In fact, the concentration variation is both consequence of insoluble sulphides salts formation and ions lower solubility in hydro-alcoholic solutions. The presence of sulphur dioxide will increase the insoluble salt formation (Catarino et al. 2006) increasing the uncertainty source during wine characterization since its concentration varies depending on both human choices and oenological needing.

What follows is just an example on how you to draw a wine model by measuring T_1 variation by changing resonant frequency: in paragraph 5.6. we discussed how the relaxation rate could be divided into individual additive contributions; what does this mean from an experimental point of view? The model in Figure 13 represents the relaxation rate readings obtained on a red Portuguese wine, namely Touriga Nacional: the black continuous line is drawn by the cumulative contributions coming by BPP model (simulating the R_{diam}, Eq. 27), together with inner-sphere (Eq. 29) and outer-sphere (Eq. 33) paramagnetic ones. In this case, the first was obtained by measuring the T_1 times on water-alcoholic solution at increasing ethanol content. Since the rotation-diffusion correlation time (τ, Eq. 27) and the corresponding longitudinal relaxation rate, was already proven to be linearly dependent on the water/ethanol molar ratio (Ludwig 1995), a linear interpolation in the 11-17%vol range was used. This approach allows to compare wines without considering solvent contributions to the relaxation rate or, it makes possible a comparison only according to the specific wine compositional variation.

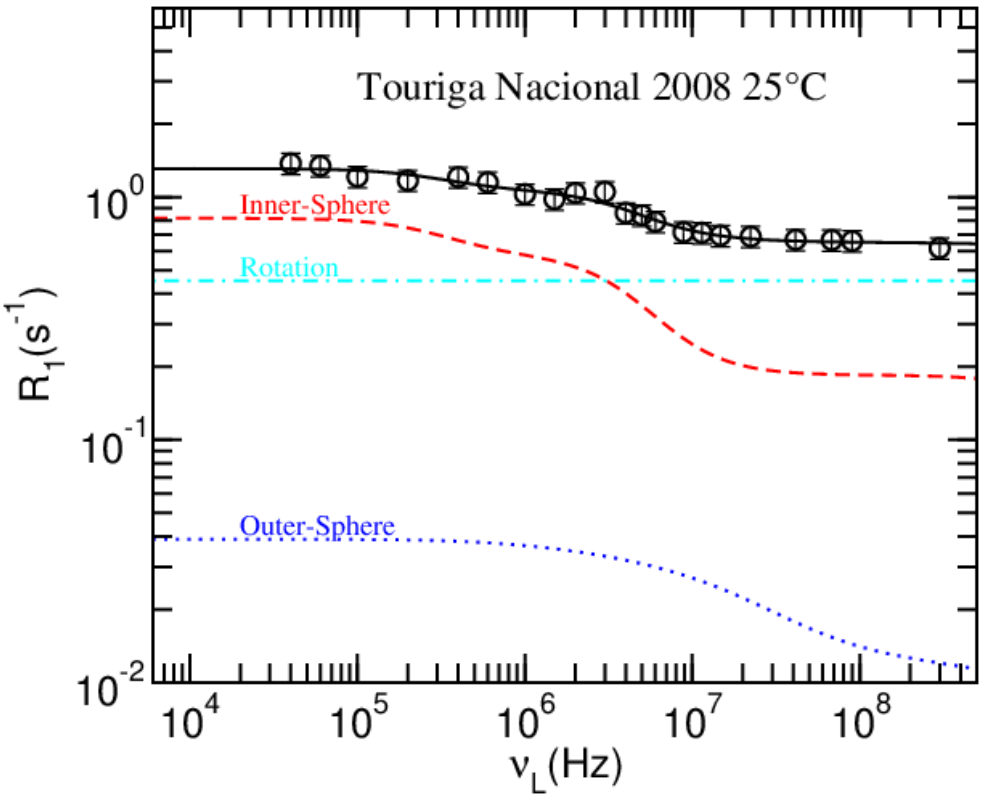

Figure 13. Relaxation rate (s^{-1}) dispersion as a function of frequency (Hz) of red wine sample (Touriga Nacional). The readings where obtained in the 0.04-300 MHz frequency range. Three independent contribution, namely inner-sphere (dashed red line), outer-sphere (dashed blue line) and rotational-diffusional (dashed cyan line), are shown.

7. General Considerations

Different approaches have been described in the categorical classification of wine samples giving greater importance to the information contained in the isotopic ratios and deriving from the chemometrics interpretation of the ^{1}H NMR spectral images: in the first case it was shown how, deeply investigating the isotopic fractionation processes, it was possible to develop an official analytical method to face chaptalization and/or water addition; in the second case the intent was to stress how the spectral information is able to code for the vintage and the geographical, varietal, technological and compositional characterization but, due to the high number of environmental factors which impact on fingerprint, the use of chemometrics tools in conjunction with an increase in the amount of available information is required. Some perplexity regarding the "a priori" samples classification through discriminant analysis (Rodionova et al. 2016) must be clarified. A solution could come from database implementation to increase both compositional and spectral available data. In conclusion, wine is a complex matrix: his composition varies as a function of environmental-genetic expression, technological practices and wine age (Cassino et al. 2019). Therefore, wine classification requires a wide range of knowledges and huge amount of data availability.

Wine modelling through relaxometry models is a recent proposal (Bodart et al. 2020). The possibility to observe sample differentiation according to the belonging categories still needs a refinement in the relaxation profiles. In order to ensure the reliability of method, wine's physical-chemical characteristics should be individually referred to variations in the relaxation rate dispersion: A deep knowledge on wine chemical composition is required together with more experimental data availability.

7. References

Albrand, J., Taieb, M., Fries, P., & Belorizky, E. (1983). NMR study of spectral densities over a large frequency range for intermolecular relaxation in liquids: pair correlation effects. *The Journal of Chemical Physics*, **78**(**9**), 5809–5815.

Anastasiadi, M., Zira, A., Magiatis, P., Haroutounian, S., Skaltsounis, A., & Mikros, E. (2009). ^{1}H NMR-based metabonomics for the classification of Greek wines according to variety, region, and vintage. Comparison with HPLC data. *Journal of Agricultural and Food Chemistry*, **57**(**23**), 11067–11074.

Aru, V., Sørensen, K., Khakimov, B., Toldam-Andersen, T., & Balling Engelsen, S. (2018). Coolclimate red wines—chemical composition and comparison of two protocols for ^{1}H–NMR analysis. *Molecules*, **23**(**1**), 160.

Asimov, E. (2009). Brunello inquiry cites five wineries. *The New York Times*, 12 August.

Ayant, Y., Belorizky, E., Aluzon, J., & Gallice, J. (1975). Calcul des densités spectrales resultant d'un mouvement aléatoire de translation en relaxation par interaction dipolaire magnétique dans les liquides. *Journal de Physique*, **36**(**10**), 991–1004.

Bautista-Ortín, A., Busse-Valverde, N., Fernández-Fernández, J., Gómez-Plaza, E., & Gil-Muñoz, R. (2016). The extraction kinetics of anthocyanins and proanthocyanidins from grape to wine in three different varieties. *OENO One*, **50**(**2**), 91–100.

Bavaresco, L., Pezzutto, S., Gatti, M., & Mattivi, F. (2007). Role of the variety and some environmental factors on grape stilbenes. *Vitis*, **46**(**2**), 57–61.

Bender, M. (1971). Variations in the ^{13}C/^{12}C ratios of plants in relation to the pathway of photosynthetic carbon dioxide fixation. *Phytochemistry*, **10**(**6**), 1239–1244.

Berrueta, L.A., Rasines-Perea, Z., Prieto-Perea, N., Asensio-Regalado, C., Alonso-Salces, R.M., Sánchez-Ilárduya, M. B., & Gallo, B. (2020). Formation and evolution profiles of anthocyanin derivatives and tannins during fermentations and aging of red wines. *European Food Research and Technology*, **246**(**1**), 149-165.

Bertini, I., Briganti, F., Xia, Z., & Luchinat, C. (1993). Nuclear magnetic relaxation dispersion studies of hexaaquo Mn (ii) ions in water-glycerol mixtures. *Journal of Magnetic Resonance*, **101**, 198–201.

Bertini, I., Luchinat, C., Parigi, G., & Ravera, E. (2017). *NMR of Paramagnetic Molecules: Applications to Metallobiomolecules and Models*. (Chap. 1, pp. 1-24). Elsevier.

Bloch, F. (1946). Nuclear induction. *Physical Review*, **70**(**7**–**8**), 460–474.

Bloembergen, N., & Morgan, L. (1961). Proton relaxation times in paramagnetic solutions. Effects of electron spin relaxation. *The Journal of Chemical Physics*, **34**(**3**), 842–850.

Bloembergen, N., Purcell, E. M., & Pound, R. V. (1948). Relaxation effects in nuclear magnetic resonance absorption. *Physical Review*, **73**(**7**), 679.

Bodart, P.R., Rachocki, A., Tritt-Goc, J., Michalke, B., Schmitt-Kopplin, P., Karbowiak, T., & Gougeon, R.D. (2020). Quantification of manganous ions in wine by NMR relaxometry. *Talanta*, **209**, 120561.

Bora, D., Donici, A., Teodor, R., Bunea, A., Popescu, D., & Bunea, C. (2018). Elemental profile and $^{207}Pb/^{206}Pb$, $^{208}Pb/^{206}Pb$, $^{204}Pb/^{206}Pb$, $^{87}Sr/^{86}Sr$ isotope ratio as fingerprints for geographical traceability of Romanian wines. *Notulae Botanicae Horti Agrobotanici Cluj*, **46**(**1**), 223–239.

Bosso, A., Guaita, M., Panero, L., Borsa, D., & Follis, R. (2009). Influence of two winemaking techniques on polyphenolic composition and color of wines. *American Journal of Enology and Viticulture*, **60**(**3**), 379–385.

Bréas, O., Reniero, F., Serrini, G., Martin, G., & Rossmann, A. (1994). Isotope ratio mass spectrometry: analysis of wines from different European countries. *Rapid Communications in Mass Spectrometry*, **8**(**12**), 967–970.

Brescia, M., Caldarola, V., De Giglio, A., Benedetti, D., Fanizzi, F., & Sacco, A. (2002). Characterization of the geographical origin of Italian red wines based on traditional and nuclear magnetic resonance spectrometric determinations. *Analytica Chimica Acta*, **458**(**1**), 177–186.

Brescia, M., Košir, I., Caldarola, V., Kidrič, J., & Sacco, A. (2003). Chemometric classification of Apulian and Slovenian wines using ^{1}H NMR and ICP-OES together with HPICE data. *Journal of Agricultural and Food Chemistry*, **51**(**1**), 21–26.

Bushberg, J., & Boone, J. (2011). *The Essential Physics of Medical Imaging*. (Chap 12, pp. 415-420). Lippincott Williams & Wilkins

Canals, R., Llaudy, M., Valls, J., Canals, J., & Zamora, F. (2005). Influence of ethanol concentration on the extraction of color and phenolic compounds from the skin and seeds of Tempranillo grapes at different stages of ripening. *Journal of Agricultural and Food Chemistry*, **53**(**10**), 4019–4025.

Cassino, C., Tsolakis, C., Bonello, F., Gianotti, V., & Osella, D. (2019). Wine evolution during bottle aging, studied by ^{1}H NMR spectroscopy and multivariate statistical analysis. *Food Research International*, **116**, 566–577.

Castellarin, S., Pfeiffer, A., Sivilotti, P., Degan, M., Peterlunger, E., & Di Gaspero, G. (2007). Transcriptional regulation of anthocyanin biosynthesis in ripening fruits of grapevine under seasonal water deficit. *Plant, Cell & Environment*, **30**(**11**), 1381–1399.

Catarino, S., Capelo, J.-L., Curvelo-García, A., & De Sousa, R. (2006). Evaluation of contaminant elements in Portuguese wines and original musts by high intensity focused ultrasound combined with inductively coupled plasma mass spectrometry. *OENO One*, **40**(**2**), 91–100.

Catarino, S., Curvelo-Garcia, A., & Sousa, R. (2008a). Revisao: Elementos contaminantes nos vinhos. *Ciência e Técnica Vitivinicola*, **23**(**1**), 3–19.

Catarino, S., Madeira, M., Monteiro, F., Rocha, F., Curvelo-Garcia, A., & De Sousa, R. (2008b). Effect of bentonite characteristics on the elemental composition of wine. *Journal of Agricultural and Food Chemistry*, **56**(**1**), 158–165.

Catarino, S., Trancoso, I., Madeira, M., Monteiro, F., Bruno de Sousa, R., & Curvelo-Garcia, A. (2011). Rare earths data for geographical origin assignment of wine: a Portuguese case study. *Bulletin de l'OIV*, **84**, 333–346.

Catarino, S., Madeira, M., Monteiro, F., Caldeira, I., Bruno de Sousa, R., & Curvelo-Garcia, A. (2018). Mineral composition through soil-wine system of Portuguese vineyards and its potential for wine traceability. *Beverages*, **4**(**4**), 85.

Cheng, J., & Liang, C. (2012). The variation of mineral profiles from grape juice to monovarietal Cabernet Sauvignon wine in the vinification process. *Journal of Food Processing and Preservation*, **36**(**3**), 262–266.

Christoph, N., Hermann, A., & Wachter, H. (2015). 25 years authentication of wine with stable isotope analysis in the European Union–review and outlook. *BIO Web of Conferences*, **5**, 02020.

Coetzee, P., & Vanhaecke, F. (2005). Classifying wine according to geographical origin via quadrupole-based ICP–mass spectrometry measurements of boron isotope ratios. *Analytical and Bioanalytical Chemistry*, **383**(**6**), 977–984.

Craig, H. (1961). Isotopic variations in meteoric waters. *Science*, **133**(**3465**), 1702–1703.

Danezis, G., Tsagkaris, A., Brusic, V., & Georgiou, C. (2016). *Food authentication: state of the art and prospects. Current Opinion in Food Science*, **10**, 22–31.

Diamond, J. (2005). *Collapse: How Societies Choose to Fail or Succeed*. 80 Strand, London, UK: Penguin Books.

Dinca, O.-R., Ursu, S., Costinel, D., Popescu, R., Miricioiu, M., Radu, G.-L., Popa, D.V., Campeanu, C.B., & Elena, R. (2015). Samburesti wines characterization in terms of their stable isotope content. *UPB Science Bulletin*, **77**(**4**), 176–187.

Doan, B.-T., Meme, S., & Beloeil, J.-C. (2013). General principles of MRI. In A. Merbach, L. Helm, & É. Tóth (Eds.), *The Chemistry of Contrast Agents in Medical Magnetic Resonance Imaging* (Chap. 1, pp. 1-23). John Wiley & Sons.

Dongmann, G., Nürnberg, H., Förstel, H., & Wagener, K. (1974). On the enrichment of $H_2{}^{18}O$ in the leaves of transpiring plants. *Radiation and Environmental Biophysics*, **11**(**1**), 41–52.

Dowdy, S., Wearden, S., & Chilko, D. (2004). *Statistics for Research*. John Wiley & Sons.

Dunbar, J. (1982). A study of the factors affecting the $^{18}O/^{16}O$ ratio of the water of wine. *Zeitschrift für Lebensmittel-Untersuchung und Forschung*, **174**(**5**), 355–359.

English, N., Betancourt, J., Dean, J., & Quade, J. (2001). Strontium isotopes reveal distant sources of architectural timber in Chaco Canyon, New Mexico. *Proceedings of the National Academy of Sciences*, **98**(**21**), 11891–11896.

Esteki, M., Shahsavari, Z., & Simal-Gandara, J. (2018). Use of spectroscopic methods in combination with linear discriminant analysis for authentication of food products. *Food Control*, **91**, 100–112.

Everstine, K., Spink, J., & Kennedy, S. (2013). Economically motivated adulteration (EMA) of food: common characteristics of EMA incidents. *Journal of Food Protection*, **76**(**4**), 723–735.

Fan, S., Zhong, Q., Fauhl-Hassek, C., Pfister, M.-H., Horn, B., & Huang, Z. (2018). Classification of Chinese wine varieties using ^{1}H NMR spectroscopy combined with multivariate statistical analysis. *Food Control*, **88**, 113–122.

Farquhar, G., O'Leary, M., & Berry, J. (1982). On the relationship between carbon isotope discrimination and the intercellular carbon dioxide concentration in leaves. *Functional Plant Biology*, **9**(**2**), 121–137.

Farrar, T., & Becker, E. (1971a), In *Pulse and Fourier Transform NMR: Introduction to Theory and Methods* (Chap. 1, pp. 1–17). Academic Press.

Farrar, T., & Becker, E. (1971b), In *Pulse and Fourier Transform NMR: Introduction to Theory and Methods* (Chap. 2, pp. 18-33). Academic Press.

Farrar, T., & Becker, E. (1971c), In *Pulse and Fourier Transform NMR: Introduction to Theory and Methods* (Chap 3, pp. 34-45). Academic Press.

Farrar, T., & Becker, E. (1971d), In *Pulse and Fourier Transform NMR: Introduction to Theory and Methods* (Chap. 4, pp. 46-65). Academic Press.

Faure, G., & Powell, J. (1972). Strontium Isotope Geology. In *Minerals, Rocks and Inorganic Materials* (Chap. 1, pp. 1-8). Heidelberg, DE: Springer-Verlag.

Ferrandino, A., Carra, A., Rolle, L., Schneider, A., & Schubert, A. (2012). Profiling of hydroxycinnamoyl tartrates and acylated anthocyanins in the skin of 34 Vitis vinifera genotypes. *Journal of Agricultural and Food Chemistry*, **60**(**19**), 4931–4945.

Ferreira, R., Monteiro, S., Piçarra-Pereira, M., Tanganho, M., Loureiro, V., & Teixeira, A. (2000). Characterization of the proteins from grapes and wines by immunological methods. *American Journal of Enology and Viticulture*, **51**(**1**), 22–28.

Ferreira, R., Piçarra-Pereira, M., Monteiro, S., Loureiro, V., & Teixeira, A. (2001). The wine proteins. *Trends in Food Science & Technology*, **12**(**7**), 230–239.

Formisyn, P., Vaillant, H., Lantreibecq, F., & Bourgois, J. (1997). Development of an enzymatic reactor for initiating malolactic fermentation in wine. *American Journal of Enology and Viticulture*, **48**(**3**), 345–351.

French, A., & Taylor, F. (2000). *An introduction to quantum physics*. Boca Raton, Florida 33431: CRC PRESS.

Fries, P., & Belorizky, E. (1978). Effets des fonctions de corrélation de paire sur la relaxation nucléaire intermoléculaire par diffusion translationnelle et rotationnelle dans les liquides. *Journal de Physique*, **39**(**12**), 1263–1282.

Geană, E.-I., Sandru, C., Stanciu, V., & Ionete, R. (2017). Elemental profile and $^{87}Sr/^{86}Sr$ isotope ratio as fingerprints for geographical traceability of wines: an approach on Romanian wines. *Food Analytical Methods*, **10**(**1**), 63–73.

Gill, R., Mayewski, P., Nyberg, J., Haug, G., & Peterson, L. (2007). Drought and the Maya collapse. *Ancient Mesoamerica*, **18**(**2**), 283–302.

Godelmann, R., Fang, F., Humpfer, E., Schütz, B., Bansbach, M., Schäfer, H., & Spraul, M. (2013). Targeted and nontargeted wine analysis by ^{1}H NMR spectroscopy combined with multivariate statistical analysis. Differentiation of important parameters: grape variety, geographical origin, year of vintage. *Journal of Agricultural and Food Chemistry*, **61**(**23**), 5610–5619.

Godelmann, R., Kost, C., Patz, C.-D., Ristow, R., & Wachter, H. (2016). Quantitation of compounds in wine using ^{1}H NMR spectroscopy: description of the method and collaborative study. *Journal of AOAC International*, **99**(**5**), 1295–1304.

Granato, D., Putnik, P., Kovačević, D., Santos, J., Calado, V., Rocha, R., Da Cruz, A., Jarvis, B., Rodionova, O., & Pomerantsev, A. (2018). Trends in chemometrics: food authentication, microbiology, and effects of processing. *Comprehensive Reviews in Food Science and Food Safety*, **17**(**3**), 663–677.

Halliday, D., Resnick, R., & Walker, J. (2013a), In *Fundamentals of Physics* (Chap. 1, pp. 2-22). Hoboken, US-NJ: John Wiley & Sons.

Halliday, D., Resnick, R., & Walker, J. (2013b), In *Fundamentals of Physics* (Chap. 11, pp. 327-360). Hoboken, US-NJ: John Wiley & Sons.

Halliday, D., Resnick, R., & Walker, J. (2013c), In *Fundamentals of Physics* (Chap. 15, pp. 458-487). Hoboken, US-NJ: John Wiley & Sons.

Halliday, D., Resnick, R., & Walker, J. (2013d). In *Fundamentals of Physics* (Chap. 18, pp. 545-577). Hoboken, US-NJ: John Wiley & Sons.

Halliday, D., Resnick, R., & Walker, J. (2013e), In *Fundamentals of Physics* (Chap. 29, pp. 904-936). Hoboken, US-NJ: John Wiley & Sons.

Halliday, D., Resnick, R., & Walker, J. (2013f), In *Fundamentals of Physics* (Chap. 30, pp. 937-978). Hoboken, US-NJ: John Wiley & Sons.

Halliday, D., Resnick, R., & Walker, J. (2013g), In *Fundamentals of Physics* (Chap. 31, pp. 979-1013). Hoboken, US-NJ: John Wiley & Sons.

Halliday, D., Resnick, R., & Walker, J. (2013h), In *Fundamentals of Physics* (Chap. 34, pp. 1075-1103). Hoboken, US-NJ: John Wiley & Sons.

Haynes, M., Lide, R., & Brun, J. (2014). *CRC Handbook of Chemistry and Physics* (pp. 1/12-1/15). Boca Raton, US-FL: CRC Press.

He, F., Liang, N., Mu, L., Pan, O., Wang, J., Reeves, M.J., & Duan, C. (2012). Anthocyanins and their variation in red wines II. Anthocyanin derived pigments and their color evolution. *Molecules*, **17**, 1420-3049.

Holmberg, L. (2010). Wine fraud. *International Journal of Wine Research*, **2**(**1**), 105–113.

OIV. International Organisation of Vine and Wine (2019a). *Compendium of International Methods of Wine and Must Analysis*. International Organisation of Vine and Wine: Paris, France, **1**.

OIV. International Organisation of Vine and Wine (2019b). *Compendium of International Methods of Wine and Must Analysis*. International Organisation of Vine and Wine: Paris, France, **2**.

Jin, Z.-M., He, J.-J., Bi, H.-Q., Cui, X.-Y., & Duan, C.-Q. (2009). Phenolic compound profiles in berry skins from nine red wine grape cultivars in northwest China. *Molecules*, **14**(**12**), 4922–4935.

Kaya, A., Bruno de Sousa, R., Curvelo-Garcia, A., Ricardo-da-Silva, J., & Catarino, S. (2017). Effect of wood aging on wine mineral composition and $^{87}Sr/^{86}Sr$ isotopic ratio. *Journal of Agricultural and Food Chemistry*, **65**(**23**), 4766–4776.

Keeler, J. (2002). *Understanding NMR Spectroscopy*. (pp. 2/1-2/19). Hoboken, New Jersey: John Wiley & Sons.

Kimmich, R., & Anoardo, E. (2004). Field-cycling NMR relaxometry. *Progress in Nuclear Magnetic Resonance Spectroscopy*, **44**(**3**-**4**), 257–320.

Košir, I., & Kidrič, J. (2002). Use of modern nuclear magnetic resonance spectroscopy in wine analysis: determination of minor compounds. *Analytica Chimica Acta*, **458**(**1**), 77–84.

Lauffer, R.B. (1987). Paramagnetic metal complexes as water proton relaxation agents for NMR imaging: Theory and design. *Chemical Reviews*, **87**(**5**), 901–927.

Lerno, L., Reichwage, M., Ponangi, R., Hearne, L., Block, D., & Oberholster, A. (2015). Effect of cap and overall fermentation temperature on phenolic extraction in Cabernet Sauvignon fermentations. *American Journal of Enology and Viticulture*, **66**(**4**), 444–453.

Loira, I., Morata, A., Palomero, F., González, C., & Suárez-Lepe, J. (2018). Schizosaccharomyces pombe: A promising biotechnology for modulating wine composition. *Fermentation*, **4**(**3**), 70.

López-Rituerto, E., Savorani, F., Avenoza, A., Busto, J. H., Peregrina, J. M., & Engelsen, S. B. (2012). Investigations of La Rioja terroir for wine production using ^{1}H NMR metabolomics. *Journal of Agricultural and Food Chemistry*, **60**(**13**), 3452–3461.

Ludwig, R. (1995). NMR relaxation studies in water-alcohol mixtures: The water-rich region. *Chemical Physics*, **195**(**1**-**3**), 329–337.

Maicas, S. (2001). The use of alternative technologies to develop malolactic fermentation in wine. *Applied Microbiology and Biotechnology*, **56**(**1**-**2**), 35–39.

Marguerit, E., Brendel, O., Lebon, E., Van Leeuwen, C., & Ollat, N. (2012). Rootstock control of scion transpiration and its acclimation to water deficit are controlled by different genes. *New Phytologist*, **194**(**2**), 416–429.

Marini, F. (2013). *Chemometrics in Food Chemistry* (Chap. 3, pp. 62-114). Elsevier.

Martin, G., Martin, M., Mabon, F., & Michon, M. (1982). Identification of the origin of natural alcohols by natural abundance hydrogen-2 nuclear magnetic resonance. *Analytical Chemistry*, **54**(**13**), 2380–2382.

Martin, G., Martin, M., Mabon, F., & Michon, M. (1983). A new method for the identification of the origin of ethanols in grain and fruit spirits: high-field quantitative deuterium nuclear magnetic resonance at the natural abundance level. *Journal of Agricultural and Food Chemistry*, **31**(**2**), 311–315.

Martin, G., Danho, D., & Vallet, C. (1991). Natural isotope fractionation in the discrimination of sugar origins. *Journal of the Science of Food and Agriculture*, **56**(**4**), 419–434.

Martins, P., Madeira, M., Monteiro, F., De Sousa, R., Curvelo-Garcia, A., & Catarino, S. (2014). ^{87}Sr/^{86}Sr ratio in vineyard soils from Portuguese denominations of origin and its potential for origin authentication. *Journal International des Sciences de la Vigne et du Vin One*, **48**(**1**), 21–29.

Mazzei, P., Francesca, N., Moschetti, G., & Piccolo, A. (2010). NMR spectroscopy evaluation of direct relationship between soils and molecular composition of red wines from Aglianico grapes. *Analytica Chimica Acta*, **673**(**2**), 167–172.

Mazzei, P., Spaccini, R., Francesca, N., Moschetti, G., & Piccolo, A. (2013). Metabolomic by ^{1}H NMR spectroscopy differentiates “Fiano di Avellino” white wines obtained with different yeast strains. *Journal of Agricultural and Food Chemistry*, **61**(**45**), 10816–10822.

Medina, B., Augagneur, S., Barbaste, M., Grousset, F., & Buat-Ménard, P. (2010). Influence of atmospheric pollution on the lead content of wines. *Food Additives & Contaminants*, **17**(**6**), 435–445.

Medina, S., Perestrelo, R., Silva, P., Pereira, J. A., & Câmara, J. (2019). Current trends and recent advances on food authenticity technologies and chemometric approaches. *Trends in Food Science & Technology*, **85**, 163–176.

Meija, J., Coplen, T., Berglund, M., Brand, W., De Bièvre, P., Gröning, M., Olden, N.E., Irrgeher, J., Loss, R.D., Walczyk, T., & Prohaska, T. (2016). Isotopic compositions of the elements 2013 (IUPAC technical Report). *Pure and Applied Chemistry*, **88**(**3**), 293–306.

Meloni, G., & Swinnen, J. (2013). The political economy of European wine regulations. *Journal of Wine Economics*, **8**(**3**), 244–284.

Melucci, D. (2015). Lezioni ed esercizi di chemometria per la chimica analitica. Retrieved from https://www.researchgate.net/publication/50432799_Lezioni_ed_esercizi_di_CHEMIOMETRIA_per_la_Chimica_Analitica.

Monakhova, Y., Godelmann, R., Hermann, A., Kuballa, T., Cannet, C., Schäfer, H., Spraul, M., & Rutledge, D. (2014). Synergistic effect of the simultaneous chemometric analysis of ^{1}H NMR spectroscopic and stable isotope (SNIF-NMR, ^{18}O, ^{13}C) data: Application to wine analysis. *Analytica Chimica Acta*, **833**, 29–39.

Moreira, C., de Pinho, M., Curvelo-Garcia, A., de Sousa, B., Ricardo-da-Silva, J., & Catarino, S. (2017). Evaluating nanofiltration effect on wine ^{87}Sr/^{86}Sr isotopic ratio and the robustness of this geographical fingerprint. *South African Journal of Enology and Viticulture*, **38**(**1**), 82-93.

Næs, T., & Mevik, B.-H. (2001). Understanding the collinearity problem in regression and discriminant analysis. *Journal of Chemometrics*, **15**(**4**), 413–426.

Ogrinc, N., Košir, I., Kocjančič, M., & Kidrič, J. (2001). Determination of authenticy, regional origin, and vintage of Slovenian wines using a combination of IRMS and SNIF-NMR analyses. *Journal of Agricultural and Food Chemistry*, **49**(**3**), 1432–1440.

Oliveira, J.. Azevedo, J., Silva, A.M.S., Teixeira, N., Cruz, L., Mateus, N., & de Freitas, V. (2010). Pyranoanthocyanin dimers: a new family of turquoise blue anthocyanin-derived pigments found in Port wine. *Journal of Agricultural and Food Chemistry*, **58**, 5154-5159.

Paris, W. (2002). Top French wine diluted and sold with fake labels. *The Observer*, 24 February.

Pereira, G., Gaudillere, J.-P., Pieri, P., Hilbert, G., Maucourt, M., Deborde, C., Moing, A., & Rolin, D. (2006). Microclimate influence on mineral and metabolic profiles of grape berries. *Journal of Agricultural and Food Chemistry*, **54**(**18**), 6765–6775.

Petrini, R., Sansone, L., Slejko, F., Buccianti, A., Marcuzzo, P., & Tomasi, D. (2015). The ^{87}Sr/^{86}Sr strontium isotopic systematics applied to Glera vineyards: a tracer for the geographical origin of the Prosecco. *Food Chemistry*, **170**, 138–144.

Pocock, K., Hayasaka, Y., McCarthy, M., & Waters, E. (2000). Thaumatin-like proteins and chitinases, the haze-forming proteins of wine, accumulate during ripening of grape (Vitis vinifera) berries and drought stress does not affect the final levels per berry at maturity. *Journal of Agricultural and Food Chemistry*, **48**(**5**), 1637–1643.

Redan, B., Jablonski, J., Halverson, C., Jaganathan, J., Mabud, M.A., & Jackson, L. (2019). Factors affecting transfer of the heavy metals arsenic, lead, and cadmium from diatomaceous-earth filter aids to alcoholic beverages during laboratory-scale filtration. *Journal of Agricultural and Food Chemistry*, **67**(**9**), 2670–2678.

Ribéreau-Gayon, P., Glories, Y., Maujean, A., & Dubourdieu, D. (2006a). *Handbook of Enology, Volume 2: The Chemistry of Wine-Stabilization and Treatments (2. ed.)*. (Chap. 1, pp. 3-49). West Sussex, UK: John Wiley & Sons.

Ribéreau-Gayon, P., Glories, Y., Maujean, A., & Dubourdieu, D. (2006b). *Handbook of Enology, Volume 2: The Chemistry of Wine-Stabilization and Treatments (2. ed.)*. (Chap. 5, pp. 109-139). West Sussex, UK: John Wiley & Sons.

Ribéreau-Gayon, P., Glories, Y., Maujean, A., & Dubourdieu, D. (2006c). *Handbook of Enology, Volume 2: The Chemistry of Wine-Stabilization and Treatments (2. ed.)*. (Chap. 6, pp. 141-203). West Sussex, UK: John Wiley & Sons.

Ribéreau-Gayon, P., Glories, Y., Maujean, A., & Dubourdieu, D. (2006d). *Handbook of Enology, Volume 2: The Chemistry of Wine-Stabilization and Treatments (2. ed.)*. West Sussex, UK: John Wiley & Sons.

Rodionova, O., Titova, A., & Pomerantsev, A. (2016). Discriminant analysis is an inappropriate method of authentication. *Trends in Analytical Chemistry*, **78**, 17–22.

Romano, P., Suzzi, G., Turbanti, L., & Polsinelli, M. (1994). Acetaldehyde production in Saccharomyces cerevisiae wine yeasts. *FEMS Microbiology Letters*, **118**(**3**), 213–218.

Rossano, E., Szilágyi, Z., Malorni, A., & Pocsfalvi, G. (2007). Influence of winemaking practices on the concentration of rare earth elements in white wines studied by inductively coupled plasma mass spectrometry. *Journal of Agricultural and Food Chemistry*, **55**(**2**), 311–317.

Sacchi, K., Bisson, L., & Adams, D. (2005). A review of the effect of winemaking techniques on phenolic extraction in red wines. *American Journal of Enology and Viticulture*, **56**(**3**), 197–206.

Schmidt, H.-L. (2003). Fundamentals and systematics of the non-statistical distributions of isotopes in natural compounds. *Naturwissenschaften*, **90**(**12**), 537–552.

Shriver, D., Weller, M., Overton, T., Rourke, J., & Armstrong, F. (2014). *Inorganic Chemistry (6. ed.)*. (Chap. 1, pp. 3-33). 41 Madison Avenue, New York, US-NY: WH Freeman and Company.

Smith, P., McRae, J., & Bindon, K. (2015). Impact of winemaking practices on the concentration and composition of tannins in red wine. *Australian Journal of Grape and Wine Research*, **21**, 601–614.

Son, H.-S., Kim, K., Van Den Berg, F., Hwang, G.-S., Park, W.-M., Lee, C.-H., & Hong, Y.-S. (2008). ^{1}H nuclear magnetic resonance-based metabolomic characterization of wines by grape varieties and production areas. *Journal of Agricultural and Food Chemistry*, **56**(**17**), 8007–8016.

Sousa, M., Teixeira, J., & Mota, M. (1991). Malo-alcoholic fermentation: the influence of operating conditions on the kinetics of deacidification. *Journal of Wine Research*, **2**(**2**), 115–124.

Šuklje, K., Lisjak, K., Baša Česnik, H., Janeš, L., Du Toit, W., Coetzee, Z., Vanzo, A., & Deloire, A. (2012). Classification of grape berries according to diameter and total soluble solids to study the effect of light and temperature on methoxypyrazine, glutathione, and hydroxycinnamate evolution during ripening of Sauvignon blanc (Vitis vinifera L.). *Journal of Agricultural and Food Chemistry*, **60**(**37**), 9454–9461.

Tcherkez, G., Mahé, A., & Hodges, M. (2011). $^{12}C/^{13}C$ fractionations in plant primary metabolism. *Trends in Plant Science*, **16**(**9**), 499–506.

Torrey, H. (1953). Nuclear spin relaxation by translational diffusion. *Physical Review*, **92**(**4**), 962.

Tóth, É., Helm, L., & Merbach, A. (2013). Relaxivity of gadolinium(III) complexes: Theory and mechanism. In A. Merbach, L. Helm, & É. Tóth (Eds.), *The Chemistry of Contrast Agents in Medical Magnetic Resonance Imaging* (Chap. 2, pp. 25-81). John Wiley & Sons.

Tramontini, S., Vitali, M., Centioni, L., Schubert, A., & Lovisolo, C. (2013). Rootstock control of scion response to water stress in grapevine. *Environmental and Experimental Botany*, **93**, 20–26.

Tyagi, S., Raghvendra, S., Kalra, T., & Munjal, K. (2010). Applications of metabolomics - a systematic study of the unique chemical fingerprints: an overview. *International Journal of Pharmaceutical Sciences Review and Research*, **3**(**1**), 83–86.

U.S. Food and Drug Administration. (2010). Adulterated food. U.S. Food and Drug Administration, Washington, DC, IV. 21, 342–402.

Vilfan, M., & Žumer, S. (1980). Theory of nuclear-spin relaxation by translational self-diffusion in liquid crystals: Smectic A phase. *Physical Review A*, **21**(**2**), 672.

Vorster, C., Greeff, L., & Coetzee, P. (2010). The determination of $^{11}B/^{10}B$ and $^{87}Sr/^{86}Sr$ isotope ratios by quadrupole-based ICP-MS for the fingerprinting of South African wine. *South African Journal of Chemistry*, **63**, 207–214.

Waters, E., Alexander, G., Muhlack, R., Pocock, K., Colby, C., O'Neill, B.K., Høj, P.B., & Jones, P. (2005). Preventing protein haze in bottled white wine. *Australian Journal of Grape and Wine Research*, **11**(**2**), 215–225.

William, W., Teukolsky, S., Vetterling, W., & Flannery, B. (2002). *Numerical Recipes in C*. (Chap. 15, pp. 656-706). Cambridge University Press.

Žumer, S., & Vilfan, M. (1978). Theory of nuclear spin relaxation by translational self-diffusion in liquid crystals: Nematic phase. *Physical Review A*, **17**(**1**), 424-433.

Experimental Part

8. Exploring ^{1}H NMR Relaxometry for Wine Traceability and Authenticity Assessment

Andrea Zava[a,*], Sofia Catarino[a,b], Pedro J. Sebastião[b,c]

[a] LEAF—Linking Landscape, Environment, Agriculture and Food, Instituto Superior de Agronomia, Universidade de Lisboa, Tapada da Ajuda, 1349-017 Lisboa, Portugal; brunosousa@isa.ulisboa.pt

[b] CEFEMA—Center of Physics and Engineering of Advanced Materials, Instituto Superior Técnico, Universidade de Lisboa, Av. Rovisco Pais, 1, 1049-001 Lisboa, Portugal

[c] Department of Physics, Instituto Superior Técnico, University of Lisbon, Av. Rovisco Pais, 1049-001 Lisboa, Portugal

[*] Corresponding author: Tel: +39 3450709125, email: a.zava92@gmail.com

8.1. Abstract

Wine profiles for proton relaxation rate have been obtained for the first time in a wide frequency range. Five Portuguese (Moscatel Graúdo, Arinto, Alvarinho, Touriga Nacional, Trincadeira) varieties and one international (Cabernet Sauvignon) variety have been used to assess possible varietal effect. Each variety have been sampled from two different years, namely 2008 and 2017. The US National Oceanic and Atmospheric Administration (NOAA) agency provided precipitation data to evaluate vintage/environmental interaction and effect on relaxation profiles. Water-ethanol mixture has been evaluated as a possibility to estimate solvent diamagnetic contribution to relaxation. Unexpected enhancement in the 1.5-6 MHz range have been attributed to wine nitrogenous compounds. A general wine characterization provided interesting observation about glycerol correlation to the relaxation rate associated to the presence of paramagnetic ions. This work provides some explorative data management for relaxation profile analysis in complex alimentary fluids.

Keywords: Wine, Authenticity, Relaxometry, Cross-Relaxation, NMR

8.2. Introduction

In the last decades many developments have been made in determining a correlation between the composition of bottled wines, the originating varietal blend, the geographical origin and the environmental impact associated with the vintage; to these are added comparisons on the impact in the use of biological, biodynamic protocols against traditional winemaking

techniques. The sum of all these factors, together with agronomic and/or process management aspects, are the basis of the uniqueness of many wine products: To summarize the complexity resulting from their interaction, the French producers coined the term "*terroir*". The growing economic interest linked to specific production areas renowned for the typicality and quality of the products led to the development of regulatory bodies and to the association of specific mentions: within the European Union, each country is granted detailed indications that can be regrouped under the Denomination of Origin (DO) and Geographical Indication (GI) categories. These certification bodies aim is to guarantee a certain quality standard to consumers and to ensure proper competitiveness by reducing the number of economically motivated adulteration (EMA) (Meloni and Swinnen 2013): among these, the use of non-authorised grapes, i.e. from non-approved varieties and/or geographical origin other than that imposed by the specification, is of particular concern.

In order to trace the compositional variability related to each specific mention different approaches have been under study. Organic compounds synthesis and berry accumulation during all the productive cycle is a consequence of plant phenotype expression which depends on each specific genotype interaction with environmental condition. Nevertheless, the variability of only a few numbers of organic chemical species can hardly be uniquely associated to a single denomination. The discriminative information source can be founded in multivariate statistical pattern both through the application of spectroscopic and classical chemical analysis. Hydrogen nuclear magnetic resonance (^{1}H NMR) spectroscopy was used to discriminate wines according to their variety, vintage, and/or geographical origin (Anastasiadi et al. 2009, Fan et al. 2018, Godelmann et al. 2013, Magdas et al. 2019). Tempranillo wines were correctly discriminated according to their geographical origin through the mass spectroscopy together with electronic nose and application of chemometric tools (Cynkar et al. 2010). Similar goals were achieved using near visible (Vis) together with near infra-red (NIR) (Liu et al. 2006) and Vis in conjunction with NIR and ultra-violet (Uv) (Martelo-Vidal & Vázquez 2014) spectroscopy. In addition, according to Cozzolino et al. (2009) MIR technology can discriminate wines produced under organic protocol from wines obtained by non-organic vineyard management. Since the organic composition undergoes to modification during alcoholic fermentation which intensity and quality depend on the type of yeasts used (Mazzei et al. 2013), particular attention should be given to specific compounds; in particular, glycerol concentration seems to be strongly affected. Beside ethanol, glycerol is the most abundant by-product during sugar consumption since its concentration varies between 5 and 20 g L^{-1} as a consequence of reduction of dihydroxyacetone during wine fermentation. Therefore, its content in the final product depends on the interaction between must chemical composition, sulphur dioxide addition before and/or during vinification, fermentation temperature and yeast's strain.

Particularly interesting is the effect on wine body or the increasing in wine viscosity which is of main interest for in determining wine fullness.

An alternative source for wines geographical characterization lies in mineral and isotopic composition. Some of these elements, namely transition metals, are known to catalyse oxidation processed during whole wine production (Elias and Waterhouse 2010). Catarino et al. (2011) reported rare earth elements (REE) to be suitable markers for geographical discrimination of specific Portuguese DO. Induced coupled plasma mass spectroscopy (ICP-MS) is an analytical technique which allows to inspect sample mineral composition even if in traces concentration. The association soil mineral composition and the originating mother rock seems to be applicable also to a soil-wine system in the absence of biotic and abiotic fractionation processes making it possible to associate wines to their soil of origin (Catarino et al. 2018). If the same restrictions are respected also some isotopic ratios, namely strontium (Martins et al. 2014), boron (Coetzee & Vanhaecke 2005 2005) and lead (Bora et al. 2018) can be used as markers for geographical origin fingerprinting. Wine is recognised to contain paramagnetic ions, namely iron(III) and manganese(II) which concentration varies as a consequence of soil composition (Catarino et al. 2018) and external contamination (Catarino et al. 2008a,b). Iron concentration seems to decrease during wine aging because of oxidation and insolubilization processes (Catarino et al. 2008a, Kaya et al. 2017). Since wine manganese content seems to be independent from hydrogeological conditions (Martin et al. 2012), no vintage effect is expected or, the variability in manganese concentration could be used as a geographic indicator of origin. In fact, Orellana et al. (2019) reported Mn to code in some extent for geographical discrimination between wines in the Washington State. Recently Bodart et al. (2020) explored for the first time the possibility to apply fast field-cycling nuclear magnetic resonance (FFC-NMR) relaxometer on wine samples for manganese and iron quantitation. According to this author a titration curve on model wine for manganese can be obtained and used to determine wine relaxivity at specific frequency. Previously, this analytical technique has been tested with the aim of detecting adulterations on balsamic vinegars (Baroni et al. 2009).

The aim of this study is to explore how wine chemical compositional differences can affect relaxometry readings and the reliability of the technique as a tool for varietal and vintage discrimination of wines. The presence of paramagnetic species in solution leads to longitudinal relaxation rate ($1/T_1$) enhancement which intensity is correlated to their concentration (Bloembergen and Morgan 1961). Nevertheless, the relaxometry models used were developed on aqueous solutions and most of studies involve the response of the relaxation rate as a consequence of solvent composition changes in the presence or not of one paramagnetic

specie (Bertini et al. 1993, Ludwig et al. 1995). Wine is a complex alimentary matrix and as far as we know his physical-chemical characterization, namely ethanol, total and volatile organic acid, phenol, glycerol, sulphur dioxide contents, density and turbidity never were inspected in a sense of relaxation rate variation in a wide range of frequency readings.

8.3. Materials and Methods

8.3.1. Wine Samples

The experiment was carried out on twelve wines produced starting by six different grape varieties (*V. vinifera L.*), namely Touriga Nacional (TN), Trincadeira (Tr), Cabernet Sauvignon (CS), Moscatel Graúdo (MG), Arinto (Ar) and Alvarinho (Al) during vintages 2008 and 2017. All samples come from two neighbouring plots located at the Instituto Superior de Agronomia (University of Lisbon). After being destemmed and crushed and sulphur dioxide added (50 mg kg^{-1}), the red grapes were fermented using a commercial yeast. Regarding the white grapes, after crushing and destemming, the must was subjected to static sedimentation for 24 hours, added in SO_2 and finally inoculated with a commercial yeast. Among these, during the 2008 vintage, both Moscatel Graúdo and Arinto varieties were fermented by indigenous yeasts. In both cases the fermentation took place in 120 litre tanks without temperature control until the sugars were completely consumed. To ensure proper fermentation, the 2017 musts have been enriched with commercial nitrogen nutrients as follows: 0.2 g kg^{-1} of Fermoplus Integrateur 20KD (AEB®) to red varieties; 0.5 g kg^{-1} of Aromax B4 (AEB®) to the whites. Due to the reduced volumes, the homogenisation of musts of the red varieties was manually facilitated three times a day per 15 maceration days with the aid of a wooden pole. All fermentation took place regularly and the temperature never exceeded 27 °C. At the end, both free-run and pressed wines were stored at room temperature in order into stainless-steel tanks to allow spontaneous malolactic to happen till the bottling day. Between the two vintages tanks and instrumentation were renewed. After the malolactic transformation, the wines were racked and bottled in 0.75 L glass bottles. During bottling Sulphur dioxide (50 mg L^{-1}) was added.

8.3.2. Wine Physical-Chemical Characterisation

The samples were taken directly sequentially from bottles. After each sampling, the bottles were closed again, inert with nitrogen and kept at a temperature of about 6 °C. As part of the experimental design included analyses at further sites, some samples were transferred in 50

mL of volume plastic flasks and inert with nitrogen for transfer. A generic physical-chemical characterization of the samples was made following the analytical procedures proposed on the Compendium of International Methods of Wine and Must Analysis (Organization of Vine and Wine, OIV) (OIV 2019a,b). Alcoholic strength by volume was determined by distillation of wine made alkaline by a suspension of calcium hydroxide followed by Measurement of the alcoholic strength of the distillate with a hydrometer (OIV-MA-AS312-01B). The total dry extract is calculated indirectly by comparing wine specific gravity at 20 °C (corrected for volatile acidity) to the specific gravity of the alcohol-free wine (20 °C) (OIV-MA-AS2-03B). During this analysis also density values were collected. Total acidity was obtained by titration till pH 7.0 against a sodium hydroxide alkaline solution; carbon dioxide is not included in the final values. Bromothymol was used as pH indicator with a blue end-point comparison to standard colour (OIV-MA-AS313-01). After carbon dioxide removal by evaporation enhanced by vacuum, volatile acids were separated from the wine by steam distillation and titrated using standard sodium hydroxide solution and phenolphthalein as indicator; after that, free and combined sulphur dioxide were sequentially titrated with iodine solution, with starch as redox indicator, and subtracted during final calculations (OIV-MA-AS313-02). Regarding the wine turbidity, first the sample were centrifuged (10 min, 10000 rpm) and then light optical diffusion through wines were compared to reference samples using a 2100N Turbidimeter (HACH®) to obtain nephelometric values (OIV-MA-AS2-08). After a respective acidification with sulphuric acid, both free and total sulphur dioxide wine content were titrated with sodium hydroxide by potentiometry through a Sulfilyser (ENARTIS®) apparatus. Wine pH were potentiometrically measured by the Thermo Scientific™ Orion Star™ A211 Benchcorp pH meter. Spectral density at 280 nm was obtained thanks to a UNICAM UV4 Uv/Vis Spectrometer and the wine total phenol index calculated according to method described by Somers and Evans (1977). Glycerol content was obtained through Fourier Transform Infrared Spectroscopy (FTIR) through the method explained by Ferreira (2015); since no titration curve was used, no quantitative observation was possible. Nevertheless, these data made it possible qualitative comparison between samples. In conclusion, the wine total iron content was determined by atomic absorption spectroscopy (AAS); the applied method refers to OIV-MA-AS322-05A whit the only exception the wine samples were not previously dealcoholized but a titration curve was obtained by using concentrated standard iron solution containing 1 gL^{-1} of iron(III) [$FeNH_4(SO_4)_2 12H_2O$] diluted into hydro-alcoholic solutions: 5 calibration sample were used corresponding to 1, 2, 3, 4 and mg L^{-1} of iron. Only decontaminated polyethylene flasks have been used.

8.3.3. NMR Relaxometers: Experimental Conditions

Wine samples were transferred to conventional 5mm NMR tubes, immediately put under vacuum, filled with nitrogen, and immediately sealed by fusing the opening. In order to guarantee the same ageing condition, the tubes have been subjected to the storage condition of the bottles (6 °C). Relaxation data were obtained in a wide frequency range (0.04-300 MHz) thanks to the use of 3 different instrumentation: a Bruker Widebore Ultra-shielded 7.1 Tesla (T) Superconducting Magnet (300 MHz), variable field 0.2 T–2.5 T solid state NMR spectrometer magnet (1.14-90 MHz) and a fast field-cycling NMR relaxometer (FFC-NMR) for proton relaxation measurements in the Larmor frequency range of 0.04-8.86349 MHz; data were collected only thill 40 kHz. Data were collected and analysed through the online fitting environment fitteia.org. Since room temperature was found to oscillate, all the measurements were carried out at 25°C thanks to the use of an air worming system. In addition to the use of a calibration curve, random temperature probing was performed to ensure the sample kinetic stability both using electronic and mercury thermometers. Relaxation rates corresponding to at least 20 different frequencies have been obtained in duplicate: in order to reduce the probability of experimental errors, repetitions were carried out on different days, at different times and room temperatures. In addition, to guarantee all the measurements to be taken at the same temperature, 5 minutes have been allowed to elapse from the moment the sample is inserted into the NMR and the start of calibration. Since these is a first approach for wine characterization, more than one set of acquisition point has been tested. Data till 11.4 MHz were collected and analysed through Topspin software (Bruker®) while the FFC-NMR output were managed thanks to a specific MATLAB environment. In all cases the results a mono-exponential decay curve was used to fit the wine relaxation rate (R) at each frequency.

Eight water/ethanol mixture samples have been prepared at increasing ethanol content, namely 10, 11, 12, 13, 14, 15, 16 and 17%vol in order to assess the individual diamagnetic contribution of wines' solvent. In order to ensure the same analytical and storage condition of the wines, the NMR tubes have been subjected to the same treatment exception for the inerting with nitrogen gas.

8.3.4. Pluviometric Data

In order to assess possible vintage correlation between wine relaxation rate dispersions and climate variation during the production year, data were collected for vintages 2008 and 2017 from the National Centers for Environmental Information (NCEI) form the US National Oceanic and Atmospheric Administration (NOAA) agency. Millimetres of rain per day have been used.

This information has been compared to the dates at which fermentation started to exclude the harvest date proximity to rain events.

8.3.5. Statistical Analysis and Data Management

The two-way analysis of variance (ANOVA) without factors interaction, correlation tests and simple linear regressions were performed using R software. Shapiro-Wilk test for normality of the distribution was used to test the ANOVA residuals. It was not possible in all cases to assess the normality, but we considered the results reliable thanks to the test robustness. In the case homoscedasticity assumption was not confirmed, White-adjusted ANOVA was used followed by Duncan post-hoc test. In the other cases to execute multiple comparisons Bonferroni post-hoc test was preferred to highlight significant differences. Two factors were chosen namely variety and vintage, and all the physical-chemical wines' data have been tested to assess statistical differences. The interaction between factors was not inspected due to the low number of repetitions. One-way ANOVA have been used to inspect statistical differences between red and white varieties following the same criteria.

The results for one-sided Correlation tests based on Pearson correlation coefficient between the relaxation rate contributions and wine physical-chemical parameters, namely ethanol, glycerol, total dry matter, total acidity, both total and free SO_2 density, turbidity, pH, total phenol index and total iron are presented. In this case, the relaxation contribution per each wine was considered as follows: total integral (TI), or the area below the modelled curve between 0.04 MHz and 300 MHz subtracted by the area drawn by the diamagnetic contribution line (this contribution was interpolated from water-ethanol mixture relaxation rate at the corresponding sample %vol), and paramagnetic integral (PI); PI was obtained subtracting the area below the $y = R_{i,\nu}$ (ν = 8.86349 MHz, i identifies the sample number) straight line in the 0.04-8.86349 MHz range to the integral calculated from the model in the same frequency range (FFC-NMR analytical spectrum). In all cases a chi-square (χ^2) minimization was used, regardless for the models' parameter physical reliability, in order to obtain the more sample representative profiles. All the procedure was carried out through the fitteia software.

Three simple linear regression, one per each chosen frequency (300 MHz, 68.3 MHz, 23.4 MHz), has been achieved to explain the wine solvent diamagnetic relaxation contribution trough a water-ethanol mixture at increasing %vol. The results will be compared to other presented in bibliographic form.

8.4. Theoretical Description

Nuclei possessing a non-null nuclear magnetic moment (^{1}H, ^{13}C, ^{14}N) experiencing a stable external magnetic field B_0 are subjected to a magnetic torque inducing a coherent precession motion. In case of proton nuclear magnetic resonance and according to the Boltzmann distribution, this situation causes the hydrogen (^{1}H) energy levels to degenerate assuming two unequal values. By switching the external magnetic field from an initial B_p to a lower B_r intensity relaxation phenomena occur or, the resulting magnetic moment re-orientates in time according to the new external field intensity. Generally, the resulting motion is described by the magnetization mono- or multi-exponential decay as a consequence of spin-lattice relaxation phenomena occurring in time (Bloch 1946). Relaxation time (T_1) and corresponding motion dynamics are explained through models depending on lattice/surrounding composition. Water sample can be represented applying the Bloembergen-Purcell-Pound (BPP) model (Bloembergen et al. 1948) since only dipolar-dipolar interactions between proton nuclei are responsible for total longitudinal relaxation rate ($R_1 = 1/T_1$):

$$R\ (s^{-1}) = A_{BPP}\left[\frac{\tau_o}{1+\omega_I^2\tau_o^2} + \frac{4\tau_o}{1+\omega_I^2\tau_o^2}\right] \tag{39}$$

with:

$$A_{BPP} \simeq 1.70888 \times 10^{-49}\left\langle\frac{1}{r^6}\right\rangle \tag{40}$$

where τ_o is the rotational-diffusional characteristic time for the specific sample, ω_I is the proton Larmor frequency which varies according to the external magnetic field (Doan et al. 2013), μ_o is the vacuum permeability, and r represents the average distance between nuclear spins obtained through molecular simulations for hydroalcoholic solutions.

The presence of paramagnetic chemical species, namely particles possessing at least an unpaired electron is source of addition relaxation rate contribution: in this case more than one mechanism should be considered. In principle, it is possible to refer to the relaxation rate enhancement per unit of paramagnetic particle through the linear relation:

$$R_{para} = r_v^{Mn}[Mn^{2+}] \tag{41}$$

where r_v^{Mn} reefers to the relaxivity at specific (v) acquisition frequency associated to each mole of manganese. Considering the bulk contribution (R_{diam}) as the total solvent relaxation rate after the removal of any paramagnetic particle, Equation 41 will become:

$$R_{obs} = R_{diam} + r_v^{\mathrm{Mn}}[\mathrm{Mn}^{2+}] \tag{42}$$

where R_{diam} can be obtained by the BPP model as the solvent longitudinal relaxation rate in the absence of paramagnetic ions. In addition, the relaxivity changes depending on solvent physical-chemical characteristics. The R_{para} can be either expressed as in Equation 42 or singularly considering the relaxation rate contributions from inner-sphere (IS) and outer-sphere (OS) both of them dependent on the zero field splitting (ZFS) spin Hamiltonian (Tóth et al. 2013). According to the Solomon-Bloembergen-Morgan model, the relaxation rate of proton directly bound to the paramagnetic species is a consequence of two mechanisms: dipole-dipole (DD) interaction and electronic relaxation itself, or scalar coupling (SC). The inner-sphere paramagnetic contribution is therefore dependent on the number of coordinated solvent molecules (q), which depends on the specific solvent composition combined by possible steric hindrance effects, and the number of unpaired electrons; considering the effect exerted by the presence of manganese:

$$\left(\frac{1}{T_1}\right)^{IS} = P_m \frac{1}{T_{1m} + \tau_m} \tag{43}$$

where T_{1m} is the relaxation time, τ_m is the duration of the solvent-manganese bound and P_m the molar fraction of the bound solvent molecules:

$$P_m = q \frac{n_m}{n_{\mathrm{Mn}}} \tag{44}$$

Since both paramagnetic (n_{Mn}) and solvent (n_m) number of moles are not always known, an estimation can be done starting by the density (ρ) measurement. In the case of not concentrated solutions or, when the changings in sample density by the adding in paramagnetic species is negligible, the Equation 45 can be rewritten as follows:

$$P_m = q[m_{\mathrm{Mn}}] \frac{m_{\mathrm{Mn}}}{\rho} \tag{45}$$

where $[m_{\mathrm{Mn}}]$ refers to the manganese molar concentration and m_{Mn} to its molar mass. It must be stressed this simplification to be valid only if the sample solvent is entirely composed by water. Therefore, some modification to the viscosity value according to the specific solvents molar fraction and number of bondable hydrogens are needed. By doing this, the reliability of bibliographic fits for the number of coordinated solvent molecules could lose robustness. Nevertheless, in most cases it is possible to assume the solvent density equal to the pure water one (0.9970479 g cm^{-3} at 25 °C) at the same sample temperature.

The DD and SC contributions can be written as:

$$\frac{1}{T_{1m}} = \frac{1}{T_1^{DD}} + \frac{1}{T_1^{SC}} \tag{46}$$

with

$$\frac{1}{T_1^{DD}} = \frac{2}{5}\frac{\gamma_I^2\gamma_S^2h^2}{r^6 4\pi^2} S(S+1)\left(\frac{\mu_o}{4\pi}\right)^2\left[\frac{7\tau_{c2}}{1+\omega_S^2\tau_{c2}^2} + \frac{3\tau_{c1}}{1+\omega_I^2\tau_{c1}^2}\right] \tag{47}$$

and

$$\frac{1}{T_1^{SC}} = \frac{2}{3} S(S+1)\left(\frac{2\pi A}{h}\right)^2\left[\frac{\tau_{e2}}{1+\omega_S^2\tau_{e2}^2}\right] \tag{48}$$

In Equations 47 and 48, S is the electron spin number, γ_I is the proton gyromagnetic ratio, γ_S is the electron gyromagnetic ratio, h is the Planck constant, ω_S the electron Larmor frequency and $2\pi A/h$ the reduced Fermi constant. The τ_{c1}, τ_{c2} and τ_{e2}^2 are the corresponding correlation times which arise from:

$$\frac{1}{\tau_{ci}} = \frac{1}{\tau_R} + \frac{1}{\tau_{ie}} + \frac{1}{\tau_m} \tag{49}$$

$$\frac{1}{\tau_{ei}} = \frac{1}{\tau_{ie}} + \frac{1}{\tau_m} \qquad with \qquad i = 1,2 \tag{50}$$

The τ_R and τ_{ie} correlation times respectively represent the rotational and the zero field splitting (ZFS) contribution. The latter quantifies the relaxation rate contribution related to the electronic energy level degeneration; therefore, it is strictly dependent on the type of paramagnetic ion.

The outer-sphere (OS) relaxation enhancement depends on random intermolecular dipole-dipole interactions which are therefore affected by translational-diffusional coefficient (D) (Tóth et al. 2013). According to Einstein-Stokes law for molecular diffusion into low-turbulent ($Re < 10^4$) fluids, solvent viscosity and its molecular radius are inversely proportional to self-diffusion. Therefore, in multiple solvent system the variation in solvent molar ratio could be responsible for most of the outer-sphere contribution:

$$\left(\frac{1}{T_1}\right)^{OS} = \frac{32\pi}{405}\,\gamma_S\gamma_I\left(\frac{h}{2\pi}\right)^2\frac{n_m N_a}{aD}\,S(S+1)[j_2(\omega_I - \omega_S) + 3j_1(\omega_I) + 6j_2(\omega_I + \omega_S)] \quad (51)$$

where N_a is the Avogadro's number, D the summation between the I and S self-diffusion coefficients ($D = D_I + D_S$), a is the distance of minimum approach, between the paramagnetic centre and water molecules, which should always results larger than r (Eq. 47), n_m is the number of moles of S spins per cubic meter and j_i are the spectral densities or the Fourier transform of the correlation functions (Ayant et al. 1975). ω_I and ω_S respectively represent the proton and electron Larmor frequencies.

To draw a model on a solvent-paramagnetic system all the three (Eq. 39, 46, 51) contributions should be considered even if, during similar sample comparison with small differences in the self-diffusion coefficient, the lower variability of OS in comparison to the IS makes it less relevant (Tóth et al. 2013). The so obtained model is valid only in mono-ionic solutions: when more than one paramagnetic centre is present it is possible to singularly consider their contribution through a cumulative model. If bibliographic data are available, both individual and overall contribution to the sample relaxation rate will be possible.

8.5. Results and Discussion

8.5.1. Environmental Conditions

Data collected by NOAA have been used as a first approach to evaluate the impact on relaxation profiles in sample differentiation into groups. The period between the first of January and the last day of October was considered. Main differences have been found on the amount of rain events, intended as mm of water and number of events. A total amount of 494 mm of water in sixty-seven different events were registered in 2008 against 260 mm and forty-three rainy days (Fig. 14). Starting from the first day in which one of the variety was collected to the last harvest day, the discrepancy was more pronounced: in 2008 between the 28th of August

2008 and 26th five rain events occurred for a total of 21 mm of water while in 2017, between the 7th and the 24th of August, no rain event took place. Together with possible dilution effect and the rootstock capability to absorb mineral elements according to the soil pedological conditions, rain events can affect the amount of soil particle settled on berry skins causing a reduction of the mineral element transferred to the wines during the harvest.

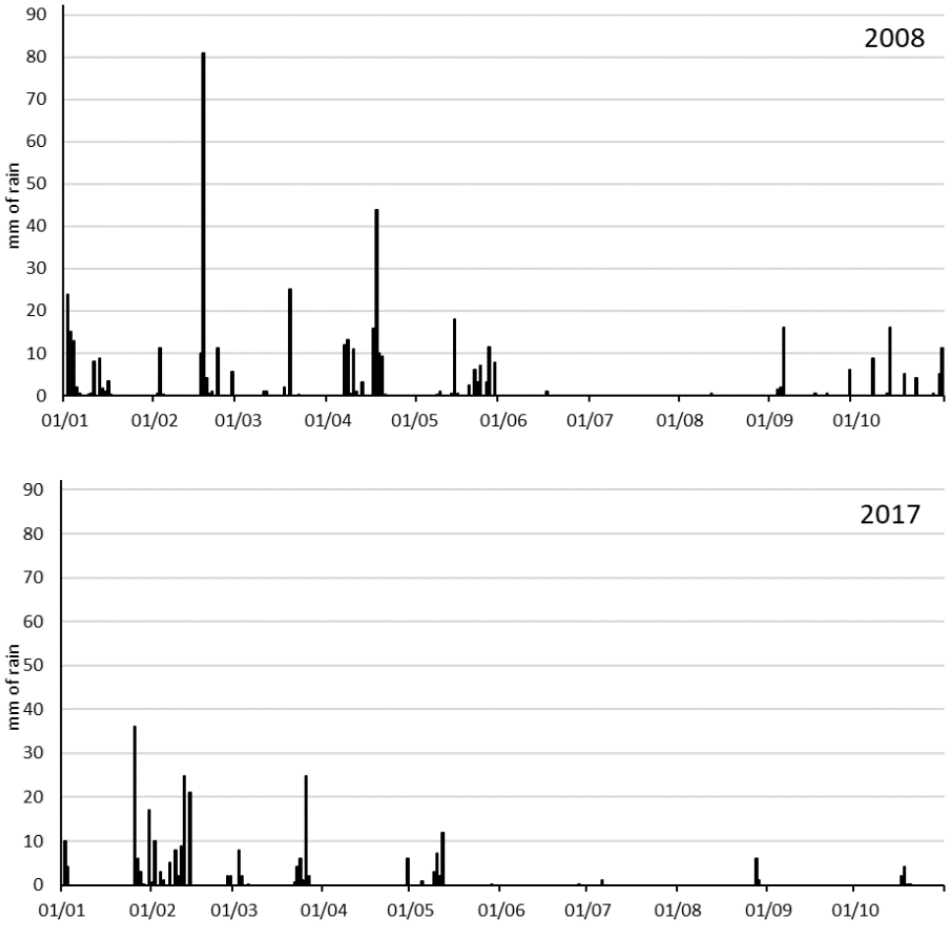

Figure 14. Rain fell (mm) in 2008 and 2017 in the Lisbon (PT) district during the period 01/01 – 31/10: data obtained from the US National Oceanic and Atmospheric Administration (NOAA) agency.

The difference in the wine samples' relaxation rate profile are shown in Figure 15. The vintage effect can be observed in terms of data variability both at high (300 MHz) and low (0.04 MHz) frequencies: this effect is more evident in the second case. A possible explanation is the preponderant effect of the relaxation contribution associated to the scalar coupling arising from the direct water molecules interaction with paramagnetic ions. The iron concentration (Tab. 3) was not able to justify the behaviour of the 2008 wine in respect to the 2017: since the relaxation rate is linearly proportional to the concentration of the paramagnetic ions (Eq. 41) and TN 2008 showed the highest relaxation rate, we expected its total iron content to be at least comparable to the others; contrary, only 1.123 mg L^{-1} were found. In addition, MG 2008, which iron content (2.224 mg L^{-1}) resulted almost the double, showed the lowest relaxation

rate dispersion (Fig. 15) suspecting iron to do not be the main responsible in wine paramagnetic relaxation rate enhancement.

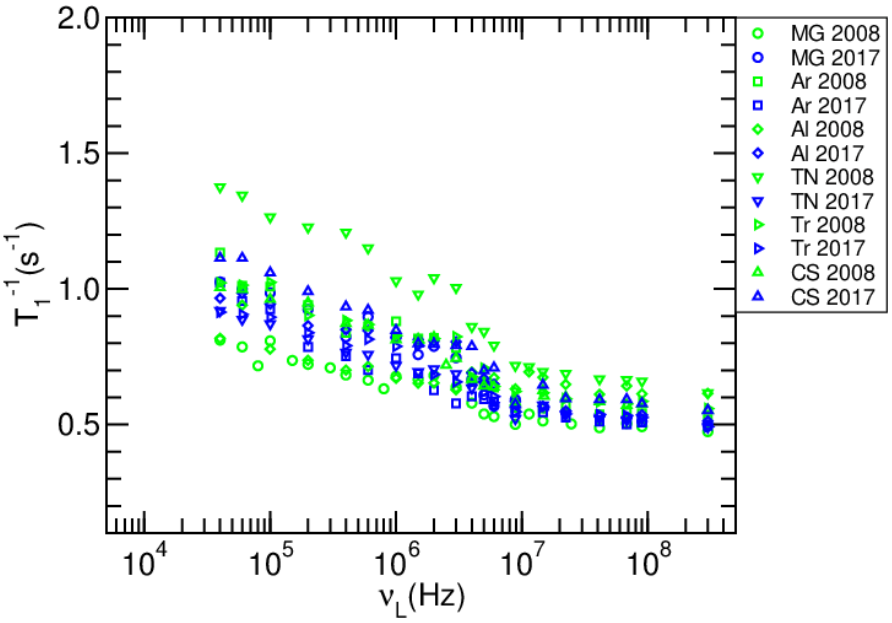

Figure 15. Relaxation rate (s^{-1}) profile obtained at different Larmor frequency (Hz) of 2008 (green) and 2017 (blue) varieties, namely MG (Moscatel Graúdo), Ar (Arinto), Al (Alvarinho), TN (Touriga Nacional), Tr (Trincadeira), and CS (Cabernet Sauvignon). Sample were analysed in the range 0.04-300 MHz. The frequencies axis is plotted in logarithmic (base 10) scale.

Bodart et al. (2020) proved relaxivity associated to manganese(II) at 19.65 MHz to be around 64% higher to the one of iron(III). Unfortunately, during this work it was not possible to measure wine manganese content. In any case, since iron is proven to be paramagnetic and to show dispersions in the FFC-NMR spectrum, its concentration should be considered. According to the ANOVA results (Annexes Tab. S1), 2008 wines statistically differ from the 2017 in iron content: Iron is well recognized to have both endogenous and exogenous origin (Catarino et al. 2008) in wine. The cellar facilities were renewed between the 2008 and 2017 vintages; since iron content was found to be not only higher but irregularly distributed between wines, some contamination could have had occurred affecting the elemental profile (Fe, Mn, Cu, …).

It must be stressed the sample differences according to the vintage to be affected from wine chemical modification during bottle ageing: the formation of insoluble salts followed by precipitation could alter the paramagnetic ions concentration depending on the wine starting composition. Bodart et al. 2020 showed relaxation rate reductions in wine samples stored at room temperature in non-sealed NMR tube per more than one year indicating also metal oxidation state to be relevant. Since manganese content is strongly affected during must fermentation, probably for insoluble sulphide salts formation (Catarino et al. 2006), total sulphur dioxide content should be considered as uncertainty source during relaxometry profile grouping according to vintage and or variety.

Table 3. Physical-chemical characteristics[b] of white and red varieties used in NMR experiments.

Variety	Vintage	pH	Alcoholic Strength by Volume (%vol)	Total Acidity ($g_{Tartaric\ Acid}$ L^{-1})	Volatile Acidity ($g_{Acetic\ Acid}$ L^{-1})	Density (10^3 kg m^{-3})	Total Dry Matter ($g_{Sucrose}$ L^{-1})	Turbidity (NTU)	Glycerol (g L^{-1})	Total Phenols Index	Total SO_2 (mg L^{-1})	Free SO_2 (mg L^{-1})	Total Iron (mg L^{-1})
MG	2008	3.19 ± 0.01	13.75 ± 0.00	5.55 ± 0.00	0.98 ± 0.03	0.9889 ± 0.0000	22.2 ± 0.0	6.0 ± 0.1	1.39 ± 0.33	10.08 ± 0.01	195 ± 9	8.00 ± 0.00	2.224 ± 0.005
MG	2017	3.29 ± 0.01	13.05 ± 0.00	4.80 ± 0.00	0.23 ± 0.00	0.9905 ± 0.0001	24.5 ± 0.1	1.2 ± 0.0	2.62 ± 0.08	8.68 ± 0.01	69 ± 3	11.75 ± 1.25	1.473 ± 0.005
Ar	2008	3.16 ± 0.01	13.80 ± 0.05	6.68 ± 0.08	0.89 ± 0.00	0.9897 ± 0.0002	23.9 ± 0.3	5.5 ± 0.0	1.60 ± 0.10	12.86 ± 0.02	93 ± 2	4.50 ± 0.00	3.456 ± 0.007
Ar	2017	3.34 ± 0.01	12.85 ± 0.08	5.63 ± 0.00	0.18 ± 0.03	0.9903 ± 0.0001	23.3 ± 0.4	3.6 ± 0.0	2.99 ± 0.04	9.85 ± 0.02	56 ± 2	5.75 ± 0.25	1.732 ± 0.006
Al	2008	3.32 ± 0.01	15.69 ± 0.00	5.67 ± 0.11	0.99 ± 0.02	0.9876 ± 0.0000	24.6 ± 0.0	2.7 ± 0.1	2.00 ± 0.01	13.80 ± 0.01	105 ± 4	4.75 ± 0.25	2.437 ± 0.010
Al	2017	3.31 ± 0.01	14.14 ± 0.00	5.70 ± 0.00	0.18 ± 0.02	0.9895 ± 0.0001	25.1 ± 0.2	10 ± 0	2.64 ± 0.17	9.68 ± 0.01	40 ± 0	6.25 ± 0.75	1.193 ± 0.006
TN	2008	3.97 ± 0.01	15.20 ± 0.00	4.24 ± 0.04	0.73 ± 0.04	0.9905 ± 0.0001	30.5 ± 0.3	2.4 ± 0.1	8.74 ± 0.26	45.15 ± 0.49	18 ± 3	5.25 ± 0.25	1.123 ± 0.008
TN	2017	3.91 ± 0.00	12.61 ± 0.00	4.40 ± 0.55	0.50 ± 0.02	0.9924 ± 0.0000	27.9 ± 0.0	26 ± 0	4.11 ± 0.02	48.85 ± 0.78	76 ± 3	19.25 ± 0.25	0.701 ± 0.001
Tr	2008	3.71 ± 0.00	13.62 ± 0.00	4.64 ± 0.06	0.75 ± 0.01	0.9907 ± 0.0001	26.4 ± 0.3	30 ± 0	4.65 ± 0.33	33.15 ± 0.21	36 ± 1	12.50 ± 0.00	1.244 ± 0.007
Tr	2017	3.73 ± 0.01	13.80 ± 0.05	4.95 ± 0.00	0.42 ± 0.02	0.9908 ± 0.0000	27.1 ± 0.0	11 ± 0	4.53 ± 0.01	31.15 ± 0.49	43 ± 1	17.25 ± 0.75	1.126 ± 0.004
CS	2008	3.92 ± 0.01	14.20 ± 0.00	5.07 ± 0.04	1.12 ± 0.02	0.9906 ± 0.0001	27.9 ± 0.0	7.3 ± 0.1	4.57 ± 0.15	34.10 ± 0.14	60 ± 3	13.25 ± 0.25	1.428 ± 0.006
CS	2017	3.41 ± 0.01	14.08 ± 0.00	6.12 ± 0.04	0.43 ± 0.04	0.9916 ± 0.0001	30.1 ± 0.1	9.5 ± 0.0	6.40 ± 0.02	37.75 ± 0.49	47 ± 10	14.75 ± 0.25	0.843 ± 0.004

[a] **Sample codes**: MG - Moscatel Graúdo, Ar - Arinto, Al - Alvarinho, TN - Touriga Nacional, Tr - Trincadeira, CS - Cabernet Sauvignon. [b] For each wine analytical parameter, average values followed by the corresponding standard deviation are shown. The determinations were carried out in duplicate (n = 2), except for glycerol and total iron content (n = 3).

8.5.2. Evaluating Water-Ethanol Mixture as Reference Sample for Wine Diamagnetic Contribution (R_{diam}) Assessment

In order to reduce the R_{obs} to the only paramagnetic relaxation rate contribution, water-alcohol mixture have been used to estimate the R_{diam} (Eq. 42). The diamagnetic relaxation rate associated to each sample have been interpolated through the linear equation (Fig. 16) and R_{diam} values are shown in Table 4. These results seem confirming the one obtained by Ludwig (1995) which readings at 300.13 MHz highlighted an increasing in the rotational correlation time (τ_o, Eq. 39) associated to samples at higher ethanol content. The effect can be explained associated to the hydrophobic hydration of ethanol methyl (-CH_3) and methylene (-CH_2) aliphatic groups. According to the same author, methanol and propanol added in water sample induce the same type of response.

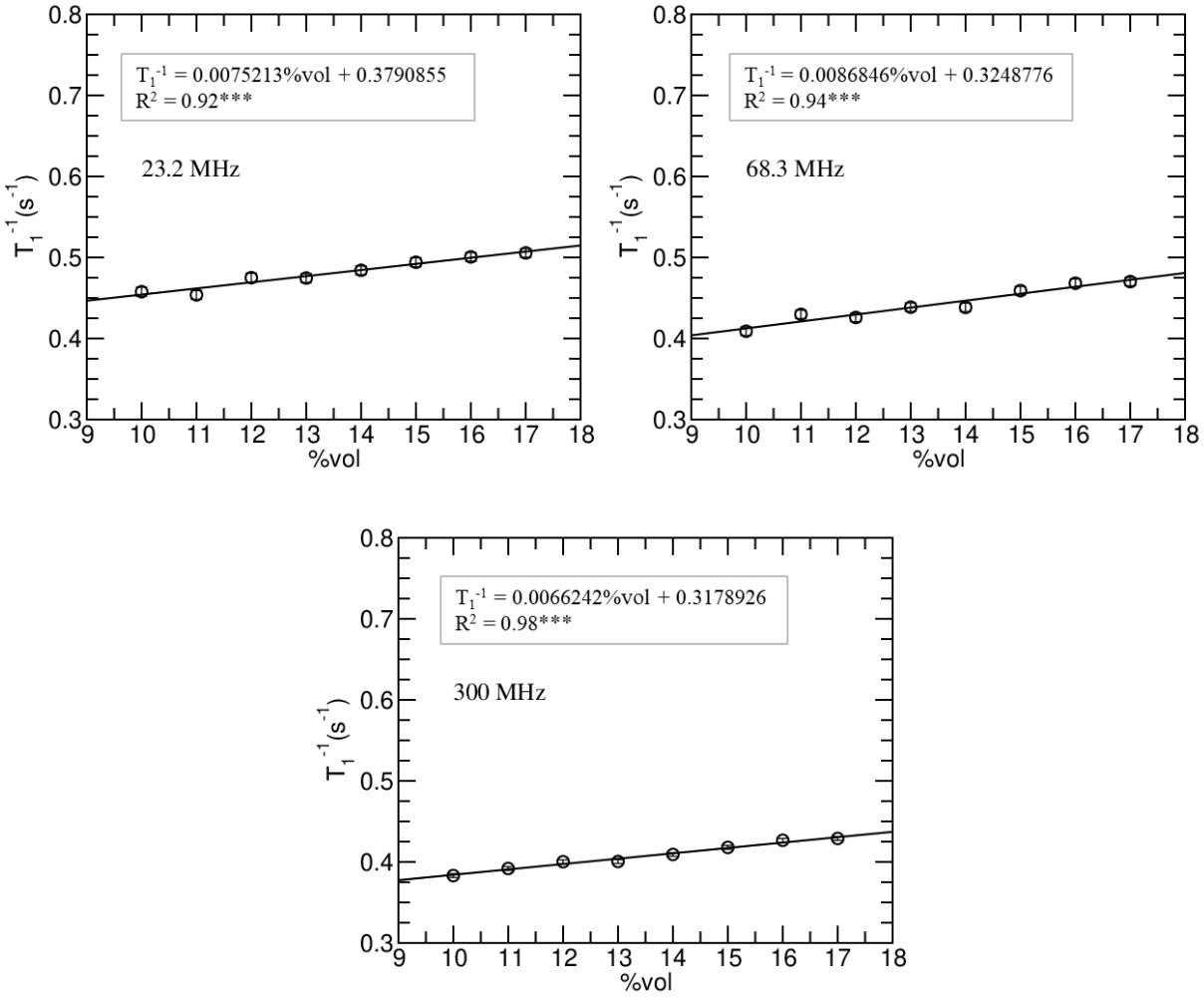

Figure 16. Results for relaxation rate dependence from %vol in water-ethanol mixture at frequencies 23.2 MHz, 68.3 MHz and 300 MHz. In all cases both estimate and intercept values were statistically significant (p < 0.001); R^2 represents the coefficient of determination.

As an alternative, Bodart et al. (2020) proposed to use the same analysed wine after ion removal on an ion exchange resin obtaining a relaxation rate close to 0.47 s^{-1}. The differences between our and their results can be explained by the higher wine compositional complexity: aliphatic groups are present in many wine's molecules (acetic acid, acetaldehyde, fatty acids, proteins, …) which effect on the wine relaxation rate still need to be quantified. In addition, the diamagnetic relaxation rate results from both rotational ad diffusional contributions. Since wine was proven to act as a Newtonian fluid at temperature higher than 10 °C (Trávníček et al. 2016) we can accept the Einstein-Stokes equation for molecular diffusion in low-turbulent ($Re < 10^4$) fluids: an increasing in wine viscosity will lead to the reduction in the diffusion coefficient. This will reflect on a decreasing in sample relaxation time (T_1).

Table 4. Values represents each sample[a] diamagnetic relaxation contribution interpolated starting from water-ethanol mixture at increasing %vol. Values arise from Bloembergen-Purcell-Pound model (Eq. 39, 40) for relaxation rate associated to molecular tumbling.

Vintage	MG	Ar	Al	TN	Tr	CS
2008	0.441475	0.441855	0.456181	0.452469	0.440489	0.444888
2017	0.436164	0.435253	0.444433	0.432825	0.441855	0.443978

[a] **Sample codes**: MG - Moscatel Graúdo, Ar - Arinto, Al - Alvarinho, TN - Touriga Nacional, Tr - Trincadeira, CS - Cabernet Sauvignon.

The increasing in wine viscosity have been proven to be linearly dependent on both ethanol and glycerol content (Yanniotis et al. 2007) but since the latter varies in wines in between of 5 and 20 mg L^{-1}, its impact on this physical property is assumed negligible. Neto et al. (2014) proved ethanol and dry extract to be the main chemical factors affecting wine viscosity and therefore the differences between our and Bodart et al. (2020) results can be ascribed to the absence in organic compounds such as polysaccharides, fructose, polyphenols and lipids. In addition, it has been proven a reduction in wine viscosity after tartaric acid, Na_2SO_3 and glucose addition (Wang et al. 2018). This will make the creation of a reference sample for assessing the diamagnetic contribution more complicated strengthening the practicality technique of the technique applied by Bodart et al. (2020). These statements can be accepted only assuming the complete independence of water-alcohol's relaxation rate values from the acquisition frequency: in this sense, a better comparison will be possible only exploring the contribution on the whole frequency range.

8.5.3. Sample Grouping According to Relaxation Rate Profiles

Relaxation rate values were proven to be in average higher in red than in white varieties (Fig. 17). One-way ANOVA results are presented as supplementary material (Annexes Tab. S2). The difference between samples is not constant in the whole frequency spectrum (Tab. 5):

even if in general the magnitude order is respected, i.e. those characterized by a longer relaxation time at high frequencies occupy the same position with respect to the others also at low frequencies and vice versa, the spacing between samples is more marked in the left side of the graph. This is valid only if we assume the reading associated error to be sample independent.

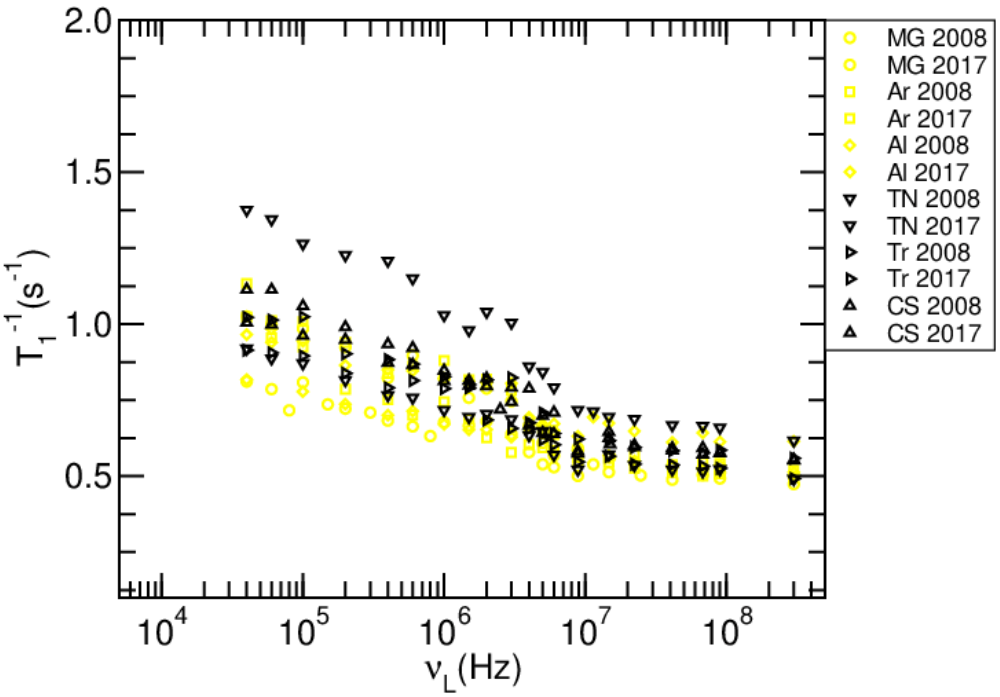

Figure 17. Relaxation profile of wines from 2008 and 2017 vintages. Yellow signs refer to white while black to red grape varieties. All the six grape varieties have been plotted: MG (Moscatel Graúdo), Ar (Arinto), Al (Alvarinho), TN (Touriga Nacional), Tr (Trincadeira) and, CS (Cabernet Sauvignon).

The frequency dependence of the relaxation rate associated to the presence of paramagnetic ions (Mn^{2+}, Fe^{3+}) in fluids arises from the contribution of each specific relaxation phenomenon and corresponding model: rotation, outer- and inner-sphere (Eq. 39, 47, 48). In other words, without knowing the responsible element for the paramagnetic enhancement, it would be difficult to obtain reliable coefficients for a correct sample modelling to explain the involved physical quantities.

Table 5. Variation indexes for relaxation rate data obtained respectively at 0.04 and 300 MHz.

Larmor Frequency	Mean	SD	Coefficient of Variation (%)
0.04	0.99	0.16	16%
300	0.53	0.05	9%

To overcome the lack of information, we tried to compare the wine profile assuming the paramagnetic ion concentration to be the same in al sample. It must be stressed the following data management procedure to do not allow extrapolating reliable physical-chemical

parameters from the models. In order to limit hour observations to the paramagnetic contribution to the sample profiles, we used the water-ethanol mixture to estimate according to each sample %vol the diamagnetic relaxation and subtracted the sample corresponding value (Tab. 4). The intent was to assess if multiplying all relaxation rate values by an arbitrary number, fixed per each sample, it would have been possible to force the profiles' overlapping and evaluate possible interference on relaxivity. Since the analytical error made it difficult to obtain a good overlapping just using one reference frequency, we decided to adapt the translation according to the goodness of the result. The obtained values maintain the same unit of the starting measurements.

Figure 18 shows the relaxation profiles of white and red wines: after the best overlapping was obtained, we decided to inspect each group separately. The main differences were found in the 1.5-6 MHz frequency range in a term of profile homogeneity. With the exception for Al 2008 data dispersion, at low frequencies all the white varieties maintained the same overlapping goodness. The data for Al 2008 are not included since it was not possible to obtain any form of profile overlapping: the absence of paramagnetic ions could explain this specific case. Contrary, all the six red wines were successfully plotted.

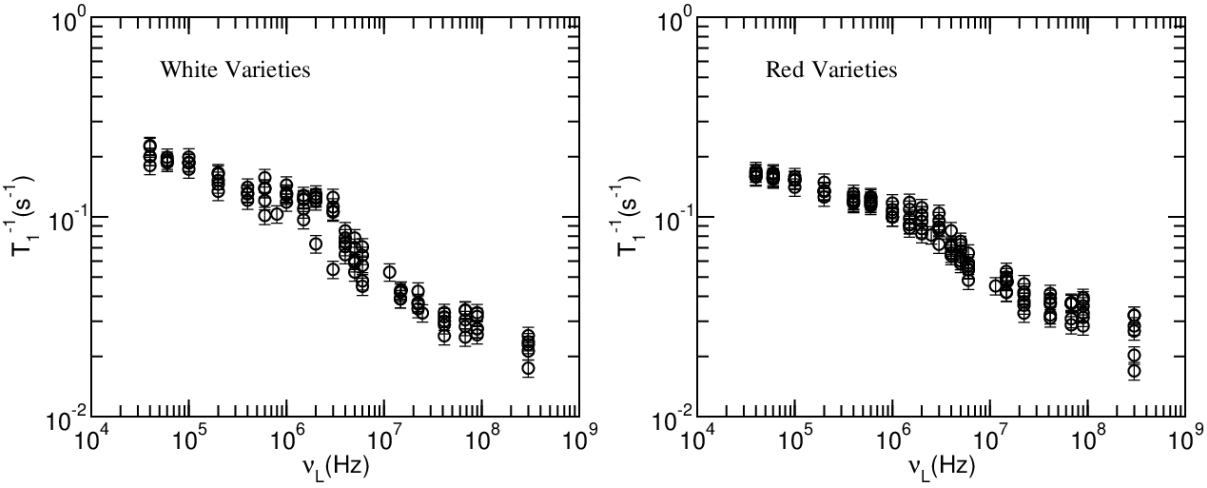

Figure 18. White and red wines' profiles after data were modified to force the best possible overlapping for relaxation rate values. Both axes are presented in logarithmic scale.

The relaxation enhancement in this frequency range in paramagnetic is referred to cross-relaxation phenomena involving nitroxide radicals ($^{14/15}$N-O•); electron spin (S) is coupled with the nuclear spin through a hyperfine scalar coupling (Eq. 38) which arises from dipole-dipole interaction between the two magnetic centres. The hyperfine coupling fluctuates in time due to rotation of the paramagnetic centre. Water protons interplay with nitroxide radicals by dipole-dipole interactions which are modulated by the two spins relative translation/diffusion motion (Kruk 2016). In this sense, diffusion and therefore viscosity, nitroxide radicals' concentration

and their rotation speed are the main physical quantity affecting the cross-relaxation. The fact we saw the presence of peaks in certain wine sample profiles can be a proof of cross relaxation phenomena presence in wines.

Nitrates (NO_3) and nitrites (NO_2^-) are allowed to be present in wine under the respective 3.0 and 50 mg L^{-1} concentration threshold (World Health Organization) (Okoye et al. 2017). Must nitrate content is extremely low (around 10% on total nitrogen content) since most of it is stored as ammonium salt and amine groups ($-NH_2$) of organic molecules such as amino acids and proteins (Ribéreau-Gayon et al. 2006). High level of nitrates can be ascribed to contamination from soils particle or raw water addition (Erdei 2014) but this is not our case. Since ammonium is the main yeast nitrogen source, it is consumed during the alcoholic fermentation. Therefore, nitrogen in wine is mainly stored in form of amino acids (proline represents around 50% of this fraction) and proteins. The only presence of nitrogen directly bounded to hydrogen atoms is registered to give relaxation enhancement (Pusiol et al. 1992); actually, the only presence of nitrogen in the proximity of hydrogen could lead to the same result. Since both nitrogen concentration and the main form in which is stored in our samples were unknown, and since other physical quantities (viscosity, rotational correlation time) are involved, in the absence of any pre-existing bibliographic reference on this topic, any sample grouping will result completely arbitrary. In addition, more information is required on the nitrogen surrounding environment: it is recognised red and white wines' free protein content to be different due to the loss in solubility acted by proanthocyanins in red wines (Ribéreau-Gayon et al. 2006) but, as far as we know, the amino acids and proteins motion in wine systems still remains to be studied. The Al 2017 profile does not show any relaxation rate enhancement but, as a result of what it was said, it does not mean its nitrogen content to be lower in respect to the others.

After data transformation, the relaxation rates variability obtained at 300 MHz was higher compared to the other cases. The paramagnetic ions at this frequency contribute to the relaxation rate in a lower extent causing possible imperfection during the R_{diam} estimation to result more evident. Since not enough repetitions per each reading were done in order to assess the associated error, any other observation regarding this type of data management could be misleading. Anyway, no particular behaviour was noticed comparing varietal groups. Since the overlapping procedure alters the relaxivity specific per each frequency, it is preferable to compare the wine physical-chemical data to the unmodified relaxation profiles.

8.5.4. Physical-Chemical Wine Properties Effect on Relaxation Rate Profiles

The paramagnetic ions diluted into wines have been proven to be responsible for creating dispersion in the FFC-NMR analytical range (Bodart et al. 2020). As far as it has been recorded till now, the impact of such chemical species at hight frequencies and in the wines' concentration range, is less relevant in comparison to the diamagnetic contribution. This is the first time it is tried to inspect wine physical-chemical properties against paramagnetic profiles: the other bibliographic sources provide only some guideline since the experiments have been carried out on more homogeneous samples. Bertini et al. (1993) showed dispersions for proton relaxation at frequencies higher than 10 MHz after the addition of glycerol to water. The increasing in glycerol/water ratio resulted proportional to the relaxation rate enhancement. Anyway, glycerol content in wine rarely exceeds 20 g L^{-1} which is five less respect to the lowest tested concentration. Therefore, no effect on our sample was expected. Results for the correlations coefficient (r) are given in Table 6.

Table 6. Pearson correlation coefficients (r) and corresponding p values for correlations between physical-chemical characters and profile of wines. The latter have been weighted considering the areas drown by the most representative models. Total integral (TI) considers the entire area below the model function subtracted by the corresponding sample R_{diam}. Paramagnetic integral (PI) represents only a portion of this contribution, namely only the fraction between the frequency range 0.04-8.86349 MHz, removed from the result of the defined integral drawn by the straight line $T_1^{-1} = R_{8.86348\,\mathrm{MHz}}$ (reading obtained for each sample) is taken into account. The statistically significant correlations have been highlighted in bold.

Whine Physical-Chemical Character	Total Integral (TI)		Paramagnetic Integral (PI)	
	r	p^b	r	p^b
pH	0.44	0.086	0.39	0.117
Alcoholic Strength by Volume	**0.69**	**0.009**	**0.78**	**0.003**
Total Acidity	-0.18	0.299	-0.02	0.472
Volatile Acidity	0.18	0.300	0.36	0.136
Density	0.33	0.159	0.26	0.217
Total Dry Matter	**0.81**	**0.001**	**0.77**	**0.003**
Turbidity[a]	-0.04	0.449	0.21	0.267
Glycerol	**0.89**	**0.000**	**0.68**	**0.011**
Total Sulphur Dioxide[a]	**-0.73**	**0.005**	-0.49	0.061
Free Sulphur Dioxide	-0.06	0.425	0.07	0.578
Total Iron[a]	-0.35	0.149	0.29	0.190
Total Phenols Index (Whites)	-0.08	0.450	0.38	0.264
Total Phenols Index (Reds)	0.15	0.389	0.15	0.387

[a] The corresponding test have been carried out after data logarithmic (base 10) transformation to force sample population to a normal distribution. [b] p values arise from one-sided correlation test based on Pearson correlation coefficient.

Alvarinho 2008 was not considered since it does not show any dispersion associable to the presence of paramagnetic ion and, as an outlier, it could alter the reliability of the test. The correlation with the total phenol index has been carried out singularly on red and withe wines groups: the impossibility to normalize the dataset for this character is explainable by the extreme compositional difference of the two classes. It must be stressed the correlations obtained for TI to be in some extent influenced from PI dependence to the wine physical-chemical characteristics since the latter represents around 2-6% of its magnitude (Fig. 19). The results for the TI correlations will be much more influenced by the profiles fluctuations in the high frequency part of the spectrum because of the larger surface drawn by the models represented in logarithmic scale.

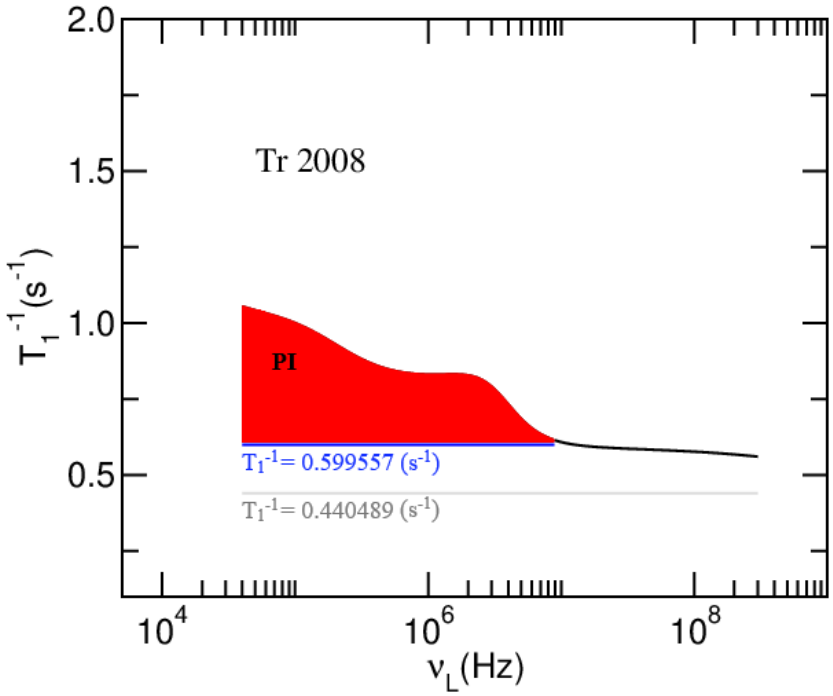

Figure 19. Most representative modelled profile for Tr 2008 wine obtained through χ^2 minimization of the cumulative BPP, IS and OS equations (Eq. 39, 43, 51). Blue line represents the relaxation rate (s^{-1}) red at 8.86349 MHz. Gray line arises from solvent (water-ethanol) diamagnetic contribution (Tab. 3). The reading surface represents the paramagnetic integral (PI). The frequency axis is plotted in logarithmic scale while T_1^{-1} values are represented in normal scale.

Total sulphur dioxide in logarithmic (base 10) scale was find strongly negatively correlated (p = 0.005) to TI (Annex Fig. S1). The correlation test between total sulphur dioxide and IP do not show a statistical relevant result even if considering the lack of information on topic makes a p close to 0.05 considerable. This result suggests a possible interaction between the paramagnetic ions and HSO_3^- diluted in wine in terms of changing their oxidation state. In fact, a reduction in the paramagnetic ion mole numbers causes a linear reduction of both inner- (Eq. 44, 45) and outer-sphere (Eq. 51) relaxation rates. The total sulphur dioxide dataset non-normality depends on the MG 2008 SO_2 concentration (Tab. 3) which differs considerably from

the others. The Shapiro-Wilk test for normality of distributions proved the population obtained after the MG 2008 removal to be normally distributed (p = 0.99). After its removal from the dataset, the new correlation still highlights the previous assumption (r = - 0.58, p = 0.016). In both cases, ethanol, glycerol, and total dry extract have been found positively correlated to PI and TI. All of them have been proven to be the main responsible physical-chemical characters determining wine viscosity (Yanniotis et al. 2007, Neto et al. 2014) even if the low glycerol concentration suggests its impact on wine profiles to be modulated by other mechanisms. The increasing in wine viscosity leads to a reduction in the diffusion coefficient (D) causing possible increasing in the outer-sphere contribution (Eq. 45). The relaxivity variation associated to viscosity changings depends on the enhancement of both the rotational correlation time (τ_R) and the correlation time modulating the zero field splitting (τ_v) (Bertini et al. 2005): the effect on the relaxation rate profile shows itself in the disappearance (or modulation) of the contact dispersion, the shift of the dipolar contribution to higher frequencies and the appearance of a second dispersion at high fields. It is not expected to observe profiles' modifications in the range of wine viscosity variation, since the relaxation rate magnitude seems mainly governed by the wine manganese(II) concentration. (Bodart et al. 2020). In addition, in the absence of information about wine manganese content, the correlation results could be misleading.

8.6. Conclusions

Wines are very complex systems: their complexity is reflected on the proton relaxation profiles in a sense of modulating the paramagnetic relaxation rate associated to manganese(II) and maybe other ions. Therefore, the relaxivity of should be considered wine dependent. We found the concentration of manganese to be an essential information for separately model the wine proton paramagnetic contributions. A possible impact of wine viscosity coded under the ethanol, glycerol and dry extract content can be explained by the simultaneous increasing in the correlation times associated to molecular rotation and the zero field splitting modulation. Since the glycerol concentration variation experienced in our samples is not enough to induce a considerable modification on wine viscosity, the result for the correlations could be explained by the concomitant effects of total dry matter and ethanol. On the other side, a cross interaction between the threes in determining the molecular organization, could lead to the same result. The presence of sulphur dioxide should be always considered because of the impact on manganese and iron oxidation state. The overlapping of wine profile highlighted the possibility to observe cross relaxation phenomena associated to the presence of nitrogen in the form of amino groups or nitrogen oxides but, in the absence of a more detailed knowledge on wine paramagnetic ions concentrations, viscosity and nitrogen profiles, the results could be

misleading. The hydroalcoholic solution models provided observations on the overall relaxation rate in wine. First, the diamagnetic contribution dominates the relaxation rate at high frequencies. In addition, the strong relaxation rate dependence ($R^2 > 0.9$) on sample ethanol content can be easily modelled through a linear regression: both intercept and slope of straight lines differed between the three inspected frequencies (23.2 MHz, 68.3 MHz, 300 MHz) even if, to exclude the analytical error to be responsible for that, data refinement is required. In conclusion, the arising diamagnetic contribution has been found to be lower if compared to the one estimated by the wine after the paramagnetic ions' removal. Wine diamagnetic contribution to the relaxation rate seems affected by other chemical species. Iron content in wine was not found to be discriminant for profile ordering; this result strengthens manganese(II) to be the most effecting ion on wine paramagnetic relaxation phenomena. The iron oxidation state should be inspected since, contrary to iron(III) no paramagnetic behaviour has been observed from iron(II) (Bodart et al. 2020). In this sense, wine sulphur dioxide can play a role. In addition, the ions concentration can be affected by contaminations occurring either during the harvest and product storage. This can be the reason why the 2008 wines' profiles have been found more informative but still, it is not possible to exclude the aging as a concomitant factor.

Manganese concentration was found required to make possible the extraction of reliable physical parameter from the fitting procedure. In addition, other variables, as the number of coordinated water molecules, modulate the ions concentration effect on the paramagnetic relaxation rate. Therefore, we stress the necessity for more wine descriptive parameters to be used during fitting procedure. Previous modelling suggested manganese to be diluted into water solvent in hexaaqua complexes $Mn(H_2O)_6^{2+}$ but recent work found the possibility for this element to be incorporated into low weighted (from 565 to 338 Dalton) molecular complexes (Latorre et al. 2019). Iron was found in three main form: free cationic (50-68%), phenolic fraction (11-39%) and residual fraction (10-24%) (Pohl et al. 2009). Creating reference sample for each of these fractions followed by proton relaxation modelling could result extremely informative on their specific contribution to the wine profiles.

9. References

Anastasiadi, M., Zira, A., Magiatis, P., Haroutounian, S., Skaltsounis, A., & Mikros, E., (2009). ^{1}H NMR-based metabolomics for the classification of Greek wines according to variety, region, and vintage. Comparison with HPLC data. *Journal of Agricultural and Food Chemistry*, **57**(**23**), 11067–11074.

Ayant, Y., Belorizky, E., Aluzon, & J., Gallice, J. (1975). Calcul des Densités spectrales résultant d'un mouvement aléatoire de translation en relaxation par interaction dipolaire magnétique dans les liquids. *Journal de Physique*, **36**(**10**), 991-1004.

Baroni, S., Consonni, R., Ferrante, G., & Aime, S. (2009). Relaxometric studies for food characterization: the case of balsamic and traditional balsamic vinegars. *Journal of Agricultural and Food Chemistry*, **57**(**8**), 3028-3032.

Bertini, I., Briganti, F., Xia, Z., & Luchinat, C. (1993). Nuclear magnetic relaxation dispersion studies of hexaaquo Mn (ii) ions in water-glycerol mixtures. *Journal of Magnetic Resonance*, **101**, 198–201.

Bertini, I., Luchinat, C., & Parigi, G. (2005). ^{1}H NMRD profiles of paramagnetic complexes and metalloproteins. *Advances in Organic Chemistry*, **57**, 140-162.

Bloch, F. (1946). Nuclear induction. *Physical Review*, **70**(**7**–**8**), 460-474.

Bodart, P.R., Rachocki, A., Tritt-Goc, J., Michalke, B., Schmitt-Kopplin, P., Karbowiak, T., & Gougeon, R.D. (2020). Quantification of manganous ions in wine by NMR relaxometry. *Talanta*, **209**, 120561.

Bora, D., Donici, A., Teodor, R., Bunea, A., Popescu, & D., Bunea, C. (2018). Elemental profile and ^{207}Pb/^{206}Pb, ^{208}Pb/^{206}Pb, ^{204}Pb/^{206}Pb, ^{87}Sr/^{86}Sr isotope ratio as fingerprints for geographical traceability of Romanian wines. *Notulae Botanicae Horti Agrobotanici Cluj-Napoca*, **46**(**1**), 223–239.

Bloembergen, N., Purcell, E.M., & Pound, R.V. (1948). Relaxation effects in nuclear magnetic resonance absorption. *Physical Review*, **73**(**7**), 679.

Catarino, S., Capelo, J.-L., Curvelo-García, A., & De Sousa, R. (2006). Evaluation of contaminant elements in Portuguese wines and original musts by high intensity focused ultrasound combined with inductively coupled plasma mass spectrometry. *OENO One*, **40**(**2**), 91–100.

Catarino, S., Curvelo-Garcia, A., & Sousa, R. (2008a). Revisão: Elementos contaminantes nos vinhos. *Ciência e Técnica Vitivinícola*, **23**(**1**), 3–19.

Catarino, S., Madeira, M., Monteiro, F., Rocha, F., Curvelo-Garcia, A., & De Sousa, R. (2008b). Effect of bentonite characteristics on the elemental composition of wine. *Journal of Agricultural and Food Chemistry*, **56**(**1**), 158–165.

Catarino, S., Trancoso, I., Madeira, M., Monteiro, F., Bruno de Sousa, R., & Curvelo-Garcia, A., (2011). Rare earths data for geographical origin assignment of wine: a Portuguese case study. *Bulletin de l'OIV*, **84**, 333–346.

Catarino, S., Madeira, M., Monteiro, F., Caldeira, I., Bruno de Sousa, R., & Curvelo-Garcia, A. (2018). Mineral composition through soil-wine system of Portuguese vineyards and its potential for wine traceability. *Beverages*, **4**(**4**), 85.

Coetzee, P., & Vanhaecke, F., (2005). Classifying wine according to geographical origin via quadrupole based ICP–mass spectrometry measurements of boron isotope ratios. *Analytical and Bioanalytical Chemistry*, **383**(**6**), 977–984.

Cozzolino, D., Holdstock, M., Dambergs, R.G., Cynkar, W. U., & Smith, P.A. (2009). Mid infrared spectroscopy and multivariate analysis: a tool to discriminate between organic and non-organic wines grown in Australia. *Food Chemistry*, **116**(**3**), 761-765.

Cynkar, W., Dambergs, R., Smith, P., & Cozzolino, D. (2010). Classification of Tempranillo wines according to geographic origin: combination of mass spectrometry based electronic nose and chemometrics. *Analytica Chimica Acta*, **660**(**1-2**), 227-231.

Kruk, D. (2016). *Understanding Spin Dynamics*. (Chap. 6-7, pp. 107-160). CRC Press.

Doan, B.-T., Meme, S., & Beloeil, J.-C. (2013). General principles of MRI. In A. Merbach, L. Helm, & É. Tóth (Eds.), *The Chemistry of Contrast Agents in Medical Magnetic Resonance Imaging* (Chap. 1, pp. 1-23). John Wiley & Sons.

Elias, R.J., & Waterhouse, A.L. (2010). Controlling the Fenton reaction in wine. *Journal of Agricultural and Food Chemistry*, **58**(**3**), 1699-1707.

Erdei, S. (2014). Monitoryng of nitrite levels in food liquid samples. *Carpathian Journal of Food Science and Technology*, **6**(**1**), 32-35.

Fan, S., Zhong, Q., Fauhl-Hassek, C., Pfister, M.-H., Horn, B., & Huang, Z. (2018). Classification of Chinese wine varieties using ^{1}H NMR spectroscopy combined with multivariate statistical analysis. *Food Control*, **88**, 113–122.

Ferreira, M.L. (2015). Automatização Da Análise de Vinhos – FTIR. Avanços Recentes No Controlo Da Qualidade de Vinhos e de Outros Produtos Vitivinícolas. In Curvelo-Garcia, A.S. & Barros, P. (Eds.), *Química Enológica - Métodos Analíticos: Avanços Recentes no Controlo da Qualidade de Vinhos e de Outros Produtos Vitivinícolas*, (pp. 101–113). Publindústria, Edições Técnicas.

Godelmann, R., Fang, F., Humpfer, E., Schütz, B., Bansbach, M., Schäfer, H., & Spraul, M. (2013). Targeted and nontargeted wine analysis by ^{1}H NMR spectroscopy combined with multivariate statistical analysis. Differentiation of important parameters: grape variety, geographical origin, year of vintage. *Journal of Agricultural and Food Chemistry*, **61**(**23**), 5610–5619.

Kaya, A., Bruno de Sousa, R., Curvelo-Garcia, A., Ricardo-da-Silva, J., Catarino, S. (2017). Effect of wood aging on wine mineral composition and ^{87}Sr/^{86}Sr isotopic ratio. *Journal of Agricultural and Food Chemistry*, **65**(**23**), 4766–4776.

Latorre, M., Herbello-Hermelo, P., Peña-Farfal, C., Neira, Y., Bermejo-Barrera, P., & Moreda Piñeiro, A. (2019). Size exclusion chromatography – Inductively coupled plasma – Mass spectrometry for determining metal-low molecular weight compound complexes in natural wines. *Talanta*, **195**, 558-565.

Liu, L., Cozzolino, D., Cynkar, W.U., Gishen, M., & Colby, C.B. (2006). Geographic classification of Spanish and Australian Tempranillo red wines by visible and near-infrared spectroscopy combined with multivariate analysis. *Journal of Agricultural and Food Chemistry*, **54**(**18**), 6754-6759.

Magdas, D.A., Pirnau, A., Feher, I., Guyon, F., & Cozar, B. I. (2019). Alternative approach of applying ^{1}H NMR in conjunction with chemometrics for wine classification. *LWT - Food Science and Technology*, **109**, 422-428.

Martelo-Vidal, M. J., & Vázquez, M. (2014). Classification of red wines from controlled designation of origin by ultraviolet-visible and near-infrared spectral analysis. *Ciência e Técnica Vitivinícola*, **29**(**1**), 35-43.

Martin, A.E., Watling, R.J., & Lee, G.S. (2012). The multi-element determination of Australian wines. *Food Chemistry,* **133**, 1081–1089.

Martins, P., Madeira, M., Monteiro, F., De Sousa, R., Curvelo-Garcia, A., & Catarino, S. (2014). ^{87}Sr/^{86}Sr ratio in vineyard soils from Portuguese denominations of origin and its potential for origin authentication. *Journal International des Sciences de la Vigne et du Vin*, **48**(**1**), 21–29.

Mazzei, P., Spaccini, R., Francesca, N., Moschetti, G., & Piccolo, A. (2013). Metabolomic by ^{1}H NMR spectroscopy differentiates “Fiano di Avellino” white wines obtained with different yeast strains. *Journal of Agricultural and Food Chemistry*, **61**(**45**), 10816–10822.

Meloni, G., & Swinnen, J. (2013). The political economy of European wine regulations. *Journal of Wine Economics*, **8**(**3**), 244–284.

OIV. International Organisation of Vine and Wine (2019a). *Compendium of international methods of wine and must analysis*. International Organisation of Vine and Wine: Paris, France, 1.

OIV. International Organisation of Vine and Wine (2019b). *Compendium of international methods of wine and must analysis*. International Organisation of Vine and Wine: Paris, France, 2.

Okoye, P.A.C., Wuana, R.A., & Ogbodo, C.V. (2017). Nitrite, nitrate and nitrosamine concentrations in common wine brands, malt drinks and fruit juices in Makurdi, Benue State. *FUW Trends in Science & Technology Journal*, **2**(**1B**), 453-549.

Orellana, S., Johansen, A.M., & Gazis, C. (2019). Geographic classification of US Washington State wines using elemental and water isotope composition. *Food Chemistry*: X, **1**, 100007.

Neto, F.S., de Castilhos, M.B., Telis, V.R., & Telis-Romero, J. (2015). Effect of ethanol, dry extract and reducing sugars on density and viscosity of Brazilian red wines. *Journal of the Science of Food and Agriculture*, **95**(**7**), 1421-1427.

Pohl, P., & Prusisz, B. (2019). Application of tandem column solid phase extraction and flame atomic absorption spectrometry for the determination of inorganic and organically bound forms of iron in wine. *Talanta*, **77**(**5**), 1732–1738.

Pusiol, D.J., Humpfer, R., & Noack, F. (1992). Nitrogen nuclear quadrupole resonance dips in the proton spin relaxation dispersion of nematic and smectic thermotropic liquid crystals. *Zeitschrift für Naturforschung A*, **47**(**11**), 1105-1114.

Ribéreau-Gayon, P., Glories, Y., Maujean, A., & Dubourdieu, D. (2006). *Handbook of Enology, Volume 2: The Chemistry of Wine-Stabilization and Treatments (2. ed.)*. (Chap. 5, pp. 109-139). West Sussex, UK: John Wiley & Sons.

Somers, T.C., & Evans, M.E. (1977). Spectral evaluation of young red wines: anthocyanin equilibria, total Phenolics, free and molecular SO_2, "Chemical Age". *Journal of the Science of Food and Agriculture*, **28**, 279-289.

Torrey, H. (1953). Nuclear spin relaxation by translational diffusion. *Physical Review*, **92**(**4**), 962.

Tóth, É., Helm, L., & Merbach, A. (2013). Relaxivity of gadolinium(III) complexes: Theory and mechanism. In A. Merbach, L. Helm, & É. Tóth (Eds.), *The Chemistry of Contrast Agents in Medical Magnetic Resonance Imaging* (Chap. 2, pp. 25-81). John Wiley & Sons.

Trávníček, P., Burg, P., Krakowiak-Bal, A., Junga, P., Vítěz, T., & Ziemiańczyk, U. (2016). Study of rheological behaviour of wines. *International Agrophysics*, **30**(**4**), 509-518.

Wang, H., Ni, Z.J., Ma, W.P., Song, C.B., Zhang, J.G., Thakur, K., & Wei, Z.J. (2019). Effect of sodium sulfite, tartaric acid, tannin, and glucose on rheological properties, release of aroma compounds, and color characteristics of red wine. *Food Science and Biotechnology*, **28**(**2**), 395-403.

Yanniotis, S., Kotseridis, G., Orfanidou, A., & Petraki, A. (2007). Effect of ethanol, dry extract and glycerol on the viscosity of wine. *Journal of Food Engineering*, **81**(**2**), 399-403.

Table S1. Two-way ANOVA results for physical-chemical data expressed according to variety and vintage effects[a]. Alcoholic strength by volume is expressed in % vol. Total acidity is expresses as g (tartaric acid) L^{-1} while volatile acidity in g (acetic acid) L^{-1} and total dry matter as g (sucrose) L^{-1}. Density is indicated in 10^{-3} kg m^3, turbidity in nephelometric turbidity units (NTU) and glycerol in g L^{-1}. Both total and free sulphur dioxide are expressed in mg L^{-1}. Total iron is expressed in mg L^{-1}.

	Variety Effect[b]	Variety (n = 2)						Vintage Effect[b]	Vintage (n = 6)	
		MG	Ar	Al	TN	Tr	CS		2008	2017
pH	***	3.24**c** ± 0.03	3.25**c** ± 0.05	3.31**c** ± 0.00	3.94**a** ± 0.02	3.72**b** ± 0.00	3.66**b** ± 0.15	ns	3.54 ± 0.10	3.50 ± 0.07
Alcoholic Strength by Volume	***	13.40**b** ± 0.20	13.36**b** ± 0.26	14.92**a** ± 0.45	13.91**b** ± 0.75	13.71**b** ± 0.06	14.14**ab** ± 0.03	**	14.38**a** ± 0.24	13.43**b** ± 0.18
Total Acidity[c]	***	5.17**abc** ± 0.23	6.15**a** ± 0.23	5.68**ab** ± 0.23	4.34**c** ± 0.23	4.79**bc** ± 0.23	5.59**ab** ± 0.23	ns	5.31 ± 0.13	5.27 ± 0.13
Volatile Acidity[d]	nd	0.60 ± 0.22	0.53 ± 0.21	0.58 ± 0.23	0.59 ± 0.06	0.58 ± 0.10	0.77 ± 0.20	***	0.91**a** ± 0.04	0.33**b** ± 0.04
Density[c]	***	0.9897**c** ± 0.0004	0.9900**c** ± 0.0002	0.9885**d** ± 0.0005	0.9915**a** ± 0.0006	0.9908**b** ± 0.0005	0.9911**ab** ± 0.0003	***	0.9900**b** ± 0.0003	0.9908**a** ± 0.0003
Total Dry Matter	***	23.4**c** ± 0.7	23.6**c** ± 0.2	24.8**c** ± 0.1	29.2**a** ± 0.7	26.7**b** ± 0.2	29.0**a** ± 0.6	ns	25.9 ± 0.7	26.3 ± 0.8
Turbidity	*	3.6**b** ± 1.4	4.6**b** ± 0.5	6.4**b** ± 2.1	14**ab** ± 7	21**a** ± 5	8.4**b** ± 0.6	ns	9.0 ± 2.0	10 ± 3
Glycerol	***	2.01**c** ± 0.28	2.30**c** ± 0.31	2.32**c** ± 0.15	6.43**a** ± 1.04	4.59**b** ± 0.04	5.49**ab** ± 0.41	ns	3.83 ± 0.32	3.88 ± 0.62
Total Phenol Index[c]	***	8.75**c** ± 1.00	10.31**c** ± 1.00	11.73**c** ± 1.00	47.00**a** ± 1.00	32.15**b** ± 1.00	35.92**b** ± 1.00	ns	24.50 ± 0.58	24.10 ± 0.58
Total SO_2	*	132**a** ± 37	74**b** ± 11	73**b** ± 19	47**b** ± 17	40**b** ± 2	52**b** ± 5	ns	84**a**± 18	55 ± 4
Free SO_2	***	9.88**b** ± 1.20	5.13**c** ± 0.38	5.50**c** ± 0.54	12.25**ab** ± 4.04	14.88**a** ± 1.40	14.00**ab** ± 0.46	**	8.04 ± 1.09**b**	12.50**a** ± 1.56
Total Iron[e]	***	1.81**b** ± 0.51	2.45**a** ± 0.60	1.70**b** ± 0.12	0.89**d** ± 0.53	1.18**c** ± 0.43	1.10**c** ± 0.55	***	1.83**a** ± 0.36	1.12**b** ± 0.32

[a] All the data are expressed as average value and standard error of the corresponding modality: each varietal value arise from averaging vintages 2008 and 2017 while for vintages the results are based on average values of the six levels (MG, Ar, Al, TN, Tr, CS) of variety. [b] Means followed by different letter in one line are significantly different at the 0.05*, 0.01** or 0.001*** of significance. ns indicates absence of significant difference between variances. [c] Statistical differences between groups have been tested with Bonferroni post-hoc test; in the other cases, Duncan multiple comparison test was preferred. [d] Data have been squared transformed before the analysis (plotted results are re-scaled). [e] Data have been transformed through the application of logarithm in base 10 (plotted results are re-scaled).

Table S2. Variance analysis (one-way ANOVA) results for physical-chemical wine characterization expressed according to colour effect[a]. Total acidity is expresses as $g_{Tartaric\ Acid}\ L^{-1}$ while volatile acidity in $g_{Acetic\ Acid}\ L^{-1}$ and total dry matter as $g_{Sucrose}\ L^{-1}$. Density is indicated in g L^{-1}, turbidity in nephelometric turbidity units (NTU) and glycerol in g L^{-1}. Both total and free sulphur dioxide are expressed in mg L^{-1}. Alcoholic strength by volume is expressed in % vol and the total iron content in mg L^{-1}.

	pH	Alcoholic Strength by Volume	Total Acidity[c]	Volatile Acidity	Density[c]	Total Dry Matter[c]	Turbidity	Glycerol[d]	Total Phenols Index	Total SO_2[d]	Free SO_2	Total Iron[c]
Colour Effect[b]	***	ns	**	ns	***	***	**	***	***	**	***	***
Red	3.77**a** ± 0.06	13.9 ± 0.2	4.9**b** ± 0.2	0.64 ± 0.07	991.0**a** ± 0.3	28.3**a** ± 0.4	14**a** ± 3	5.3**a** ± 0.3	38**a** ± 2	42.5**b** ± 0.5	14**a** ± 1	1.1**b** ± 0.1
White	3.26**b** ± 0.02	13.9 ± 0.3	5.7**a** ± 0.2	0.6 ± 0.1	989.3**b** ± 0.3	23.9**b** ± 0.4	4.8**b** ± 0.8	2.1**b** ± 0.3	10.3**b** ± 0.6	81.5**a** ± 0.5	6.8**b** ± 0.8	2.1**a** ± 0.1

[a] Each value represents the respective average for the corresponding group (Red, White) together with the standard error. [b] Different letters in the same line do not indicate statistical differences; *, ** and *** respectively indicate the significance level namely 0.05, 0.01 and 0.001. [c] Differences between groups have been tested with the Bonferroni post-hoc test; in the other cases Duncan test were preferred. [d] Data have been transformed through the application of logarithm in base 10 (results are re-scaled).

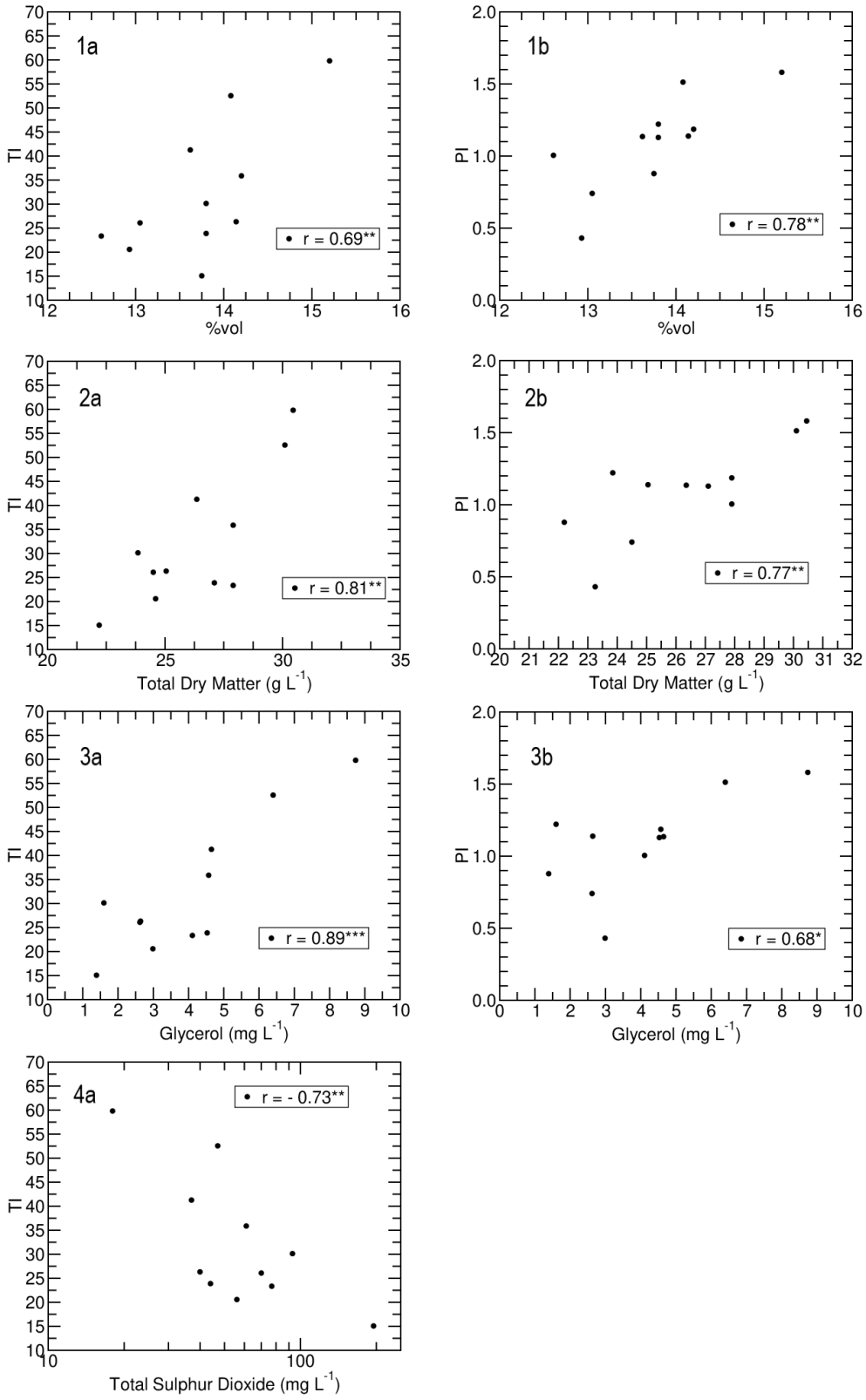

Figure S1. Plotted results for correlation respectively between (1a) total integral (TI) and alcoholic strength by volume, (1b) paramagnetic integral (PI) and alcoholic strength by volume, (2a) TI and dry matter, (2b) PI and dry matter, (3a) TI and glycerol, (3b) PI and glycerol, (4a) TI and total sulphur dioxide. The corresponding Pearson correlation coefficient (r) are given per each correlation test. *, **, *** respectively indicate statistically significant correlation at 0.05, 0.01 and 0.001 of significance.